SOLUBILITIES AND MASS TRANSFER COEFFICIENTS OF GASES IN HEAVY SYNTHETIC HYDROCARBON LIQUIDS

by

Yeldos Rakymkul

Drilling Engineer, Kazakh National Technical University, 2007

Submitted to the Graduate Faculty of

the Swanson School of Engineering in partial fulfillment

of the requirements for the degree of

Master of Science in Petroleum Engineering

University of Pittsburgh

2011

UNIVERSITY OF PITTSBURGH

SWANSON SCHOOL OF ENGINEERING

This thesis was presented

by

Yeldos Rakymkul

It was defended on

November 30, 2011

and approved by

Badie I. Morsi, Ph.D., Professor, Department of Chemical and Petroleum Engineering

Shiao-Hung Chiang Ph.D., Professor, Department of Chemical and Petroleum Engineering

George E. Klinzing, Ph.D., Professor, Department of Chemical and Petroleum Engineering

Thesis Advisor: Badie I. Morsi, Ph.D., Professor, Department of Chemical and Petroleum Engineering

SOLUBILITIES AND MASS TRANSFER COEFFICIENTS OF GASES IN HEAVY SYNTHETIC HYDROCARBON LIQUIDS

Yeldos Rakymkul, M.S.

University of Pittsburgh, 2011

The equilibrium gas solubility (C^*) and the volumetric liquid-side mass transfer coefficient (k_La) of N_2, He, H_2 and CO and their mixtures were measured in two liquids (C_{12}-C_{13} paraffins mixture and Sasol molten reactor wax) using a 4-liter agitated reactor operating in the gas-inducing mode under typical Fischer-Tropsch conditions. The experimental C^* and k_La values were obtained in wide ranges of pressure (4-45 bar), temperature (300-500 K), mixing speed (800-1400 RPM), alumina particles concentration (0-20 vol%) and gas composition (0.25, 0.5, 0.75 mole fraction of He in N_2 and H_2 in CO). Within these experimental conditions, the following results were obtained:

- The solubilities of the four gases in the two liquids at constant temperature followed the order $C^*_{CO} > C^*_{N2} > C^*_{H2} > C^*_{He}$ and obeyed Henry's Law as their values linearly increased with pressure up to 30 bar. The solubilities of the four gases in both liquids at constant pressure increased with temperature; and an Arrhenius-type equation was used to model the dependency of their Henry's Law constants on the temperature. The solubilities of the four gases were greater in the paraffins mixture than those in the molten reactor wax. The solubility and diffusivity values showed that He and N_2 could be used as surrogates for H_2 and CO, respectively.
- The mass transfer coefficients of the four gases each as a single-component or in gaseous mixtures in the two liquids increased with mixing speed, pressure and temperature at constant solid concentration. At constant mixing speed, pressure and temperature, k_La values of the four gases in the two liquids decreased with increasing solid concentration

above 10 vol%. Also, k_La values for H_2 were greater than those of CO and k_La values for He were greater than of N_2 in the two liquids. Again, k_La values showed that He and N_2 could be used as surrogates for H_2 and CO, respectively.

- A new empirical relationship was developed to predict k_La of each individual component in a gaseous mixture in liquids/slurries, if the overall k_La of this gas mixture and the diffusivities and solubilities of its components in those liquids/slurries were known.

TABLE OF CONTENTS

LIST OF TABLES

LIST OF FIGURES

NOMENCLATURE

v_1^L	Molar volume of component 1 at temperature T, $cm^3\ mol^{-1}$
a	Gas-liquid interfacial area per unit liquid volume, m^{-1}
a_p	Solid-liquid interfacial area, m^{-1}
C	Concentration, mol/m^3
C^*	Solubility of the gas at equilibrium, kmol m^{-3}
C_L	Concentration of the gas in the liquid bulk, kmol m^{-3}
C_S	Volumetric concentration of solid particles, vol%
d_{32}	Sauter mean bubble diameter, m
D_{ij}	Diffusivity of component i in j, $m^2\ s^{-1}$
$d_{imp.}$	Impeller diameter, m
d_p	Particle diameter, m
d_T	Diameter of the reactor, m
g	Gravitational constant, 9.81 $m\ s^{-2}$
H_{0a}	Pre-exponential constant in equation (7-2)
He	Henry's law constant, $Pa.m^3.mol^{-1}$
H_L	Liquid height above the impeller, m
H_V	Molar heat of vaporization, $J.mol^{-1}$
k_La	Volumetric liquid-side mass transfer coefficient, s^{-1}
m	Phase weight, kg
MW	Phase molecular weight, kg $kmol^{-1}$
N	Mixing speed, Hz or RPM
n	Carbon number, -
N_A	Avogadro Number, 6.022141 $10^{23}\ mol^{-1}$
N_{CRI}	Critical mixing speed for gas induction, Hz or RPM

P	Pressure, bar
P_c	Critical pressure, bar
P_V	Vapor pressure, Pa
R	Ideal gas constant, 8.314 $J.mol^{-1}.K^{-1}$
s	Dimensionless coefficient in equation (2-2)
T	Temperature, K
t	time, s
T_b	Boiling point, C
T_c	Critical temperature, K
TD	Tank diameter, cm
T_r	Reduced temperature, -
TV	Tank volume, Liter
V_c	Critical volume, m^3 kmol
V_G	Volume of the gas phase, m^3
V_L	Volume of the liquid phase, m^3
x	Molar fraction, -
x_i	Mole fraction of species i
y	Molar fraction (gas phase), -
Z_c	Compressibility factor, -

Greek symbols

ω	Acentric factor, -
ε_G	Gas holdup, -
ε_G	Gas holdup, -
ΔE	Apparent activation energy of absorption, $kJ.kmol^{-1}$
μ	Viscosity, Pa.s
ρ	Density, $kg.m^{-3}$
σ	Surface tension, $N.m^{-1}$
Ω	Cross section area, m^2
α	Growth probability factor, -
δ_{ij}	Interaction parameter between components i and j, -

Subscripts

0	Initial (t=0)
b	Bulk
C	Critical
G	Gas phase
G	Gas phase
i	Component i
i	Component i
L	Liquid phase
L	Liquid phase
R	Reduced
S	Sauter mean

Abbreviations and acronyms

AEO	Annual Energy Outlook
ASF	Anderson-Schulz-Flory (Distribution)
bbl	barrel
CTL	Coal-to-Liquid
EIA	Energy Information Administration
EVA	Energy Ventures Analysis
F-T	Fischer-Tropsch
GIR	Gas Inducing Reactor
GSR	Gas Sparging Reactor
GTL	Gas-to-Liquid
IEA	International Energy Agency
IHSGI	IHS Global Insight
INFORUM	Interindustry Forecasting Project at the University of Maryland
PR-EOS	Peng-Robinson Equation of State
SAR	Surface Aeration Reactor
SBCR	Slurry bubble column reactor
WGS	Water Gas Shift

ACKNOWLEDGMENTS

It is with immense gratitude that I acknowledge the sincere support, invaluable advice and compassionate guidance of my advisor, Professor Badie I. Morsi during my participation in this research project and in the preparation of this thesis. I would like to extend my thanks to Professor Shiao Hung Chiang and Professor George E. Klinzing for serving at my committee.

I do appreciate the exceptional cooperation of my labmates Yannick J. Heintz and Laurent Sehabiague. I would like also to thank Manuel Götz, Dr. Peiqian Yu and Mariela Sanoja for their constructive comments, being good teammates and making my life in Pittsburgh memorable. I consider it an honor to have worked with them.

I owe my deepest gratitude to my parents for their profound support and inspiration during my study at the University of Pittsburgh. It is a great pleasure to thank all my friends and relatives for their extensive support and encouragement during my studies abroad. I would like to give special thanks to my wife Zhibek, her love and comfort made my academic life and especially the work on this thesis an enjoyable task.

Last, but not the least, I would like to acknowledge the financial support of this research project by Sasol Technology Netherlands bv.

1.0 INTRODUCTION

In 2011, the world's population has reached 7 billion and at the 2010 world oil consumption rate of 87 million bbl/day [1], the estimated proven oil reserve worldwide will only last for 46.2 years [2]. In 2008, oil represented 37.1% of the total worldwide energy supply of which 71%, 23%, 5% and 1% were consumed in transportation sector, industrial applications, residential and commercial applications and electric power generations, respectively [3]. According to the projections made in the 2011 Annual Energy Outlook [4], in 2015 the worldwide oil will be at ~ $95/bbl and in 2035 it will rise to ~ $125/bbl (estimated at the 2009 dollars per barrel) as presented in Table 1.1. These projections could suddenly change considering the current political instabilities and turmoil within the major oil producing countries in the Middle East, Iran and Nigeria, which could jeopardize the secure oil supply to the entire world.

Table 1.1 Projections of world oil prices, 2015-2035 (2009 dollars per barrel)

Projection	2015	2020	2025	2030	2035
AEO2011(Reference case)	94.58	108.10	117.54	123.09	124.94
AEO2010 (Reference case)	94.51	109.30	116.12	124.66	134.47
Deutsche Bank	81.06	91.77	99.75	105.39	109.09
ICF Q4 2010 Integrated Energy Outlook	77.86	77.86	77.86	77.86	77.86
INFORUM	90.97	102.25	108.91	117.02	125.07
IEA (current policy scenario)	94.00	110.00	120.00	130.00	135.00
EVA	87.02	91.97	99.71	110.85	--
IHSGI	90.44	86.15	80.17	82.31	--
-- = not reported					

Although new oil deposits would be discovered in the future, the worldwide growing demand for energy, particularly by the developing countries, such as China and India, will certainly gulp all

oil production from such discoveries. Therefore, there is a pressing need for worldwide diversification of energy sources to produce the mostly needed chemicals and transportation fuels.

Synthetic chemicals and fuels produced through Fischer-Tropsch (F-T) technology are considered to be one the main viable solutions for such an increasing demand. This is due to the availability of F-T feedstock, such as coal with its abundant global reserves of 1 trillion tonnes in 2009 [5] and natural gas in remote gas reservoirs with its proven reserves of about 190 trillion cubic meters in 2011 [5], biomass with its increasing projected availability in the future [5], and heavy vacuum residue which is available in all refineries worldwide. These feedstocks can all be converted to synthetic chemical and fuels through Fischer-Tropsch (F-T) synthesis via Gas-To-Liquid (GTL), Coal-To-Liquid (CTL) and Biomass-To-Liquid (BTL) processes. It should be mentioned that research and development in F-T synthesis had been primarily driven by strategic rather than economic reasons. For instance F-T synthesis was developed in Germany during World War II and in South African Republic during the apartheid era.

In recent decades, however, there has been a growing interest in F-T technologies since it might become a substitute for crude oil for the production of fuels and other petrochemical products. In fact, F-T synthesis has been applied on a large scale in some countries, such as South Africa, Malaysia and Qatar; however, its widespread commercialization worldwide has been hampered by relatively high operating and maintenance costs and volatility of the global crude oil prices. Nonetheless, the current and projected hikes in the oil prices as given in Table 1.1 have renewed strong interest in F-T technology. In 2001-2004, F-T synthesis was projected to be economically viable, if crude oil prices were about 20-24$/bbl [6-8]. Recent estimate, on the other hand, showed that F-T would be viable at oil price of $59-65/bbl [9].

The F-T process produces many hydrocarbons through the following main reactions in the presence of cobalt or iron catalyst:

Olefins: $2nH_2 + nCO \rightarrow C_nH_{2n} + nH_2O \qquad (2 < n < N)$

Paraffins: $(2n+1)H_2 + nCO \rightarrow C_nH_{2n+2} + nH_2O \qquad (1 < n < N)$

Alcohols: $2nH_2 + nCO \rightarrow C_nH_{2n+2}O + (n-1)H_2O$

Where n is the average carbon number. The main side reaction in F-T process is the Water gas shift (WGS), which occurs in the presence of the iron catalyst as: $H_2O + CO \rightarrow CO_2 + H_2O$.

2.0 BACKGROUND

The F-T synthesis is commercially carried out in 3-phase reactors whether fixed-beds or slurry-phase reactors. This study is focusing on slurry reactors, particularly, 3-phase agitated reactors. Three-phase agitated reactors are widely used in industrial applications due to their low initial and operating costs, versatility, ease of operation, and control flexibility. For instance, in complex gas-liquid-solid systems, different modes of operation can be followed to achieve thorough mixing of all three phases. Depending on the process requirements, agitated reactors can be operated in 3 modes as Surface-Aeration Reactor (SAR), Gas-Sparging Reactor (GSR), and Gas-Inducing Reactor (GIR). In this study, a 3-phase GIR was used.

2.1 DESIGN CRITERIA OF 3-PHASE GAS-INDUCING REACTORS

The design and scaleup of GIRs require precise knowledge of the following:

1. gas induction;
2. solid suspension;
3. hydrodynamics (gas holdup, axial/radial catalyst distribution);
4. mass and heat transfer (heat and mass transfer coefficients, gas-liquid interfacial area, liquid-solid interfacial area); and
5. reaction kinetics and stoichiometry (orders with respect to reactants, products, rate constants, mechanism).

2.1.2 Gas induction and solid suspension

In the GIR, a hollow shaft is installed with holes in the gas-phase and the slurry-phase. With this configuration, GIR will function as a SAR at low mixing speeds. When mixing speed is increased, the reduction in pressure beneath the impeller becomes significant, and at a critical mixing speed for gas induction, the pressure inside the hollow shaft overcomes the hydrostatic head of the slurry, and the gas bubbles are induced from the holes into the slurry. Thus, knowing the critical mixing speed for gas induction N_{CRI} is vital for the operation of a GIR. According to Lemoine et al.[10], the critical mixing speed for gas induction could be calculated by the following equation:

$$\frac{N_{CRI}^2 d_{imp}}{g} = 0.512 * \left(\frac{\mu_L}{\mu_{water}}\right)^{0.146} * \left(\frac{\sigma_L}{\sigma_{water}}\right)^{-0.18} * \left(\frac{\rho_L}{\rho_{water}}\right)^{-0.265} * \left(\frac{H_L}{d_T}\right) \quad (2\text{-}1)$$

The physical properties of the liquid are expressed at the operating temperature, whereas those for water are taken at the ambient temperature. This correlation was developed taking into account various reactor sizes (up to 1.5 m) and different gas-liquid systems.

Also, in 3-phase reactors, a complete solid suspension must be achieved. The correlation developed by Zwietering [11] was proposed to calculate the critical mixing speed required for solid suspension.

$$N_{suspension} = \frac{s v^{0.1} d_p^{0.2} (g\Delta\rho/\rho_L)^{0.45} C_V^{0.13}}{d_{imp}^{0.85}} \quad (2\text{-}2)$$

Where v is the kinematic viscosity, $\Delta\rho$ is the density difference between the solid-phase and the liquid-phase and s is a dimensionless coefficient depending on the reactor design (d_T/d_{imp} ratio). Equation (2-2) is valid only where the particles could remain at the bottom of the reactor for less than 2 seconds. This correlation, however, was developed for liquid-solid systems and does not take into account the possible effect of the gas being induced into the slurry. Zwietering's correlation was modified by several investigators [12-14] to account for different reactor and impeller geometries, different liquid-solid systems and multiple impellers. On the other hand, the work by Murugesan [15] suggested that the gas species might be contributing to the critical mixing speed for solid suspension as well.

2.1.3 Mass transfer characteristics

The following steps, schematically represented in Figure 2.1, should be followed in order for the chemical reaction to take place in 3-phase systems:

- Step 1: Transfer of the reactants from the gas-phase bulk to the gas-liquid interface through the gas film.
- Step 2: Transfer of the reactants from the gas-liquid interface through the liquid film into the liquid bulk
- Step 3: Transfer of the reactants from the liquid bulk to the liquid-solid interface.
- Step 4: Adsorption and the reaction of the reactants on the catalyst active sites.

The resulting products will then desorb from the catalyst surface and will transfer back either to the liquid-phase or the bulk gas-phase.

According to the two-film theory, initially developed by Lewis and Whitman [16], all the steps listed above can be described by a pseudo steady-state mass transfer across a stagnant gas-liquid and liquid-solid interface by the following equations:

$$R_S = k_G a(P_G - P^*) \tag{2-3}$$

$$R_S = k_L a(C^* - C_L) \tag{2-4}$$

$$R_S = k_S a_P (C_L - C_S) \tag{2-5}$$

P^* in Equation (2-3) is the equilibrium solute gas partial pressure at the gas-liquid interface, respectively, defined as:

$$P^* = C^* * He \tag{2-6}$$

Where C^* is the equilibrium solubility and He is Henry's Law constant.

The pseudo kinetic rate of reaction can be expressed by Equation (2-5) as:

$$R_S = K_r a_P C_S \tag{2-7}$$

Combining Equations (2-3) through (2-7) leads to:

$$R_S = \frac{C_G - C_S}{\frac{1}{k_G a\, He} + \frac{1}{k_L a} + \frac{1}{k_S a_P} + \frac{1}{K_r\, a_P}} \tag{2-8}$$

In the F-T process, syngas (CO and H_2) are used which can be considered as pure components and since the liquid (wax) vapor in the gas-phase is small, the gas-phase resistance term can be neglected. Also, the solid-phase resistance can be neglected due to the small micron sized

particles used which have a huge specific surface area (a_P). Therefore, the gas-liquid film resistance ($1/k_La$) and kinetic resistance ($1/K_r$) are governing the overall rate of reaction.

In this study, however, the equilibrium gas solubility (C^*) and the volumetric liquid-side mass transfer coefficients (k_La) will be investigated in a 3-phase agitated reactor. In the following, the effects of the main operating variables (pressure, temperature, mixing speed and solid concentration) on C^* and k_La are discussed.

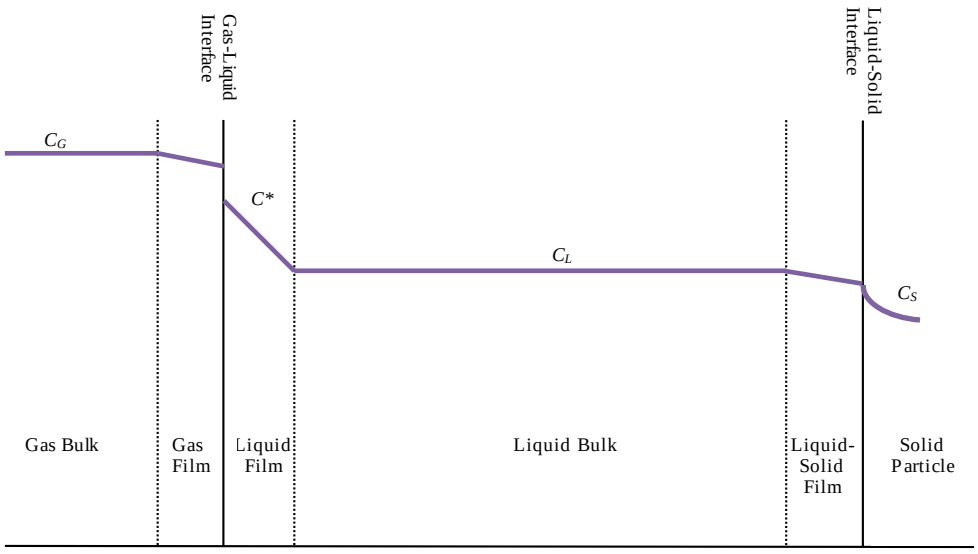

Figure 2.1: Concentration profile in a 3-phase reactor

3.0 LITERATURE REVIEW ON C^* AND k_La IN 3-PHASE REACTORS

3.1 FACTORS AFFECTING C^*

As Equation (2-4) shows, the equilibrium solubility C^* is an important factor in determining the mass transfer rate in 3-phase processes. In the following, various factors affecting k_La are discussed. Table 3.1 presents an extensive literature survey on the solubilities of gases in organic liquids under high temperature and pressure conditions. It was reported that, for the most of these gas-liquid systems, the solubility appeared to increase linearly with pressure and therefore Henry's Law is applicable within the pressure range examined. The solubilities of gases were also reported to decrease [17-19] with increasing the molecular weight/carbon number of organic liquids. Depending on the gas-liquid system and the temperature range used, C^* values can either increase or decrease with increasing temperature. For example, the solubilities of Ar, H_2, N_2, He and CO in n-paraffins were reported to increase [20-24], while the solubilities of CO_2, CH_4, C_2H_6, C_2H_4 and C_3H_8 were reported to decrease [21, 24-26] with increasing temperature. Several investigators [21, 24, 27-29] measured the solubility of different gases in n-alkanes and reported that the solubility values follow the order:

$$C^*_{He} < C^*_{H2} < C^*_{N2} < C^*_{CO} < C^*_{CH4} < C^*_{CO2} < C^*_{C2H4} < C^*_{C2H6} < C^*_{C3H8}$$

Table 3.1: Literature survey on solubilities of gases in hydrocarbon liquids

Reference	Gases	Solvent	MW	T (K)	P (bar)	System
Chou et al.[21]	$H_2/CO/CH_4/CO_2/C_2H_6/C_2H_4$	Sasol wax (n-$C_{43}H_{88}$)	605	473-573	10-50	Diffusion cell (Shaking mech.)
Albal et al.[20]	H_2/CO	Gulf wax	380	348-523	10-35	Stirred reactor (SAR)
Van Vuuren et al.[24]	$H_2/CO/CO_2/Ar/CH_4/C_2H_6/C_2H_4/C_3H_8/C_4H_{10}$	Sasol Wax	464±53	433-513	3-11	Diffusion cell (Shaking mech.)
Tsai et al.[30]	$CH_4/C_2H_6/CO_2$	Mobil wax (n-$C_{61}H_{124}$)	857	473-573	10-50	Equilibration cell
Huang et al.[31]	CO/H_2	n-C_{20}/C_{28}/C_{36}/ Mobil F-T wax	282-857	373-573	10-50	Equilibration cell
Chou et al.[32]	$CO/H_2/CO_2/CH_4/C_2H_6/C_2H_4$	n-C_{20}/C_{28}/C_{30}/C_{43}/C_{61}/C_{95}/ Sasol wax Mobil F-T wax	282-1332	-	-	Lacombe-Sanchez EOS Correlation (for heavy n-paraffin)
Gao et al.[33]	$H_2/N_2/CO$	n-C_{12}	170	344-410	7-132	Rocking cell
Karandikar et al.[34]	$CO/H_2/CH_4/CO_2$	F-T heavy fraction	368	423-498	7-45	Stirred reactor (GIR)
Karandikar et al.[35]	CO/H_2	F-T medium fraction (C_{11}-C_{20})	201	423-498	10-40	Stirred reactor (GIR)
Campanella[29]	$H_2/CO/CH_4/CO_2/C_2H_6/C_2H_4$	Light & heavy n-paraffins n-$C_{20}H_{42}$/n-$C_{28}H_{58}$/n-$C_{36}H_{74}$ Sasol wax ($C_{43}H_{88}$) Mobil wax ($C_{61}H_{124}$)	282-506	-	-	Correlation based on fluctuation solution theory
Huang et al.[36]	H_2/CO	n-$C_{20}H_{42}$/n-$C_{28}H_{58}$/ n-$C_{61}H_{124}$	282-857	373-573	10-50	Equilibration cell
Chang et al. [17]	CO	n-C_6H_{14}/n-$C_{10}H_{22}$/n-$C_{14}H_{30}$	86-198	328-428	1-50	Stirred reactor (GIR)
Campanella[37]	$H_2/CO/CO_2$	n-paraffins C_{20}-C_{44}	282-618	-	-	Correlation using a lattice-gas model

Table 3.1 (continued)

Reference	Gases	Solvent	MW	T (K)	P (bar)	System
Inga [38]	$H_2/CO/N_2/CH_4/C_2H_4$	Hexane mixture: 2 methyl pentane (6.73%)/ 3 methyl pentane (14.17%)/ Hexane (64.55%)/ Methylcylopentane (14.55%)	85.88	398-303	5-25	Stirred reactor (SAR)
Tekie et al. [39]	N_2/O_2	Cyclohexane	78	330-430	7-35	Stirred reactor
Ghosh et al. [26]	$CH_4/C_2H_6/CO/H_2$	n-Alkanes (up to C_{16})/ 1-alkenes (C_2 to C_{16})	28-226	-	-	Statistical Associating Fluid Theory EOS
Ronze et al. [40]	H_2	Cyclohexane/Gas oil	78	298-675	Up to 40	Stirred reactor (GIR)
Breman et al. [41]	$H_2/CO/CO_2/H_2O$/n-C_2H_6 to C_6H_{14}/ CH_3OH/C_2H_5OH/ 1-C_3H_7OH/ 1-C_4H_9OH/ 1-$C_5H_{11}OH$/ 1-$C_6H_{13}OH$	Tetraethyleneglycol ($C_8H_{18}O_5$)/n-$C_{16}H_{34}$/ n-$C_{28}H_{58}$/1-$C_{16}H_{33}OH$/ phenanthrene ($C_{14}H_{10}$)/	178-394	293-553	0.6-55	Stirred reactor (SAR)
Hichri et al. [42]	H_2	2-propanol/o-cresol	60-108	303-393	0-30	Stirred reactor (GIR)
Behkish et al. [43]	$H_2/CO/N_2/CH_4$	Isopar-M (n-C_{10}-n-C_{16})/ hexane mixture	85.88-192	298	1.7-8	SBCR
Tong et al. [23]	N_2	n-$C_{10}H_{22}$/n-$C_{20}H_{42}$/ n-$C_{28}H_{58}$/n-$C_{36}H_{74}$	142-506	323-423	Up to 180	Equilibrium cell
Miller et al. [44]	H_2/CO	n-$C_{28}H_{58}$	394	528	10-30	Stirred reactor (SAR)
Deimling et al.[19]	CO/H_2	F-T heavy/medium/light	114-368	373-523	10-40	Stirred reactor (SAR)

3.2 FACTORS AFFECTING k_La

The volumetric liquid-side mass transfer coefficient, k_La is one of the important parameters in Equation (2-4). The k_La is commonly measured either by chemical or physical methods. In the following, various factors affecting k_La are discussed.

3.2.1 Effect of pressure on k_La

A literature survey on the effect of pressure on k_La is presented in Table 3.2; and as can be seen, k_La values appear to be strongly dependent on the gas-liquid system and the range of pressures investigated. Some investigators reported that k_La increased [17, 19, 34, 39, 45], while others reported that k_La remained unaffected [20, 44, 46] with increasing pressure. The majority of these investigators, however, agreed that the effect of pressure on k_La is related to the alteration of the liquid-phase physico-chemical properties due to the increase of gas solubility with pressure, which leads to the decrease of the viscosity and surface tension of the liquid-phase.

3.2.2 Effect of temperature on k_La

Table 3.3 presents a literature survey on the effect of temperature on k_La. Resembling the effect of pressure, increasing temperature could lead to an increase [19, 20, 35, 39], no effect [45, 47], or even a decrease [19] of k_La values. With increasing temperature, the liquid viscosity and surface tension decrease, whereas the diffusivity of the gas in the liquid increases. The decrease of viscosity and surface tension leads to a decrease of the average bubble size, and therefore the gas-liquid interfacial area, a, increases. The increase of the gas diffusivity into the liquid increases k_L since it is proportional to the diffusivity to the power 0.5 or 1.0. Therefore, increasing temperature is supposed to increase k_La. Depending on the gas-liquid system,

however, if the gas solubility decreases with increasing temperature, the solubility effect on k_La could offset the expected increase of k_La with increasing temperature of the liquid.

3.2.3 Effect of mixing speed on k_La

A literature review on the mixing speed effect on the k_La is presented in Table 3.4. Increasing mixing speed was reported to increase k_La [17, 19, 34, 35, 39, 45, 48]. The gas holdup and gas-liquid interfacial area (a) increase with increasing mixing speed. Additionally, increasing mixing speed increases the shear rate applied at the bubbles gas-liquid interface which reduces the liquid film thickness and, according to the two-film model, it will increase k_L. Several investigators [49-51], however, reported no significant increase in k_La when reaching high mixing speeds (>1200 RPM) in small size reactors. This behavior was related to the fact that the pumping capacity of the impeller reaches its maximum and would not provide any further increase in the gas holdup and subsequently k_La.

3.2.4 Effect of solid concentration on k_La

According to a literature review presented in Table 3.5, the addition of solid particles to the liquid-phase can have different effects on k_La. In some cases, low solid concentration can have a small effect [42, 52] on, or increase k_La [45, 46, 53, 54], whereas at high solid concentrations, k_La values dramatically decrease [19, 45, 46, 53]. Low concentrations of small particles have only a limited impact on the slurry viscosity and can inhibit the coalescence tendency or promote breakup of gas bubbles by interacting directly with the gas-liquid interface, resulting in a small increase of k_La values. High solid concentrations, on the other hand, are more likely to increase the slurry viscosity which in turn will promote gas bubbles coalescence and will lead to a decrease of the gas-liquid interfacial area, a. Increasing bubble size, however, can increase the mass transfer coefficient k_L and as a result k_La might increase, decrease or remain unaffected by the solid concentration depending on the resultant effect on both k_L and a.

3.2.5 Effect of liquid nature on $k_L a$

A summary of the available literature data on the effect of liquid nature on $k_L a$ is presented in Table 3.6. When considering hydrocarbon series such as alkanes C_nH_{2n+2}, Karandikar et al. [19, 34, 35] and Chang et al. [17] reported a decrease in $k_L a$ values with increasing carbon number or average chain length. Albal et al. [46] reported that increasing the liquid-phase viscosity decreases $k_L a$, whereas when lowering the surface tension of the liquid they observed an increase of $k_L a$. These observed effects on $k_L a$ are largely due to the decrease of the gas diffusivity into the liquid when the viscosity is increased and to the decrease in the average bubble size when surface tension is decreased.

3.2.6 Effect of gas nature on $k_L a$

The effect of the gas nature on $k_L a$ could be rather complex. In n-hexane, Chang et al. [17] and Inga et al. [45] reported similar $k_L a$ behavior when comparing gases with close diffusivities. They reported similar $k_L a$ values for N_2 and CO and attributed this behavior to the fact that both gases have similar molecular weight and close diffusivities (i.e., k_L) in n-hexane and hexane mixture. However, it is quite difficult to explain the effect of gas nature on $k_L a$ based solely on its impact on k_L since an effect of the interfacial area (a) has to be considered, particularly, for low molecular weight gases, such as H_2 and He.

Table 3.2: Literature survey on the effect of pressure on $k_L a$

Reference	Gas	Liquid/Slurry	Operating Conditions	Reactor	Remarks
Hichri et al.[42]	H_2	2-propanol/o-cresol/ mixture (2/3 2-propanol+ 1/3 o-cresol)/ Pyrex beads ($40<d_p<300\mu m$)	303-393 K, 800-1500 RPM, TD 5 cm, 0-30 bar, solid up to 5 vol%	GIR	No influence of P
Sridhar et al. [51]	N_2	Cyclohexane	297-423 K, 480-1800 RPM, 1-10 bar, TD 13 cm	GSR	P↑ a↑ ε_G↑ no significant increase after 10 atm
Teramoto et al.[55]	H_2/He/N_2/ CO_2/Ar	Ethanol/p-xylene/water	273 K, 2-100 bar, 150-1400 RPM, TD 5.6 cm	SAR	No effect of P on k_L for H_2O and ethanol For p-xylene P↑ k_L slightly↓
Albal et al. [46]	He/O_2	Glycerin/water+CMC/ glass beads (75-150μm)/ oil shale particles	295 K, 13.8-96.5 bar, 400-1000 RPM, TD 10.2 cm, Solid up to 30 vol%	SAR	No influence of P
Albal et al.[20]	H_2/CO	Gulf wax, MW 380	348-523 K, 10-35 bar, 800-1000 RPM	SAR	$k_L a$ independent of P
Tekie et al. [39]	N_2/O_2	Cyclohexane	330-430 K, 7-35 bar, 400-1200 RPM	GIR/SAR	P↑ $k_L a$ slightly↑
Inga et al.[45]	H_2/CO/N_2/ CH_4/C_2H_4	Hexane mixture/ Iron oxide catalyst	298-373 K, 2-25 bar, 400-1200 RPM	SAR	P↑ $k_L a$↑ (H_2/CO/N_2) No effect or slight decrease for (CH_4/C_2H_4)
Miller et al. [44]	H_2/CO	n-Octacosane (n-$C_{28}H_{58}$)/ iron-based catalyst	523 K, 10-30 bar, 250-1750 RPM, TV 0.3L	SAR	Effect of P not significant

Table 3.2 (continued)

Reference	Gas	Liquid/Slurry	Operating Conditions	Reactor	Remarks
Deimling et al.[56]	H_2/CO	F-T light(C_6-C_{11})/ F-T medium (C_{12}-C_{21})/ F-T heavy($\geq C_{22}$)/solid: glass bed (125-177μm)	373-523K, 10-40 bar, TV 2.0L, 800-1100 RPM, Solid up to 30 wt.%	SAR	P↑ k_La↑
Karandikar et al. [35]	H_2/CO	F-T medium (C_{11}-C_{22}) M.W. 201.5	423-498K, 10-40 bar, TV 4L, 700-1200 RPM	GIR	P↑ k_La↑↑ Effect of H_2O: ↑ k_La values for CO ↓ k_La values for H_2
Karandikar et al. [34]	H_2/CO/ CH_4/CO_2	F-T heavy ($\geq C_{22}$) M.W. 368.5	423-498K, 10-40 bar, TV 4L, 700-1200 RPM	GIR	P↑ k_La↑↑ Effect of H_2O: ↑ k_La for $CO/H_2/CH_4/CO_2$ at 700 RPM ↓ k_La for H_2/CO_2 at 1000-1200 RPM No clear effect on k_La for CO/CH_4
Chang et al. [17]	CO	n-hexane/n-decane/ n-tetradecane	328-428 K, 1-50 bar, 800-1200 RPM, TV 4L	GIR	P↑ k_La slightly↑
Maalej et al.[57]	N_2	Water	293 K, 1-100 bar, TV 1.6L	GSR	P↑ k_La↓

Table 3.3: Literature survey on the effect of temperature on k_La

Reference	Gas	Liquid/Slurry	Operating Conditions	Reactor	Remarks
Hichri et al. [42]	H_2	2-propanol/o-cresol/ mixture (2/3 2-propanol+ 1/3 o-cresol)/ Pyrex beads ($40<d_p<300\mu m$)	303-393 K, 800-1500 RPM, TD 5 cm, 0-30 bar, solid up to 5 vol%	GIR	T↑ k_La ↑
Sridhar et al. [51]	N_2	Cyclohexane	297-423 K, 480-1800 RPM, 1-10 bar, TD 13 cm	GSR	Effect of T on a is Complex
Dietrich et al. [58]	N_2/H_2	Ethanol/water/ hydrogenation mixture/ Ni Raney particles (10-15μm)	293-353 K, 10-50 bar, TV 0.5L	GIR	T↑ k_La ↑
Albal et al.[20]	H_2/CO	Gulf wax, MW 380	348-523 K, 10-35 bar, 800-1000 RPM	SAR	T↑ k_La ↑
Tekie et al. [39]	N_2/O_2	Cyclohexane	330-430 K, 7-35 bar, 400-1200 RPM	GIR/SAR	T↑ k_La ↑
Inga et al.[45]	H_2/CO/N_2/ CH_4/C_2H_4	Hexane mixture/ Iron oxide catalyst	298-373 K, 2-25 bar, 400-1200 RPM	SAR	Very small effect of temperature on k_La
Deimling et al.[56]	H_2/CO	F-T light(C_6-C_{11})/ F-T medium (C_{12}-C_{21})/ F-T heavy($\geq C_{22}$)/solid: glass bed (125-177μm)	373-523K, 10-40 bar, TV 2.0L, 800-1100 RPM, Solid up to 30 wt.%	SAR	T↑ k_La ↑ (for F-T light & heavy) T↑ k_La ↓ (for F-T medium)
Karandikar et al. [35]	H_2/CO	F-T medium (C_{11}-C_{22}) M.W. 201.5 +effect of water	423-498K, 10-40 bar, TV 4L, 700-1200 RPM	GIR	T↑ k_La ↑ For F-T liquid saturated with water
Chen et al. [59]	O_2	water	293-313 K, 1-1.2 bar, 900-1300 RPM, TD 29 cm	GIR	T↑ k_La ↑

Table 3.4: Literature survey on the effect of mixing speed on $k_L a$

Reference	Gas	Liquid/Slurry	Operating Conditions	Reactor	Remarks
Chang et al. [17]	CO	n-hexane/n-decane/ n-tetradecane	328-428K, 1-50 bar, 800-1200 RPM, TV 4L	GIR	N↑ $k_L a$↑
Hsu et al.[50]	O_3	Water	Ambient conditions, 500-1600 RPM	GIR	N↑ $k_L a$↑ Level off at 1400 RPM (ε_G↑ but more coalescence)
Hichri et al.[42]	H_2	2-propanol/o-cresol/ mixture (2/3 2-propanol+ 1/3 o-cresol)/ Pyrex beads ($40<d_p<300\mu m$)	303-393K, 800-1500 RPM, TD 5 cm, 0-30 bar, solid up to 5 vol%	GIR	N↑ $k_L a$↑↑
Sridhar et al. [51]	N_2	Cyclohexane	297-423K, 480-1800 RPM, 1-10 bar, TD 13 cm	GSR	N↑ a↑, reaches asymptotic value at high N
Albal et al. [46]	He/O_2	Glycerin/water+CMC/ glass beads (75-150μm)/ oil shale particles	295K,13.8-96.5 bar, 400-1000 RPM, TD 10.2 cm solid up to 30 vol%	SAR	N↑ $k_L a$↑
Dietrich et al.[58]	N_2/H_2	Ethanol/water/ hydrogenation mixture/ Ni Raney particles (10-15μm)	293-353K, 10-50 bar, TV 0.5L	GIR	N↑ $k_L a$↑
Tekie et al. [39]	N_2/O_2	Cyclohexane	330-430K, 7-35 bar, 400-1200 RPM	GIR/SAR	N↑ $k_L a$ ↑ for both operating modes. N↑ ε_G ↑, a↑, no effect on Bubble size
Inga et al.[45]	$H_2/CO/N_2/CH_4/C_2H_4$	Hexane mixture/ Iron oxide catalyst	298-373K, 2-25 bar, 400-1200 RPM	SAR	N↑ $k_L a$↑
Ledakowicz et al.[48]	$H_2/CO/N_2/CO_2$	Vestowax SH105	1-60 bar, 453-553 K, TV 1L	SAR	N↑ $k_L a$↑

Table 3.4 (continued)

Reference	Gas	Liquid/Slurry	Operating Conditions	Reactor	Remarks
Lekhal et al. [60]	H_2/CO	n-Octene/ethanol/water	323K, 10-150 bar, TV 0.6L, 1100-2500 RPM	GIR	N↑ k_La ↑↑
Karandikar et al. [35]	H_2/CO	F-T medium (C_{11}-C_{22}) M.W. 201.5 +effect of water	423-498K, 10-40 bar, TV 4L, 700-1200 RPM	GIR	N↑ k_La ↑↑ Effect of H_2O: ↑ k_La values for CO ↓ k_La values for H_2
Karandikar et al.[34]	H_2/CO/ CH_4/CO_2	F-T heavy ($\geq C_{22}$) M.W. 368.5 + effect of water	423-498K, 10-40 bar, TV 4L, 700-1200 RPM	GIR	N↑ k_La↑↑ Effect of H_2O: ↑ k_La for $CO/H_2/CH_4/CO_2$ at 700 RPM ↓ k_La for H_2/CO_2 at 1000-1200 RPM No clear effect on k_La for CO/CH_4
Deimling et al.[56]	H_2/CO	F-T light(C_6-C_{11})/ F-T medium (C_{12}-C_{21})/ F-T heavy($\geq C_{22}$)/solid: glass bed (125-177μm)	373-523K, 10-40 bar, TV 2.0L, 800-1100 RPM, Solid up to 30 wt.%	SAR	N↑ k_La↑↑
Hsu et al.[49]	O_3	Water	290-303K, 600-1300 RPM, TD 29 cm	GIR	N↑ k_La↑, levels off above 1000 RPM
Chen et al.[59]	O_2	water	293-313K, 1-1.2 bar, 900-1300 RPM, TD 29 cm	GIR	N↑ k_La↑

Table 3.5: Literature survey on the effect of solid concentration on $k_L a$

Reference	Gas	Liquid/Slurry	Operating Conditions	Reactor	Remarks
Hichri et al.[42]	H_2	2-propanol/o-cresol/ mixture (2/3 2-propanol+ 1/3 o-cresol)/ Pyrex beads ($40<d_p<300\mu m$)	303-393K, 800-1500 RPM, TD 5 cm, 0-30 bar, solid up to 5 vol%	GIR	$C_S\uparrow$ low effect on k_La. At $40<d_p<200\mu m$ no k_La influence
Joosten et al.[53]	He/N_2	Kerosene/sieved fraction of polypropylene/sugar/ glass beds, ($53<d_p<250\mu m$)	TV 6.1L, Solids up to 45 vol%	GSR	$k_La\uparrow$ by 10-20% at low Cs; $k_La\downarrow$ at higher C_S
Albal et al. [46]	He/O_2	Glycerin/water+CMC/ glass beads (75-150μm)/ oil shale particles	295K,13.8-96.5 bar, 400-1000 RPM, TD 10.2 cm solid up to 30 vol%	SAR	$C_S\uparrow$ (2-5 vol%) $k_La\uparrow$ by 10-30% Further $C_S\uparrow$ $k_La\downarrow$
Dietrich et al.[58]	N_2/H_2	Ethanol/water/ hydrogenation mixture/ Ni Raney particles (10-15μm)	293-353K, 10-50 bar, TV 0.5L	GIR	C_S (to 3 wt.%)$\uparrow$ $k_La\uparrow$ by 20% at low speed and 90% at high speed, C_S (above 3 wt.%)$\uparrow$ $k_La\downarrow$
Inga et al.[45]	$H_2/CO/N_2/CH_4/C_2H_4$	Hexane mixture/ Iron oxide catalyst	298-373K, 2-25 bar, 400-1200 RPM	SAR	C_S (to 12.5 wt.%)$\uparrow$ $k_La\uparrow$, $C_S\uparrow$ (above 12.5 wt.%) $k_La\downarrow$
Deimling et al.[56]	H_2/CO	F-T light(C_6-C_{11})/ F-T medium (C_{12}-C_{21})/ F-T heavy($\geq C_{22}$)/solid: glass bed (125-177μm)	373-523K, 10-40 bar, TV 2.0L, 800-1100 RPM, solid up to 30 wt.%	SAR	$C_S\uparrow$ k_La significantly $\downarrow$
Kluytmans et al.[61]	O_2	Water +electrolyte (sodium gluconate)/ solid: carbon particles (30μm)	298K, TV 1.5L, 500-1500 RPM, solid up to 0.4 wt.%	SAR/GIR	$C_S\uparrow$ $k_La\uparrow$, at C_S=const, the increase in k_La becomes smaller with N$\uparrow$

Table 3.5 (continued)

Reference	Gas	Liquid/Slurry	Operating Conditions	Reactor	Remarks
Ruthiya et al. [54]	O_2/H_2	Glucose solution/ α-methyl styrene (AMS)/ solid: SiO_2/carbon particles ($30<d_p<40\mu m$)	323 K (glucose) 303 K (AMS)	GIR	$k_La\uparrow$ at low solid concentrations
Oguz et al. [52]	O_2	Water +solid (Al_2O_3, Fe_2O_3, TiO_2, ZnO, sea sand, Kieselguhr)	298 K, 500-800 RPM, TV 4L, C_S up to 10 vol% ($0.5<d_p<80\mu m$)	GSR	No effect of sand. $C_S\uparrow$ $k_La\downarrow$ for TiO_2 and ZnO, for Fe_2O_3 and Kieselguhr little effect at low C_S then $k_La\downarrow$

Table 3.6: Literature survey on the effect of liquid nature on k_La

Reference	Gas	Liquid/Slurry	Operating Conditions	Reactor	Remarks
Hsu et al.[50]	O_3	Water	Ambient conditions, 500-1600 RPM	GIR	$HL\downarrow$ $k_La\uparrow$, $HL\uparrow\varepsilon_G\downarrow$ Liq. Height↑ Bubble size↓
Hichri et al.[42]	H_2	2-propanol/o-cresol/ mixture (2/3 2-propanol+ 1/3 o-cresol)/ Pyrex beads ($40<d_p<300\mu m$)	303-393K, 800-1500 RPM, TD 5 cm, 0-30 bar, solid up to 5 vol%	GIR	$HL\downarrow$ $k_La\uparrow$, $k_La_{proanol}>k_La_{cresol}>k_La>_{mixture}$
Albal et al. [46]	He/O_2	Glycerin/water+CMC/ glass beads (75-150μm)/ oil shale particles	295K,13.8-96.5 bar, 400-1000 RPM, TD 10.2 cm Solid up to 30 vol%	SAR	$\mu_L\uparrow$ $C^*\downarrow$ $k_La\downarrow$ $\sigma\downarrow$ $k_La\uparrow$
Karandikar et al.[19, 34, 35]	H_2/CO	F-T light(C_6-C_{11})/ F-T medium (C_{12}-C_{21})/ F-T heavy($\geq C_{22}$)	373-523K,10-40 bar, TD 10.1 cm, 700-1200 rpm	SAR/GIR	Carbon No.↑ $k_La\downarrow$
Chang et al. [17]	CO	n-hexane/n-decane/ n-tetradecane	328-428K, 1-50 bar, 800-1200 RPM, TV 4L	GIR	Carbon No.↑ $k_La\downarrow$

4.0 OBJECTIVE

As can be concluded from the preceding extensive literature review, most of the hydrodynamic and mass transfer data in the gas-inducing reactors were obtained using different gases (as single component) in various inorganic and organic liquids as well as slurries under different pressures and temperatures. Unfortunately, no data are available for syngas (CO + H_2 mixture) in actual reactor wax containing all heavy products of F-T synthesis. Therefore, the main objectives of this study are:

- To obtain the equilibrium solubilities (C^*) and the volumetric liquid-side mass transfer coefficient ($k_L a$) for various gases (CO, H_2), their surrogates (N_2, He) and CO/H_2 as well as N_2/He gaseous mixtures in C_{12}-C_{13} paraffins liquid mixture and Sasol molten reactor wax in the presence and absence of solid particles (Puralox Alumina) mimicking the F-T catalyst using a 4-liter ZipperClave agitated reactor; and
- To investigate the effects of pressure (15-30 bar), temperature (300-500 K), mixing speed (800-1400 RPM) gas composition (0, 0.25, 0.50, 0.75, 1.0 mole fraction), and catalyst concentration (0 - 20 vol%) on C^* and k_La in the two liquids.

5.0 EXPERIMENTAL

5.1 GAS-LIQUID-SOLID SYSTEMS

The gas-liquid and solid systems and the ranges of operating variables used in this study are:

Gases:	He, N_2, H_2, CO, He/N_2, H_2/CO mixtures
Liquids:	C_{12}-C_{13} paraffins mixture, Sasol reactor wax
Solid:	Puralox alumina particles, Al_2O_3
Pressure:	4-40 bars
Temperature:	300 to 500 K
Mixing speed:	800 to 1400 RPM
Solid concentration:	0 to 20 vol%
Reactor operating mode:	Gas-Inducing Reactor (GIR)

5.1.1 Gas-phase

The gases used (N_2, He, H_2 and CO) have a purity of 99.998%, 99.997%, 99.99% and 99.3% respectively. These gases were purchased from Valley National Gases (USA). Some basic thermodynamic properties [62] of these gases are given in Table 5.1. The mixtures were made by mixing He and N_2 or CO and H_2 to precisely obtain 25, 50, and 75% mole factions of one component in the mixture.

Table 5.1: Thermodynamic properties of the gases used

Gases	MW *(kg/kmol)*	Tb *(K)*	T_C *(K)*	P_C *(bar)*	V_C *(m^3/kmol)*	Z_C -	ω -
N_2	28.013	77.35	126.10	33.94	0.0901	0.292	0.040
He	4.003	4.22	5.20	2.28	0.0573	0.302	-0.390
CO	28.010	81.70	132.92	34.99	0.0931	0.295	0.066
H_2	2.016	20.39	33.18	13.13	0.0642	0.305	-0.220

5.1.2 Liquid-phase

The liquids used are a C_{12}-C_{13} paraffins liquid mixture and a Sasol molten reactor wax produced by Sasol, South Africa using F-T process. The composition of the paraffins liquid mixture, shown in Table 5.2, was provided by Sasol.

Table 5.2: Paraffins mixture composition

C_{11} and lighter	~ 3 wt.%
C_{12}	50 wt.%
C_{13}	47 wt.%
C_{14+}	< 1 wt.%

The Sasol reactor wax is solid at room temperature with a melting point around 70 ºC (343 K). It consists of saturated and straight chain hydrocarbons with almost no branches, however, its actual molar composition was not provided. Therefore, the composition of the Sasol reactor wax was estimated assuming the F-T product composition follows the superposition of 2 Anderson-Schulz-Flory (ASF) distribution [63] (or 2-α distributions) which was experimentally found to

give a good approximation of the chain length distribution of products for both iron and cobalt catalysts [64]. Since the volatile components with low carbon number do not remain in the final reactor wax, only products with carbon number ≥ 20 were considered for the estimation of the physical properties of the Sasol reactor wax.

5.1.2.1 Molecular weight and critical properties

The molecular weights of the paraffins liquid mixture and the reactor wax are 176.36 kg/kmol and 408.08 kg/kmol, respectively, as calculated from their compositions according to the following equation:

$$MW_{Wax} = \sum_{i=1}^{n} x_i MW_i \tag{5-1}$$

Where x_i represents the mole fraction of species *i*.

Other important thermodynamic properties of both liquids, given in Table 5.3 were also estimated [65] from their composition.

Table 5.3: Thermodynamic properties of reactor wax and paraffins mixture

	MW *(kg/kmol)*	T_C *(K)*	P_C *(bar)*	Z_C -	ω -
Paraffins Mixture	176.36	666.13	17.764	0.2485	0.5876
Reactor Wax	408.08	823.74	7.455	0.2266	1.1785

5.1.2.2 Liquid-phase density

The densities of the paraffins mixture and the molten reactor wax were measured in our laboratory over a wide range of temperature (290 to 500 K). They were also predicted using the Asymptotic Behavior Correlations (ABC) developed by Marano and Holder [66, 67].

The density of the paraffins mixture was correlated as a function of temperature using the following equation:

$$\rho_L = -0.7119 \times T + 958.79 \quad (5\text{-}2)$$

The measured liquid density of the paraffins mixture is shown as a function of temperature in Figure 5.1 along with the predicted values obtained using Marano and Holder [66, 67] correlations.

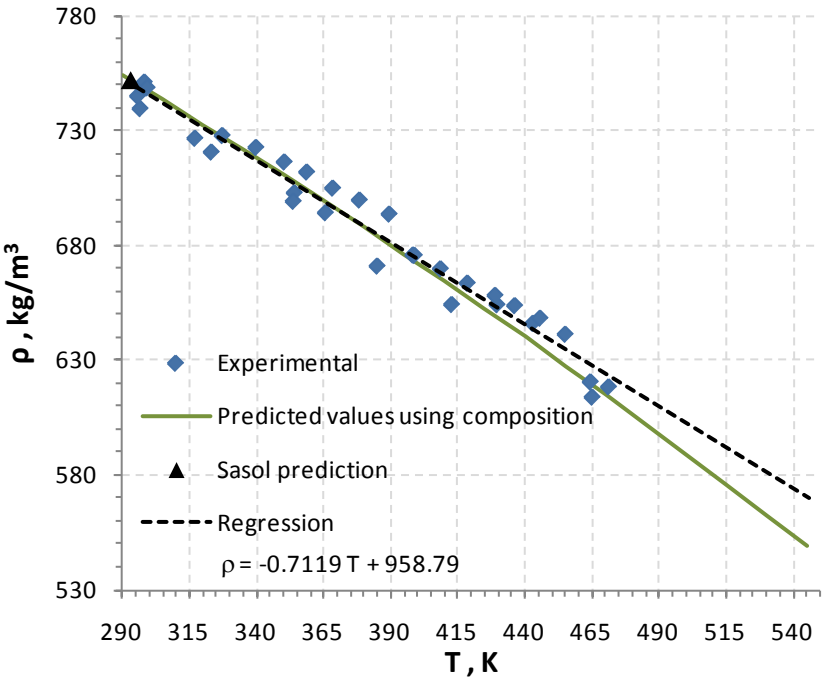

Figure 5.1: Effect of temperature on the density of the paraffins mixture

The density of the molten Sasol reactor wax was correlated as a function of temperature by the following equation:

$$\rho_L = -0.5106 \times T + 937.86 \quad (5\text{-}3)$$

The measured liquid density of the molten reactor wax is shown as a function of temperature in Figure 5.2 along with the predicted values using Marano and Holder [66, 67] correlations when considering only an average carbon number of 28 and the composition obtained in section 5.1.2.

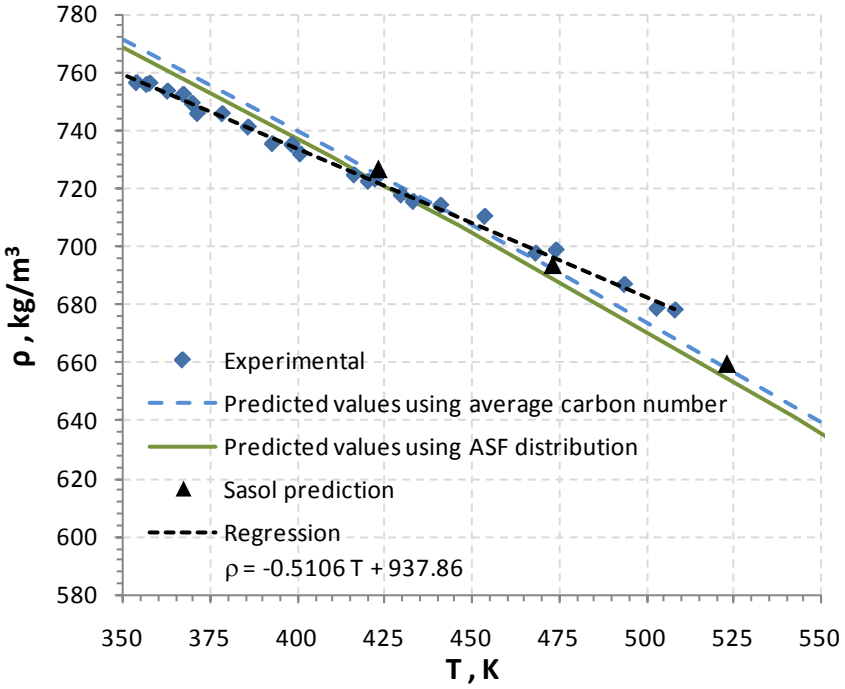

Figure 5.2: Effect of temperature on the density of the reactor wax

5.1.2.3 Liquid-phase viscosity

The viscosities of the molten reactor wax and the paraffins mixture were measured in our laboratory over a wide range of temperatures (290 to 500 K) using the Cannon-Fenske routine viscometers. They were also predicted using the ABC developed by Marano and Holder [66, 67]. The viscosity of the paraffins mixture was also measured in our laboratory and correlated as a function of temperature using the following equation:

$$\mu_L = \frac{exp\left(\frac{8.321 \times 10^4}{T^2} + \frac{1043.0}{T} - 3.9708\right)}{1000} \tag{5-4}$$

The liquid viscosity of the paraffins mixture is shown in Figure 5.3 as a function of temperature along with the predicted values obtained using Marano and Holder [66, 67] correlations.

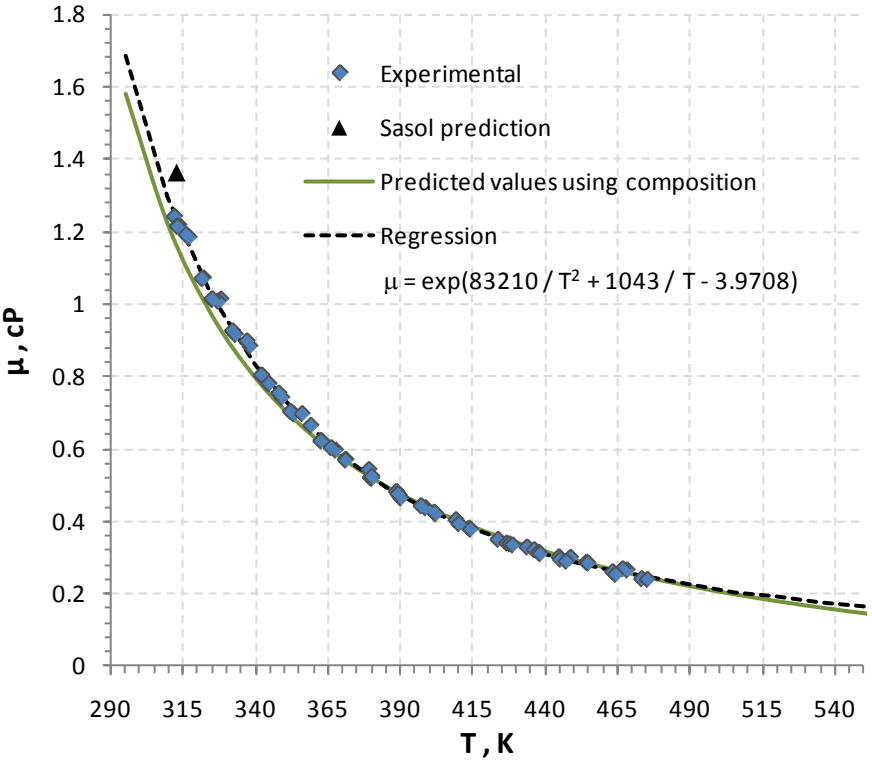

Figure 5.3: Effect of temperature on viscosity of the paraffins mixture

The viscosity of the molten reactor wax was correlated as a function of temperature by the following equation:

$$\mu_L = \frac{exp\left(\frac{1.875 \times 10^5}{T^2} + \frac{1302.7}{T} - 3.5733\right)}{1000} \quad (5\text{-}5)$$

The viscosity of the molten reactor wax is shown as a function of temperature in Figure 5.4 along with the predicted values obtained using Marano and Holder [66, 67] correlations when considering only an average carbon number of 28 as well as when considering the composition obtained in section 5.1.2.

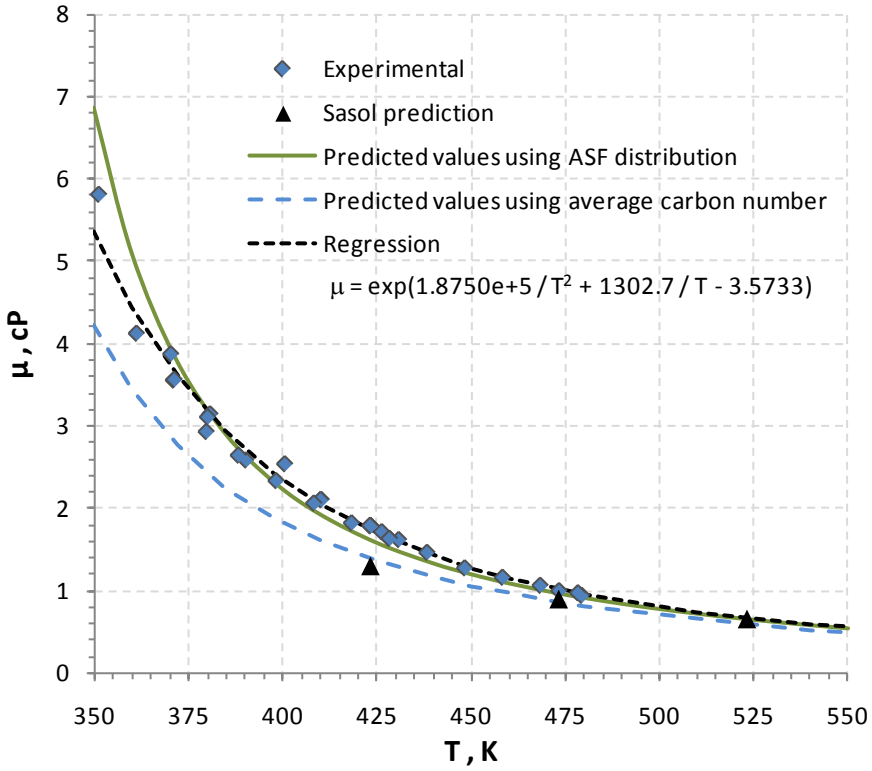

Figure 5.4: Effect of temperature on viscosity of the reactor wax

Liquid-phase surface tension

The surface tensions of the paraffins mixture and the molten reactor wax were predicted using the ABC developed by Marano and Holder [66, 67]. The liquid surface tension of the paraffins mixture is shown as a function of temperature in Figure 5.5. Also, the liquid surface tension of the reactor wax is also shown as a function of temperature in Figure 5.6 when considering only an average carbon number of 28 as well as when considering the composition obtained in section 5.1.2.

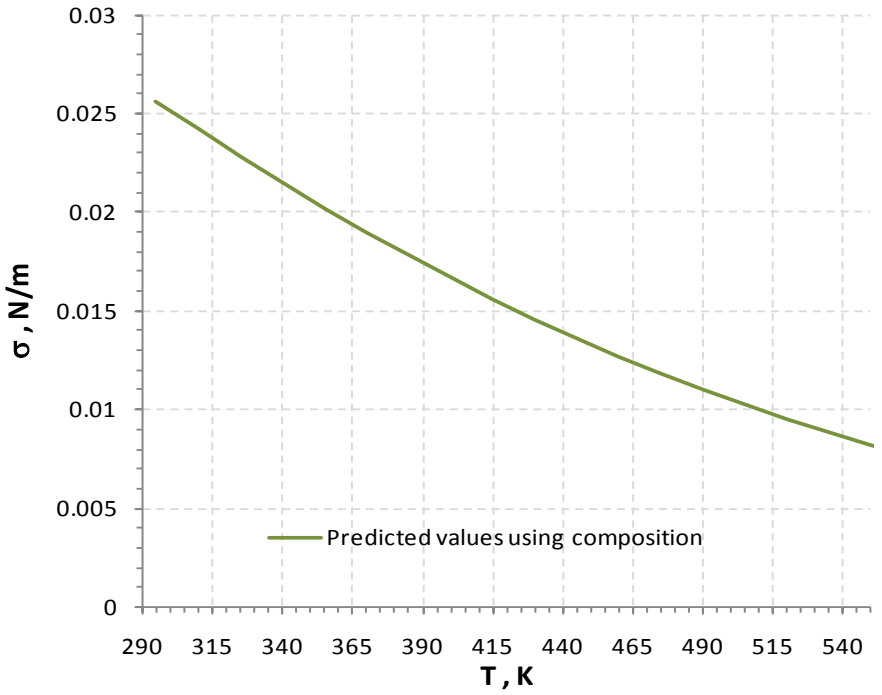

Figure 5.5: Effect of temperature on surface tension of the paraffins mixture

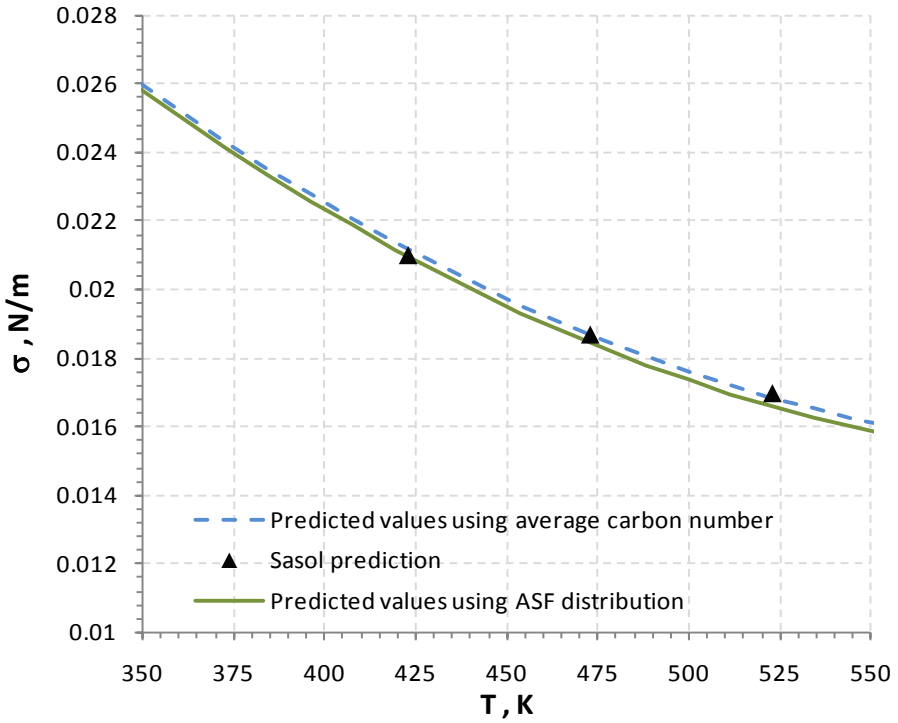

Figure 5.6: Effect of temperature on surface tension of the reactor wax

5.1.2.4 Vapor pressure

The vapor pressure of the paraffins mixture and the molten reactor wax were predicted using the ABC developed by Marano and Holder [66, 67].

The vapor pressure of the paraffins mixture is shown as a function of temperature in Figure 5.7. Also, the vapor pressure of the Sasol wax is shown as a function of temperature in Figure 5.8 when considering only an average carbon number of 28 as well as when considering the composition obtained in section 5.1.2.

For practical purposes, the vapor pressures of the paraffins mixture and the molten reactor wax were correlated as a function of temperature using Equations (5-6) and (5-7), respectively:

$$log_{10}(P_S) = -\frac{9.0041 \times 10^5}{T^2} - \frac{583.04}{T} + 2.7911 \tag{5-6}$$

$$log_{10}(P_S) = -\frac{2.6755 \times 10^5}{T^2} - \frac{1439.5}{T} + 3.9819 \tag{5-7}$$

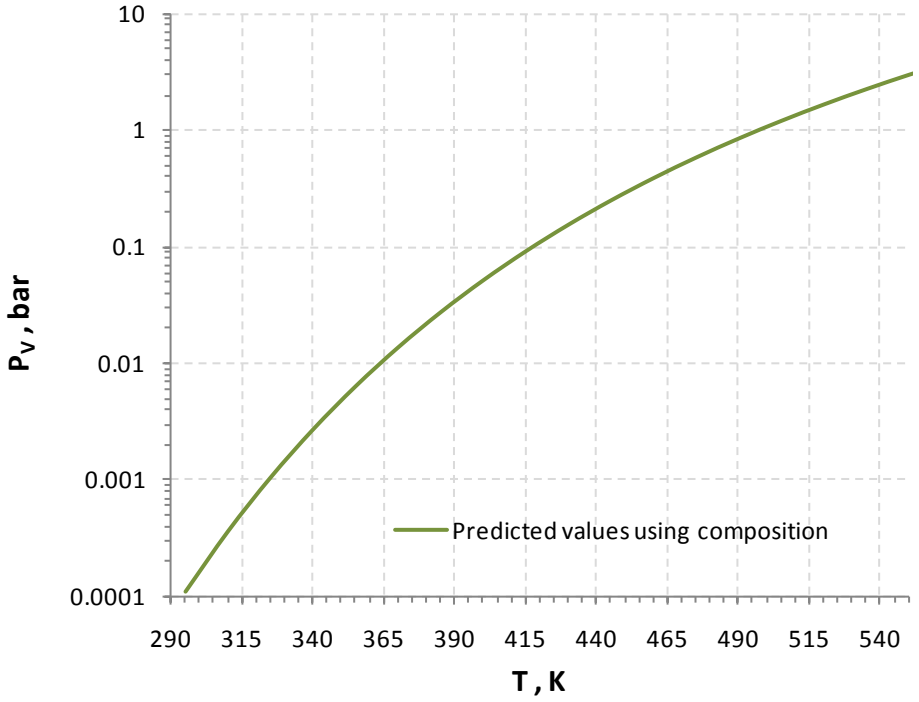

Figure 5.7: Effect of temperature on the vapor pressure of the paraffins mixture

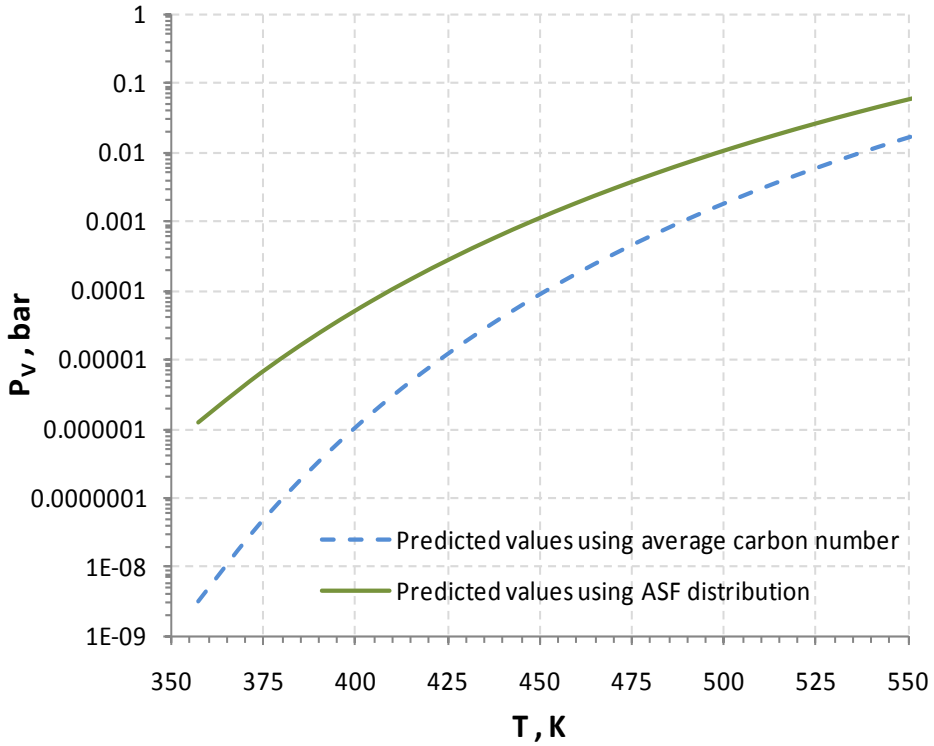

Figure 5.8: Effect of temperature on the vapor pressure of the reactor wax

5.1.3 Gas-liquid diffusivities

The diffusivities of the four gases (H_2, N_2, He and CO) used in the paraffins mixture and the molten reactor wax were calculated using the Wilke and Chang [68] equation:

$$D_{AB} = 0.1728 * 10^{-16} \frac{(\lambda MW_B)^{0.5} T}{\mu_L \upsilon_A^{0.6}} \quad (5\text{-}8)$$

The subscripts A and B represent the gas and the liquid component, respectively; λ is the association factor of the liquid-phase ($\lambda = 1$); and υ_A is the gas molar volume. Figure 5.9 and Figure 5.10 depict the diffusivities of the four gases in the paraffins mixture and the molten reactor wax as a function of temperature, respectively.

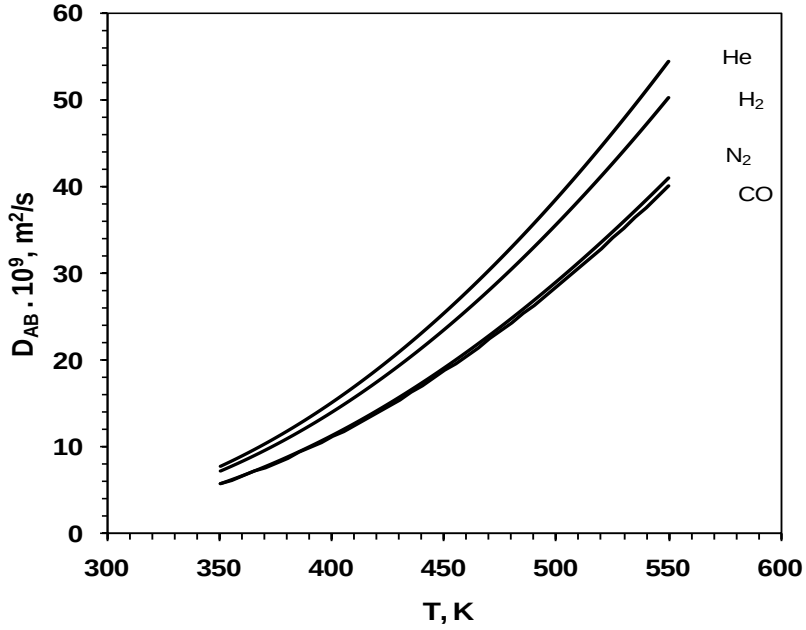

Figure 5.9: Diffusivities of gases in the paraffins mixture

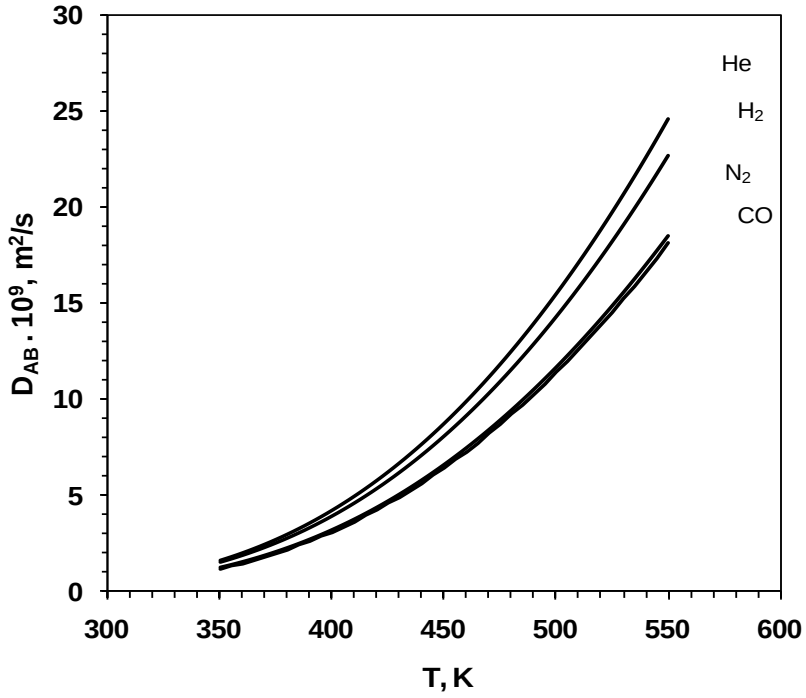

Figure 5.10: Diffusivities of gases in the molten reactor wax

5.1.4 Solid-phase

The solid-phase used is Puralox Alumina particles (provided by Sasol) that can be used as support for the actual F-T catalyst. The skeletal density of this material is about 3,900 kg/m^3 with a porosity of 70%. The size distribution of these particles, listed in Table 5.4, was obtained from Sasol.

Table 5.4: Size distribution of the solid particles

Diameter	Volume % finer than
22 μm	1%
44 μm	10%
150 μm	65%
250 μm	98%

5.2 EXPERIMENTAL SETUP

A schematic of the experimental setup and a photograph of the agitated reactor are shown in Figure 5.11 and Figure 5.12, respectively. The reactor used is a 4-liter ZipperClave with an effective volume of 3.86×10^{-3} m^3. A Pyrex glass liner with an internal diameter of 0.1128 m and height of 0.320 m is inserted inside the stainless steel reactor. The reactor is equipped with two Jerguson sight-windows, four symmetrically located baffles, a cooling coil and a heating jacket. An agitator with a six-flat blade impeller and a hollow shaft is used for mixing. The agitator is driven by a magnetic drive motor with enough capacity to avoid any eccentricity. Four holes of 0.0015 m diameter are located along the hollow shaft. Two are located in the upper part in the gas-phase and two are located in the lower end of the hollow shaft. A thermo-well provided with a K-type Chromel-Alumel thermocouple is used to measure the liquid temperature. Also, two K-type thermocouples are used to measure the gas temperature and the heating jacket temperature. A 0-1000 psia pressure transducer from Setra model 280E is located at the top of the reactor to

measure the total pressure. This reactor is able to operate up to 62 bar at a temperature of 580 K. A rupture disk rated at 60 bar and 295 K is fitted to the reactor for safety purposes. The reactor was operated as a Gas Inducing Reactor (GIR).

The preheater is a high pressure vessel with an effective volume of 1.176×10^{-3} m^3. It is heated in a convection furnace controlled with a thermostat. One K-type thermocouple and one 0-3000 psig pressure transducer are located at the outlet of the preheater.

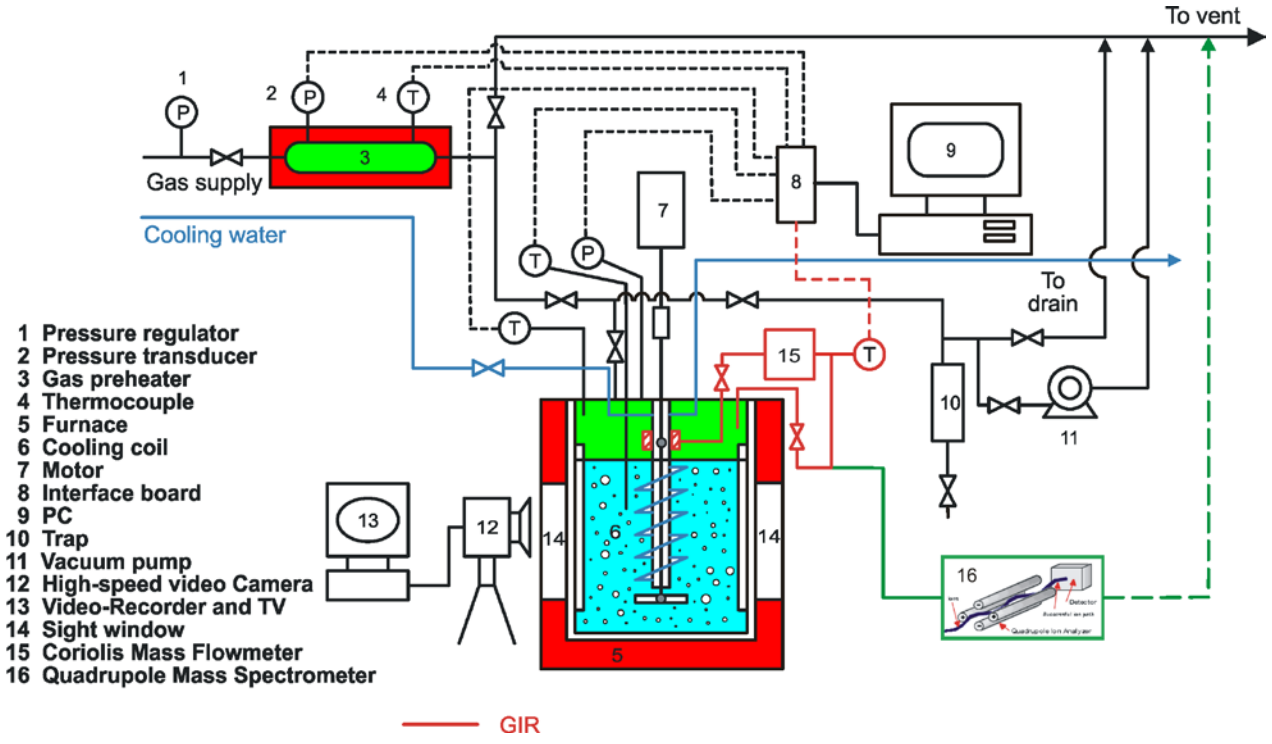

Figure 5.11: Schematic of the experimental setup for the agitated reactor

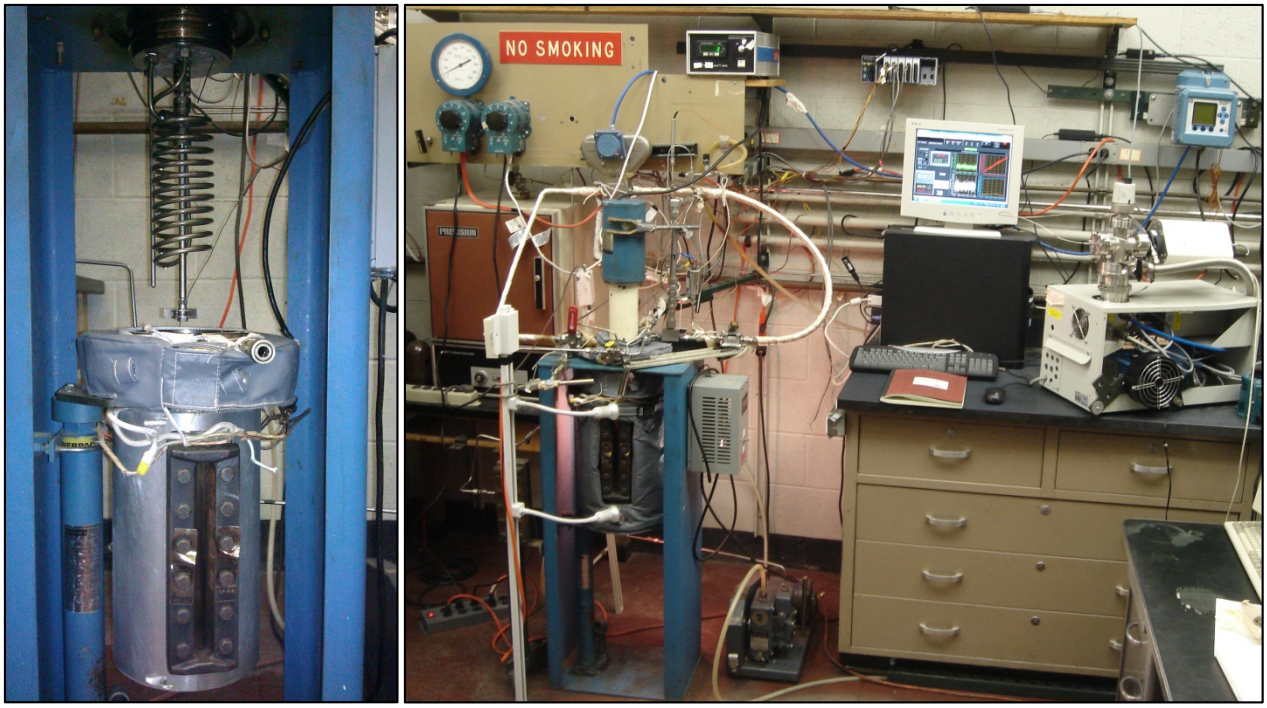

Figure 5.12: 4-liter agitated ZipperClave reactor

The gas flow rate is measured using a Coriolis mass flow meter, type CMF-010M, manufactured by Micro Motion Inc., Boulder, Co. A Welch Duo-Seal vacuum pump, model 1400, is used to vacuum the reactor contents as needed. It is able to reach an absolute pressure of 0.005 bar. Between the reactor outlet and the vacuum pump, a trap is installed to collect any condensed vapor. The outlet of the vacuum pump is connected to the exhaust.

A Balzers quadrupole Mass Spectrometer (MS) QME 200 (Quad Mass Spectrometer), is equipped with 2 roughing pumps (Vacuubrand Diaphragm vacuum pump MZ 2T and Trivac D8A) and a molecular pump (Pfeiffer TMU 065), and a pressure gauge PKR 250 to monitor the pressure inside the mass spectrometer. The MS is connected to the split stream of the gas mixture circulation loop in the experimental setup. A needle valve was installed between the circulation loop and a stainless steel capillary tube of 0.1 mm ID in order to control the flow of gas to the MS. The capillary tube was also connected to a bubbler containing water which allowed visualization of the gas flow. During absorption, the concentration of the gas measured by the MS as a function of time was converted to a pressure-time function from which the mass transfer coefficients corresponding to each component in the mixture were calculated. In addition, the

measured transient total pressure decline as a function of time allowed the calculation of the overall mass transfer coefficient of the gas mixture. The different molecules are identified in the MS using a Faraday cup detector. The Mass Spectrometer is also connected to a computer interface and is controlled using the Balzers AG QUADSTAR 422 software version 6.02. Connection of the Mass Spectrometer to a split stream of the gas mixture in the reactor is shown in Figure 5.13.

All pressure transducers and thermocouples are interfaced with an on-line personal computer through a National Instruments interface system. National Instruments LabView 2009 software is used to acquire and monitor the system pressures and temperatures as well as to control the reactor heating elements.

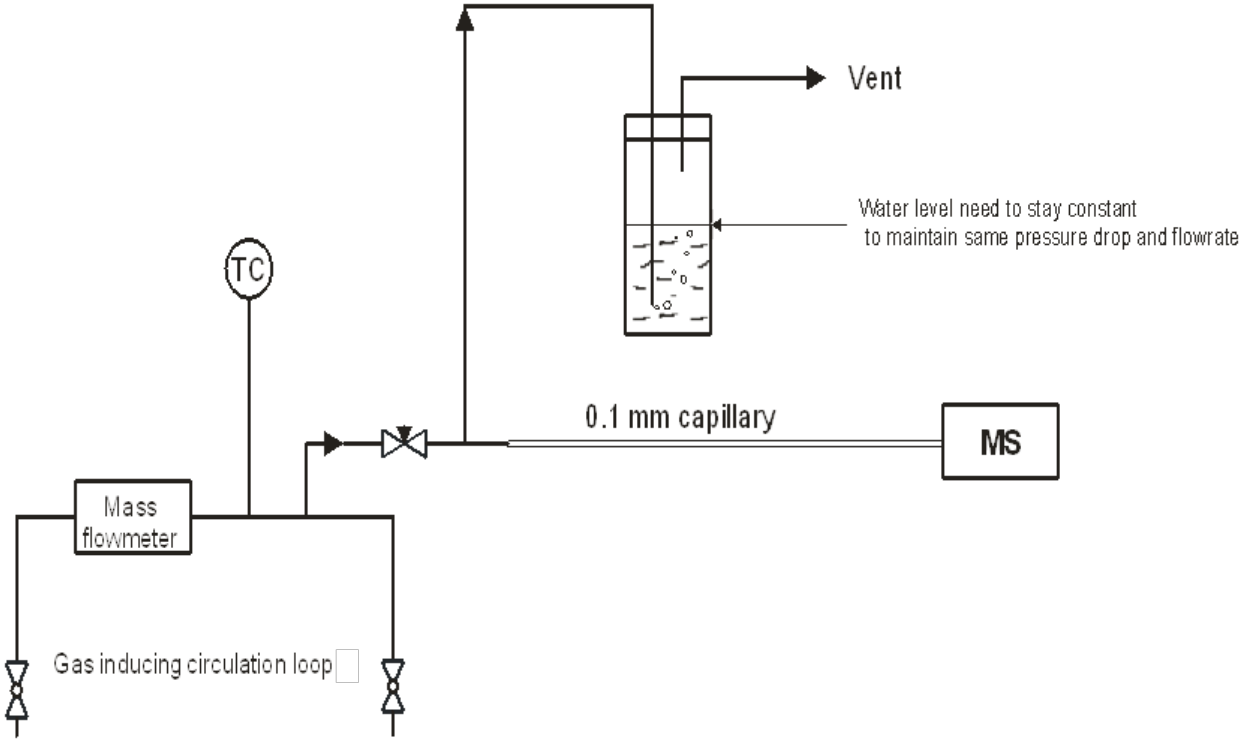

Figure 5.13: Mass spectrometer connection to the reactor system

5.3 EXPERIMENTAL PROCEDURES

The multi-step physical gas absorption method was employed to obtain the equilibrium solubility and the volumetric mass transfer coefficient values for He, N_2, H_2 and CO each as a single-gas and as various mixtures of He/N_2 and H_2/CO in the two liquids used (C_{12}-C_{13} paraffins mixture and molten reactor wax). The experimental procedure followed is given below:

1. A predetermined amount of the liquid or slurry is charged into the reactor.
2. The reactor is closed and the whole system, including the liquid-phase is degassed using the vacuum pump.
3. The gas is charged into the preheater.
4. The contents of the reactor and the preheater are heated to a desired temperature.
5. The initial conditions (pressure and temperature) in the preheater are recorded.
6. The gas is then charged into the reactor until the desired pressure is reached.
7. The needle valve connecting the reactor to the mass spectrometer is opened and a constant flow is set.
8. The data acquisition of the temperature of the gas and liquid- or slurry-phase, pressure, peaks intensities from the Mass Spectrometer is started.
9. The reactor content is stirred at a given mixing speed until the thermodynamic equilibrium, characterized by a constant final pressure in the reactor is reached. The relevant data (pressure, temperature, peak intensity, etc…) are recorded as a function of time.
10. Once the thermodynamic equilibrium is reached, the mixing is stopped as well as the data acquisition, except for the mass spectrometer where a slight delay in the measurements is observed because of the time it takes the gas to travel through the capillary tube and reach the Mass Spectrometer.

    When the peak intensities level off, the data acquisition of the Mass Spectrometer is stopped.
11. Steps 6 through 9 were repeated to collect multiple data points at different pressures as shown in Figure 5.14.

The experimental procedure given above was followed at each run with different temperature, mixing speed, solid concentration and gas composition. After each run, C^* and k_La values were calculated.

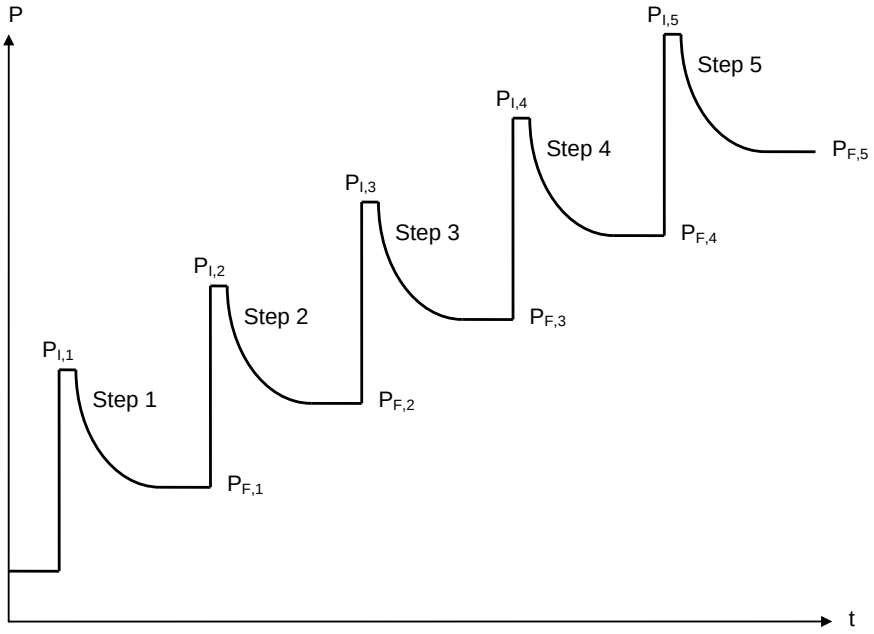

Figure 5.14: Schematic of the multi-step procedure at constant temperature (T), mixing speed (N) and liquid height (H_L)

6.0 CALCULATIONS

The equilibrium solubility (C^*) for the each gas used in the paraffins mixture and the molten reactor wax was calculated from the steady-state portion of the pressure decline (Pressure -Time) curve, whereas the volumetric liquid-side mass transfer coefficient ($k_L a$) was obtained from the transient portion of the same curve. The calculations were performed by building mass balances, on the preheater and the reactor coupled with the Peng-Robinson Equation of State (PR-EOS).

The following assumptions were made in order to calculate C^* and $k_L a$:

1. The gas-phase in the preheater and the reactor behaves as non-ideal gas and the Peng-Robinson Equation-of-State (PR-EOS) is applicable.
2. The gas and liquid phases are well mixed, resulting in homogeneous concentrations for each phase.
3. No gas absorption prior to mixing.
4. The liquid volume is constant during the absorption process, which is true, if the gas has low solubility in liquid-phase.

6.1 PENG-ROBINSON EOS

The PR-EOS was used to calculate the number of moles of gas in the feed tank before and after charging the reactor, and to calculate the number of moles remaining in the reactor after gas absorption. A general form of the PR-EOS can be written as:

$$P = \frac{RT}{v - b} - \frac{a(T)}{v(v + b) + b(v - b)} \tag{6-1}$$

This equation can be expressed in terms of the compressibility factor, Z as:

$$Z^3 - (1 - B)Z^2 + (A - 3B^2 - 2B)Z - (AB - B^2 - B^3) = 0 \tag{6-2}$$

Where:

$$A = \frac{aP}{R^2T^2} \tag{6-3}$$

$$B = \frac{bP}{RT} \tag{6-4}$$

$$z = \frac{Pv}{RT} \tag{6-5}$$

For a multi-component, one-phase system, the solution of Equation (6-2) results in three real roots or one real (single-phase) and two imaginary roots. The coefficients in Equations (6-3) and (6-4) are listed below.

$$a = \sum_i \sum_j y_i y_j a_{ij} \tag{6-6}$$

$$b = \sum_i y_i b_i \tag{6-7}$$

$$a_{ij} = \left(1 - \delta_{ij}\right) a_i^{1/2} a_j^{1/2} \tag{6-8}$$

$$a_i = 0.45724 \frac{R^2 T_C^2}{P_C^2} \left[1 + \kappa\left(1 - T_R^{1/2}\right)\right]^2 \tag{6-9}$$

$$b_i = 0.0778 \frac{RT_C}{P_C} \tag{6-10}$$

$$\kappa = 0.37464 + 1.5422\omega - 0.26992\omega^2 \tag{6-11}$$

Equation (6-2) was used to calculate the number of moles before and after absorption in the gas-phase in order to calculate the gas solubility.

6.2 EQUILIBRIUM SOLUBILITIES, *C**

The equilibrium solubility, *C**, is defined as the number of moles of gas absorbed into the liquid at equilibrium and can be defined by the following:

$$C_i^* = \frac{N_{i,I} - N_{i,F}}{V_L} \tag{6-12}$$

Where $N_{i,I}$ is the initial number of moles of the gaseous species (*i*) in the reactor prior to absorption and $N_{i,F}$ is the number of moles of the gaseous species (*i*) remaining in the reactor at thermodynamic equilibrium. $N_{i,I}$ and $N_{i,F}$ are calculated as follows:

$$N_{i,I} = \frac{V_G}{Z_{i,I} R.T_I}(P_{i,I} - P^S) \tag{6-13}$$

$$N_{i,F} = \frac{V_G}{Z_{i,F} R.T_{F,avg}}(P_{Fi,I} - P^S) \tag{6-14}$$

Where T_I is the initial temperature before the start of the absorption and $T_{F,avg}$ is the average temperature of the gas phase during the thermodynamic equilibrium. The volume of the gas phase, V_G, is calculated by subtracting the reactor volume and the liquid volume as follows:

$$V_G = V_{reactor} - (\frac{m_{liquid}}{\rho_{liquid}}) \tag{6-15}$$

In the above equation, m_{liquid} and ρ_{liquid} are the mass and density of the liquid-phase, respectively. The solubility, *C** is then obtained by substituting Equations (6-13) or (6-14) into Equation (6-12).

6.3 VOLUMETRIC LIQUID-SIDE MASS TRANSFER COEFFICIENT, $k_L a$

The volumetric liquid-side mass transfer coefficient, $k_L a$, was calculated using the Transient Physical Gas Absorption technique. During the absorption of the gas into the liquid, the decline of reactor pressure was recorded as a function of time until the equilibrium was reached. The composition data collected from the Mass Spectrometer were converted to partial pressures as

functions of time. From the decline of the total and partial pressures, the calculations of the overall as well as the individual volumetric mass transfer coefficient of each gaseous component were performed.

6.3.1 Single-gas mass transfer coefficient

The rate of mass transfer of the solute gas into the liquid phase can be calculated using the two-film model as:

$$\frac{dn_L}{dt} = k_L a(C^* - C_L)V_L \tag{6-16}$$

The rate of solute gas uptake by the liquid can be related to the decline in pressure as a function of time by the mean of a differential form of the general gas law shown in equation (6-17) below:

$$\frac{dn_L}{dt} = -\frac{V_G}{ZRT}\frac{dP_{i,t}}{dt} \tag{6-17}$$

C_L, the bulk concentration of the solute gas in the liquid, can be expressed as follows:

$$C_L = \frac{V_G}{ZV_L RT}(P_{i,I} - P_{i,t}) \tag{6-18}$$

If the gas solubility at constant temperature is linear function of pressure, Henry's law can be written as:

$$He = \frac{P_{i,t}}{C^*} \tag{6-19}$$

Substituting Equations (6-17), (6-18), and (6-19) into Equation (6-16) yields the following equation:

$$-\frac{V_G}{ZRT}\frac{dP_{i,t}}{P_{i,t}\left(\frac{V_L}{He}+\frac{V_G}{ZRT}\right)-\frac{V_G P_{i,I}}{ZRT}} = k_L a dt \tag{6-20}$$

Let $Y = P_{i,t}\left(\frac{V_L}{He}+\frac{V_G}{ZRT}\right)-\frac{V_G P_{i,I}}{ZRT}$; This gives $dY = dP_{i,t}\left(\frac{V_L}{He}+\frac{V_G}{ZRT}\right)$

By integrating between the limits of P_I at t = 0 and $P_{i,t}$ at any time (t) the following relationship can be obtained:

$$\ln\left[\frac{P_{i,t}\left(\frac{V_L}{He}+\frac{V_G}{ZRT}\right)-\frac{V_G P_{i,I}}{ZRT}}{\frac{P_{i,I}V_L}{He}}\right]=-\left[\frac{V_L ZRT}{V_G He}+1\right]k_L a.t \tag{6-21}$$

By multiplying the numerator and denominator of the left-hand-side of Equation (6-21) by (ZRT/V_G) and by rearranging, the following relationship can be obtained:

$$\ln\left[\frac{P_{i,t}(\psi+1)-P_{i,I}}{\psi P_I}\right]=-[\psi+1]k_L a.t \tag{6-22}$$

The function ψ is defined as $\psi = (V_L\ ZRT/V_G\ He)$.

At equilibrium, the final pressure ($P_{i,F}$), the final equilibrium concentration, C^*_{eq} is defined as follows:

$$C^*_{eq}=\frac{V_G}{V_L ZRT}(P_{i,I}-P_{i,F}) \tag{6-23}$$

Also, C_{eq}* can be expressed as:

$$C^*_{eq}=\frac{P_{i,F}}{He} \tag{6-24}$$

By equating equations (6-23) and (6-24), one can obtain:

$$\frac{P_{i,I}-P_{i,F}}{P_{i,F}}=\frac{V_L ZRT}{HeV_G}=\psi \tag{6-25}$$

By substituting Equation (6-25) into (6-22) and multiplying the left-hand-side of Equation (6-22) by $(P_{i,F}/P_{i,I})$, the following working equation can be obtained:

$$\frac{P_{i,F}}{P_{i,I}}ln\left[\frac{P_{i,I}-P_{i,F}}{P_{i,t}-P_{i,F}}\right]=k_L a\,t \tag{6-26}$$

If $k_L a$ is a constant, Equation (6-26) becomes a linear function of time and can be written as:

$$F(t)=k_L a\,t \tag{6-27}$$

If the left side of Equation (6-27) is plotted versus time and a linear relationship is obtained, the slope of the line will be $k_L a$.

6.3.2 Gas mixture mass transfer coefficients

When a gas mixture is used, Equation (6-27) cannot be employed to calculate $k_L a$ since $P_{i,t}$ is unknown, therefore another method as described below was followed.

The rate of mass transfer of each solute gas into the liquid phase is written as:

$$\frac{dn_{i,L}}{dt} = k_L a_i (C_i^* - C_{i,L}) V_L \tag{6-28}$$

Also, the total rate of mass transfer for all components can be expressed as:

$$\frac{dn_L}{dt} = \sum_i \frac{dn_{i,L}}{dt} = \sum_i k_L a_i \ (C_i^* - C_{i,L}) V_L \tag{6-29}$$

The rate of solute gas uptake by the liquid can be related to the decline in pressure as a function of time by the means of a differential form of the general gas law shown below:

$$\frac{dn_L}{dt} = -\frac{dn_G}{dt} = -\frac{d}{dt}\left(\frac{P_G V_G}{ZRT}\right) \tag{6-30}$$

This leads to the following equation:

$$-\frac{d}{dt}\left(\frac{P_G V_G}{ZRT}\right) = \sum_i k_L a_i \ (C_i^* - C_{i,L}) V_L \tag{6-31}$$

At every pressure, C_i* can be estimated from the experimental C* values of N_2 and He as a single-gas obtained in the paraffins mixture or in the reactor wax. The $k_L a$ for He and N_2 can be estimated by solving numerically Equation (6-31) and using the following relationship between the $k_L a$ of N_2 and He [69]:

$$k_L a_{He} = k_L a_{N_2} \left[\frac{D_{He}}{D_{N_2}}\right]^{0.5} \tag{6-32}$$

D_{He} and D_{N2} are the diffusivities of He and N_2 in the paraffins mixture or in the reactor wax, respectively.

7.0 RESULTS AND DISCUSSION

In the following sections, the equilibrium gas solubility (C^*) and the volumetric liquid-side mass transfer coefficient (k_La) data obtained in the 4-liter agitated reactor are presented and discussed.

7.1 EQUILIBRIUM SOLUBILITIES (C^*) IN THE AGITATED REACTOR

The solubility values of N_2, He, H_2 and CO were measured in the (C_{12}-C_{13}) paraffins liquid mixture and the molten Sasol reactor wax within the temperature range of 300-500 K, a pressure range of 4-45 bar and in the presence and absence of Puralox solid particles ranging from 0-20 vol%. The error analysis on C^* along with some numerical examples are provided in Appendix A. The effects of the operating variables on the solubilities of gases in the two liquids are presented in the following.

7.1.1 Effect of pressure on C^*

Within the range of operating conditions used in this study, the equilibrium solubilities of H_2, CO, N_2 and He in the paraffins mixture and in the molten reactor wax appear to linearly increase with the gas partial pressure as shown in Figures 7.1 through 7.4. The solubility values can therefore be correlated using Henry's Law as:

$$C^* = \frac{P_{i,F}}{He} \tag{7-1}$$

Where, *He* is the Henry's Law constant and $P_{i,F}$ is the partial pressure of the solute gas in the reactor at the thermodynamic equilibrium.

This increase in solubility with pressure can be related to the increase of the concentration difference (driving force) between the concentrations in the gaseous and the liquid phases when increasing the system pressure. This behavior is in a good agreement with the data reported in literature [17, 20, 21, 34, 35, 40, 43, 44, 56], presented in Table 3.1, for similar and different systems.

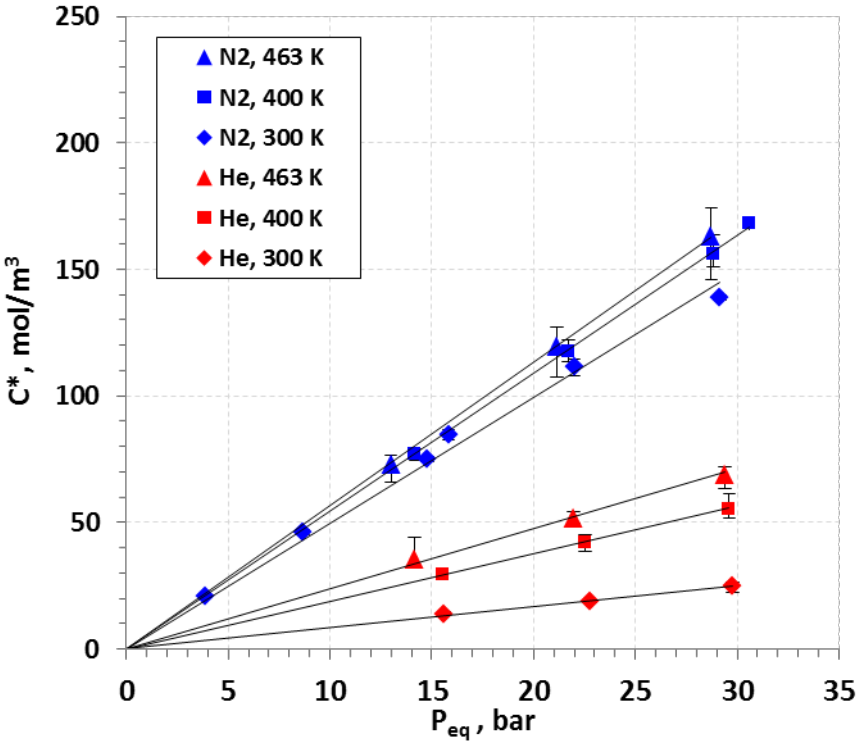

Figure 7.1. . Effect of pressure and temperature on the solubility of N_2 and He in the paraffins mixture

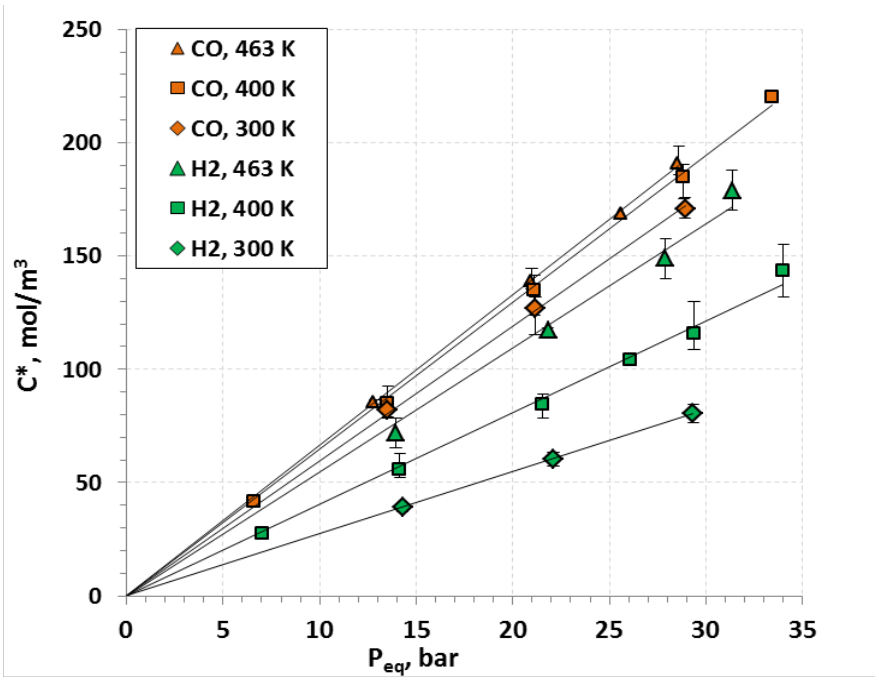

Figure 7.2 Effect of pressure and temperature on the solubility of H_2 and CO in the paraffins mixture

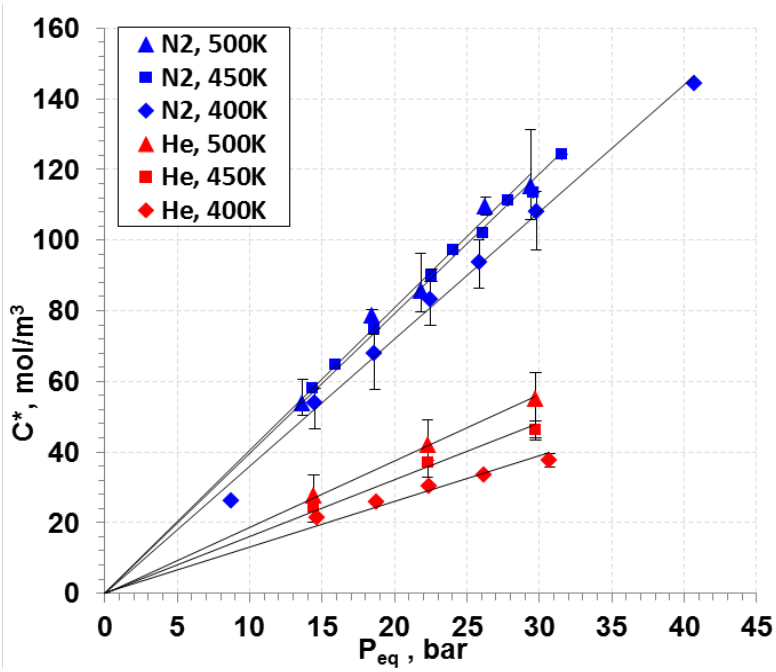

Figure 7.3. Effect of pressure and temperature on the solubility of He and N_2 in the reactor wax

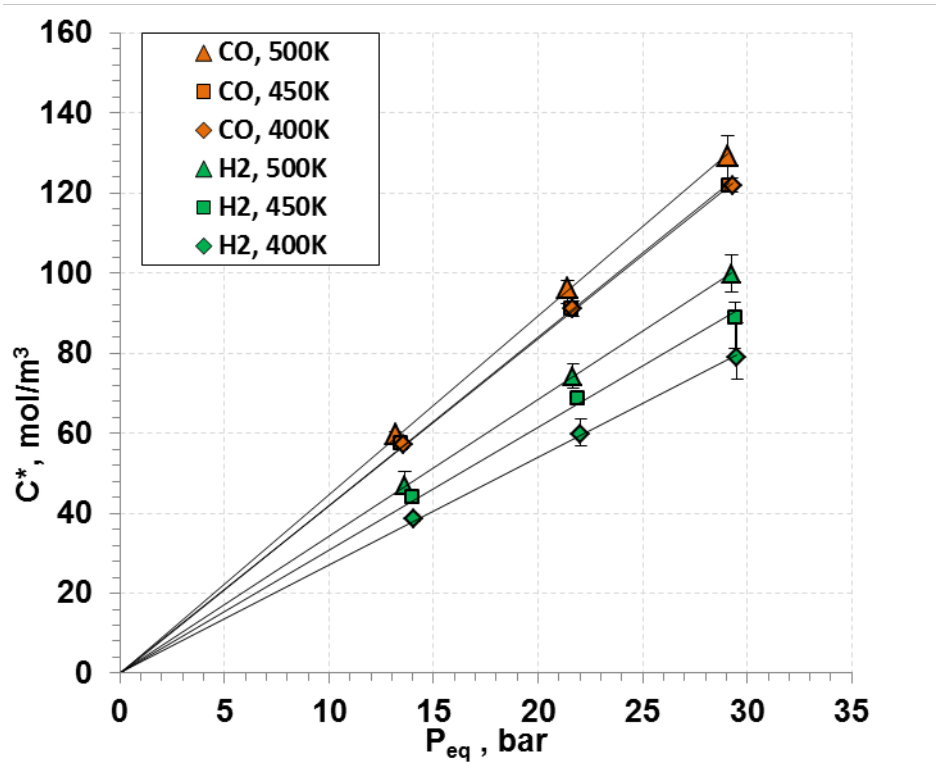

Figure 7.4. Effect of pressure and temperature on the solubility of H_2 and CO in the reactor wax

7.1.2 Effect of temperature on *C**

Depending on the gas-liquid system used and the range of temperatures studied, the gas solubility in liquids was reported in literature to increase [17, 18, 20, 21, 23, 24, 39, 43, 56, 70] or decrease [17, 21, 24, 41] with increasing temperature.

Figures 7.1 through 7.4 also show the effect of temperature on the solubility for H_2, CO, He and N_2, in the C_{12}-C_{13} paraffins mixture and in the reactor wax; and as can be seen, *C** values for the 4 gases increase with increasing temperature. Soriano [71] observed similar in magnitude behavior with identical system using refined Sasol wax as a liquid phase when compared to the data with Sasol's actual reactor wax used in this study. Also, it should be noted that the solubilities of H_2 and He were more sensitive to the changes in temperature than those of CO and N_2.

The effect of temperature on the Henry's Law constant (*He*) can be described with an Arrhenius-type equation [17, 24, 39, 70] as:

$$He = H_0 e^{\frac{\Delta H^0}{RT}} \tag{7-2}$$

Where H_0 represents the pre-exponential constant; and ΔH^0 is the heat of solution.

The effect of temperature on Henry's Law constant for four gases is depicted in Figure 7.5; and the pre-exponential constant and the heat of solution values are calculated and listed in Table 7.1.

The calculated equilibrium gas solubilities and Henry's Law constants underlined the argument that N_2 and He could be used as surrogates for CO and H_2, respectively. As can be seen the calculated values corresponding to CO and N_2 are in good agreement with each other and, H_2 and He have showed fairly similar trends both in the C_{12}-C_{13} paraffins liquid mixture and in the Sasol reactor wax. This difference in H_2 and He values could be related to their molecular weight contrast.

The heat absorbed when a gas dissolves in a liquid has essentially two contributions: (1) energy is absorbed to open a pocket in the solvent. Solvent molecules attract each other and pulling them apart to make a cavity will require energy, and heat is absorbed in this step for most solvents; and (2), energy is released when a gas molecule is popped into the pocket. Intermolecular attractions between the gas molecule and the surrounding solvent molecules lower its energy, and heat is released. The stronger the attractions are, the more heat is released. There is usually net absorption of heat when gases are dissolved in organic solvents because the pocket-making stage contribution is bigger. Le Chatelier's principle predicts that when heat is absorbed by the dissolution process it will be favored at higher temperature. Thus, the solubility would be expected to increase when temperature rises as in the present study.

Table 7.1. Coefficients in Henry's Law equation (7-2)

Gas	Reactor Wax		Paraffins Mixture	
	ΔH^0	H_0	ΔH^0	H_0
	$kJ.kmol^{-1}$	$kJ.kmol^{-1}$	$kJ.kmol^{-1}$	$kJ.kmol^{-1}$
CO	1,107.84	17,269.55	710.36	12,606.91
N_2	1,411.80	11,864.43	500.13	15,905.18
H_2	3,941.25	11,338.96	4,481.50	6,167.20
He	6,596.83	10,387.93	7,464.64	5,831.33

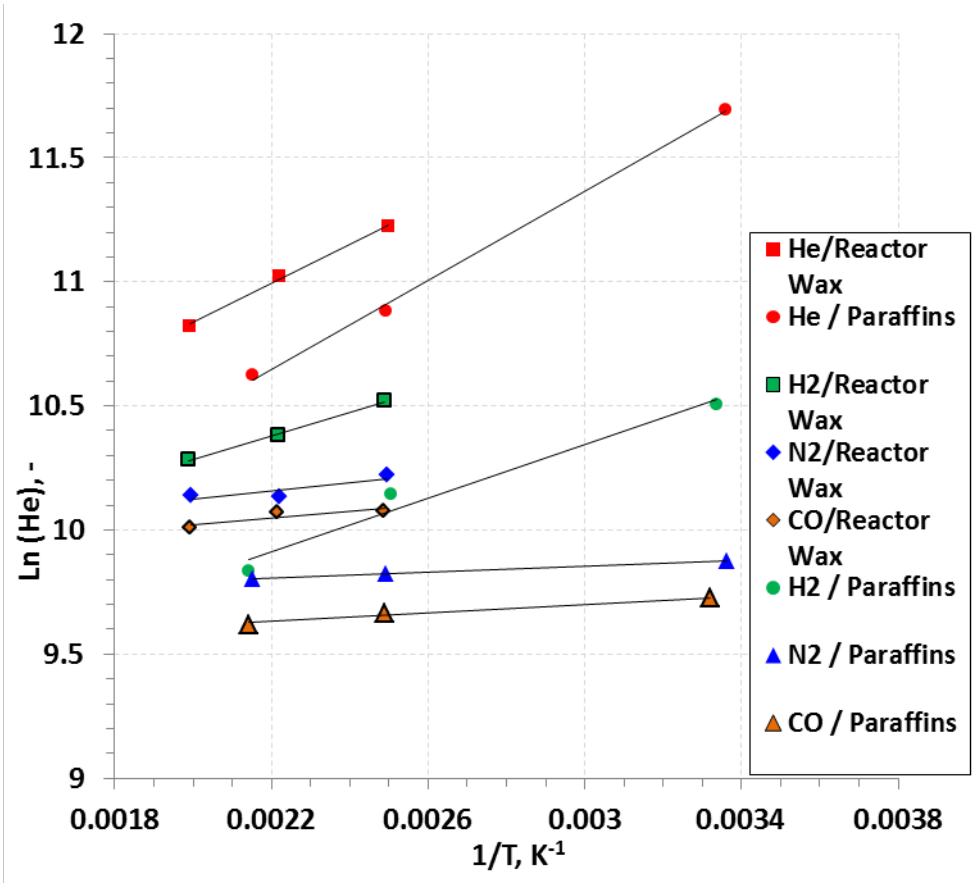

Figure 7.5: Effect of temperature on Henry's Law constant

7.1.3 Effect of solid concentration on *C**

Under the operating conditions used, solid concentration in the liquid phase had no effect on the equilibrium solubility of N_2, He, H_2 and CO. This is in agreement with other numerous investigations as presented in Table 3.1.

7.1.4 Effect of gas nature on *C**

The effect of gas nature on the equilibrium solubility is shown in Figures 7.6 and 7.7 for the paraffins mixture and the reactor wax, respectively. As can be seen, the solubility values follow the order: $C^*_{CO} > C^*_{N2} > C^*_{H2} > C^*_{He}$ in the paraffins mixture and the reactor wax under similar operating conditions. This behavior can be explained using the solubility parameter (δ) concept developed by Hildebrand [72]. The solubility parameters can be calculated from the molar heat of vaporization data using Equation (7-3) as follows:

$$\delta = \sqrt{\frac{H_v - RT}{v}} \tag{7-3}$$

Where H_v is the molar heat of vaporization and v is the molar volume.

The solubility parameters for the paraffins mixture and the reactor wax were estimated from Equation (7-3), by calculating the corresponding Hv and v values using the asymptotic behavior correlations from Marano et al. [67]. Table 7.2 shows the calculated solubility parameters for the gases and liquids used in addition to those of other selected normal hydrocarbons.

Using the calculated solubility parameter values, the solubility expressed as a mole fraction (x_1) can be formulated with the following equation:

$$x_1 \propto \exp\left(-\frac{v_1^L * (\delta_1 - \delta_2)^2 * \phi_2^2}{RT}\right) \tag{7-4}$$

Where v_1^L is the molar volume of component 1 (gas) at temperature T; ϕ_2 is the volume fraction of component 2 (liquid); and δ_1 and δ_2 are the solubility parameters of components 1 and 2 respectively.

According to Equation (7-4), a smaller difference between the solubility parameters of the gas and the liquid phases should result in a higher solubility value. Thus, the values of the solubility parameters listed in Table 7.2 can be used to explain the observed behavior of the solubility of the gases used in the paraffins mixture and the reactor wax.

Table 7.2: Solubility parameters of selected compounds

Component	δ, $(J/m^3)^{0.5}$
He	1222
H_2	6648
N_2	10800
CO	11700
n-C_8H_{18}	15300
n-$C_{16}H_{34}$	16300
C_{12}-C_{13} Paraffins mixture	16123
Reactor wax	16789

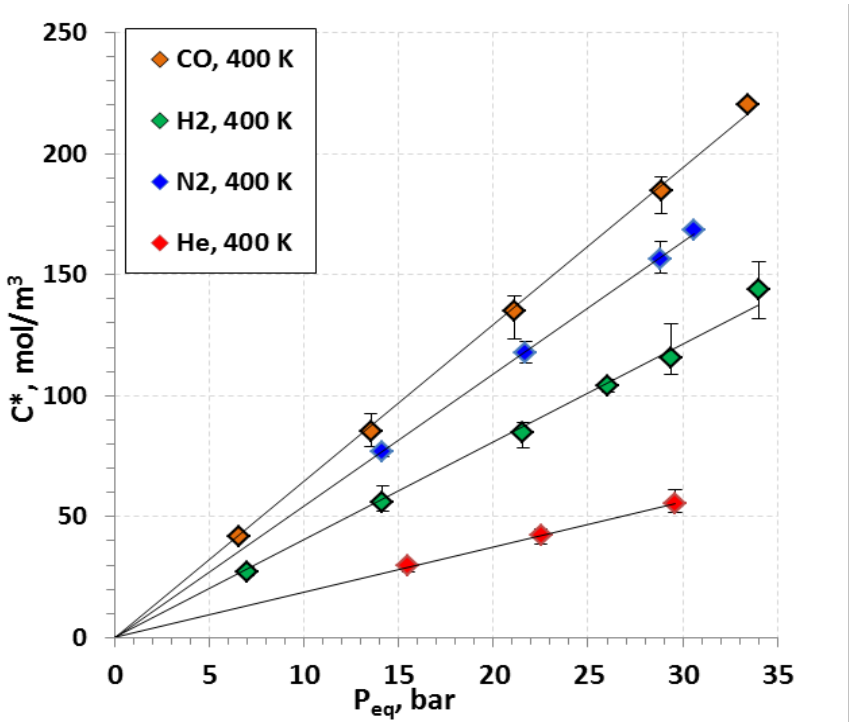

Figure 7.6: Effect of gas nature on *C** of H_2, CO, He and N_2 in the C_{12}-C_{13} paraffins mixture

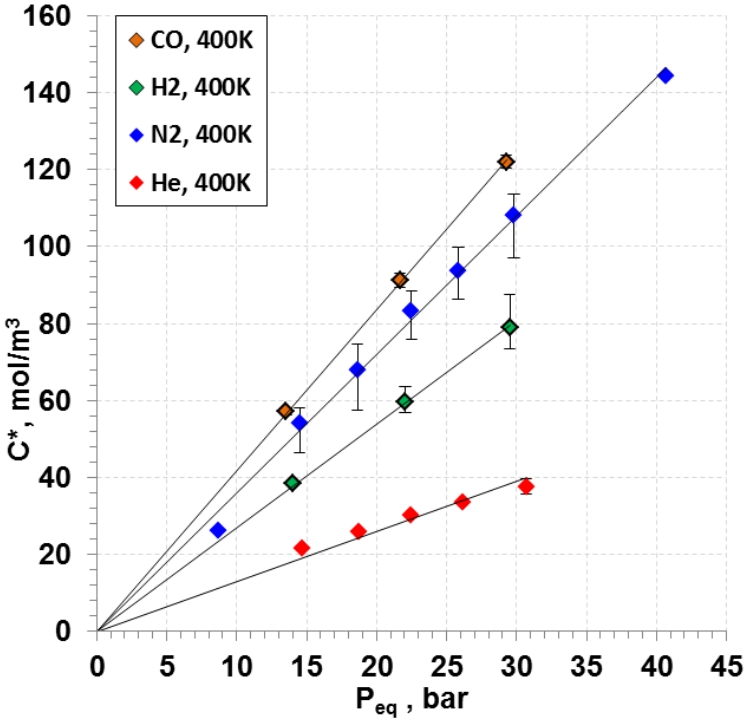

Figure 7.7: Effect of gas nature on *C** of H_2, CO, He and N_2 in the reactor wax

7.1.5 Effect of liquid nature on C^*

The effect of liquid nature on C^* can also be pointed out by comparing Figures 7.6 and 7.7 for the paraffins mixture and the reactor wax, respectively. As can be observed the solubility values decrease with increasing the molecular weight of the hydrocarbons used. Since the liquids studied are mixtures of paraffins, the exact effect of carbon number is not obvious; however, its effect can be evaluated qualitatively. Under the conditions studied it was found that the solubilities of the four gases followed the order: $C^*_{\text{paraffins mixture}} > C^*_{\text{reactor wax}}$. This implies that with increasing chain length of the paraffins, the solubility of the gas decreases. Similar behavior was reported by other investigators for comparable gas-liquid systems [17-19].

7.2 MASS TRANSFER COEFFICIENTS, (k_La)

The volumetric liquid-side mass transfer coefficients of 4 gases (N_2, He, H_2 and CO) as pure gases and in gaseous mixtures of various compositions were measured in the (C_{12}-C_{13}) paraffins mixture and in the Sasol reactor wax in the temperature range of 300-500 K, pressure range of 4-45 bar, mixing speed of 800-1400 RPM, and the Puralox alumina particles concentration of 0-20 vol%. The data obtained are discussed in the following sections. The error analysis on k_La along with some numerical examples are provided in Appendix A

7.2.1 Effect of solid concentration on the overall k_La

Figure 7.8 shows the effect of the presence of Puralox alumina particles in the paraffins mixture on the k_La values of N_2 and He each as a single-gas at 400 K and 1100 RPM. As can be seen the presence of particles increased k_La values of N_2 and decreased the k_La values of He. Low concentrations of small solid particle could increase the mass transfer by the shuttle or grazing effect according to Kluytmans [61] who mentioned that small solid particles adsorb gas from the gas-liquid diffusion layer and desorbs it into the liquid bulk, increasing as such the mass transfer

rate. Also, low solid concentrations could create turbulences at the gas-liquid interface which decrease the effective diffusion layer and increase the mass transfer coefficient k_L and subsequently $k_L a$. High concentrations of small particles, on the other hand, increase the slurry viscosity which decreases the gas diffusivity and subsequently k_L. Also, the increase of slurry viscosity promotes gas bubbles coalescence and decreases the gas-liquid interfacial area, a. At concentration of 5 vol% which is relatively small, the increase of $k_L a$ values of N_2 is in agreement with what was previously reported in the literature. Also, the decrease of $k_L a$ values of He is not necessarily in disagreement with previous findings as the concentration of 5 vol% used in the experiments might lie within the range of concentrations where the presence of solids could decrease the rate of mass transfer. Following this reasoning, it appears that this range is shifted towards higher concentrations when using denser gas (N_2).

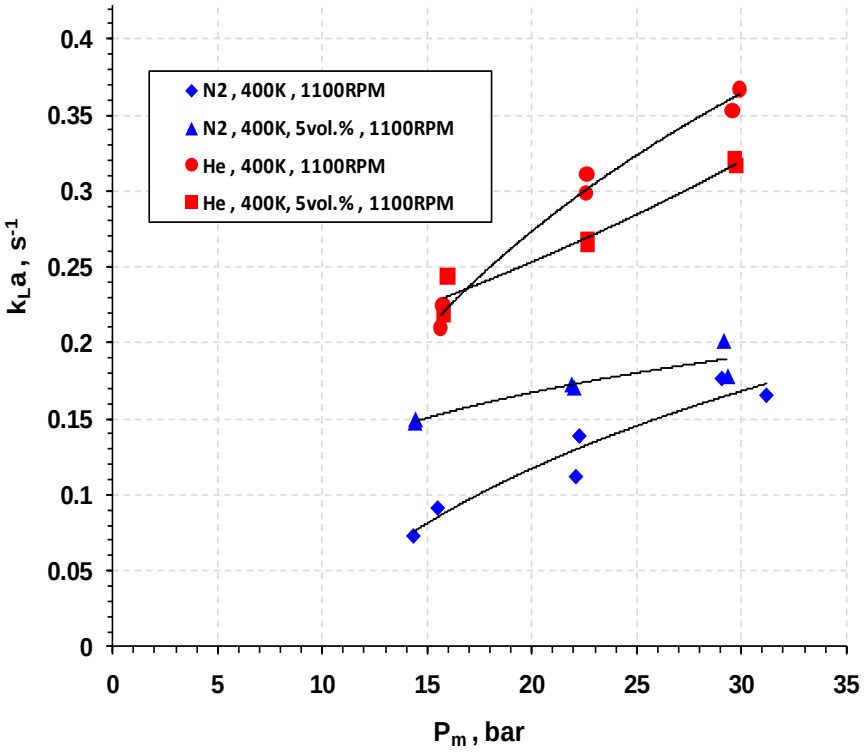

Figure 7.8 Effect of solid concentration on $k_L a$ of He and N_2 in the paraffins mixture

Figure 7.9 shows the effect of higher solid concentrations (> 5 vol%) up to 20 vol% on $k_L a$ values for He and N_2 in the paraffins mixture. Under the conditions investigated, increasing solid

concentration is found to decrease the overall volumetric mass transfer coefficient when using a gas mixture as shown in Figure 7.9. This is similar to the behavior of He discussed above, although no enhancement in the volumetric mass transfer coefficient values as in the case of N_2 as a single gas can be seen. Also, the effect of solid concentration appears stronger at high pressure. It is important to note that the effect of pressure (or gas density) appears to level off when increasing the solid concentration above 10 vol%. In the absence of solids, there is an increase in the overall k_La values of about 80 to 125% when increasing the total pressure from 15 to 30 bar, while this increase is reduced to about 25-55% and 15 % in the presence of 5 vol% solids and 10 vol% solids, respectively. Thus, it appears that the effect of the slurry viscosity, which promotes gas bubbles coalescence, on k_La is stronger than that of the gas density. At 463 K, Figures 7.10 and 7.11 show that at higher solid concentrations, i.e. 10, 15 and 20 vol%, k_La values for both He and N_2 as a single gas and as 50/50 mixture increase when the solid concentration is increased from 10 vol% to 15 vol% by an average of 13% for He and N_2 and by 18% for the gas mixture. However, upon further increase of solid concentration to 20 vol%, k_La values appeared to decrease by an average 4% for N_2, 12% for He and 16% for the mixture.

In the molten reactor wax, the effect of solid concentration on k_La was investigated up to 20 vol% for the four gases (He, N_2, H_2 and CO) at 500 K, 1100 RPM, as illustrated in Figures 7.12 and 7.13. As can be seen in these figures, k_La values decrease by an average of 23% for He and 50% for N_2 when the solid concentration is increased from 5 to 20 vol%. The k_La values for H_2 and CO were also observed to be lower by an average of 28% and 16% respectively, when increasing solid loading from 5 to 20 vol%.

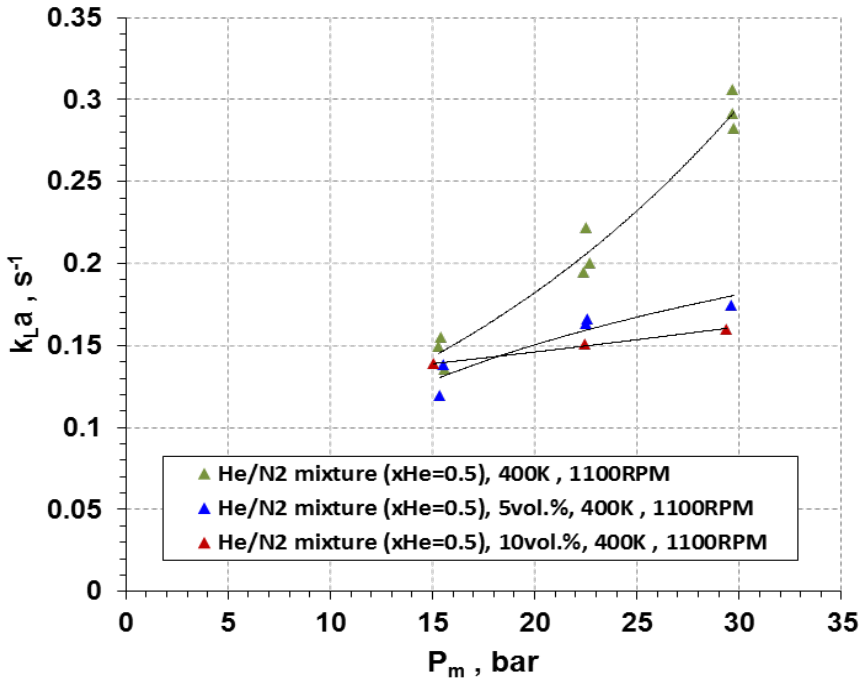

Figure 7.9 Effect of solid concentration on the overall k_La in the paraffins mixture (He/N_2=1)

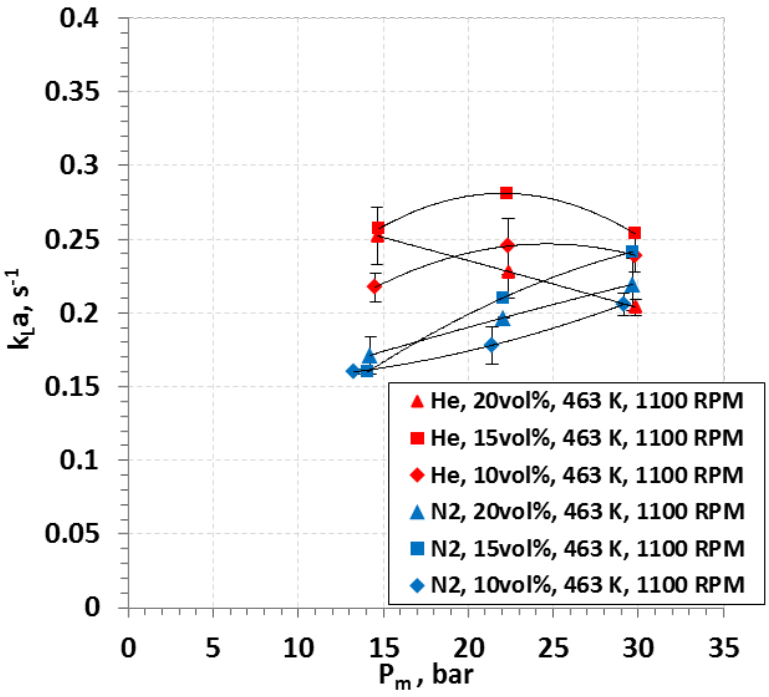

Figure 7.10: Effect of solid concentration on the overall k_La in the paraffins mixture (He and N_2)

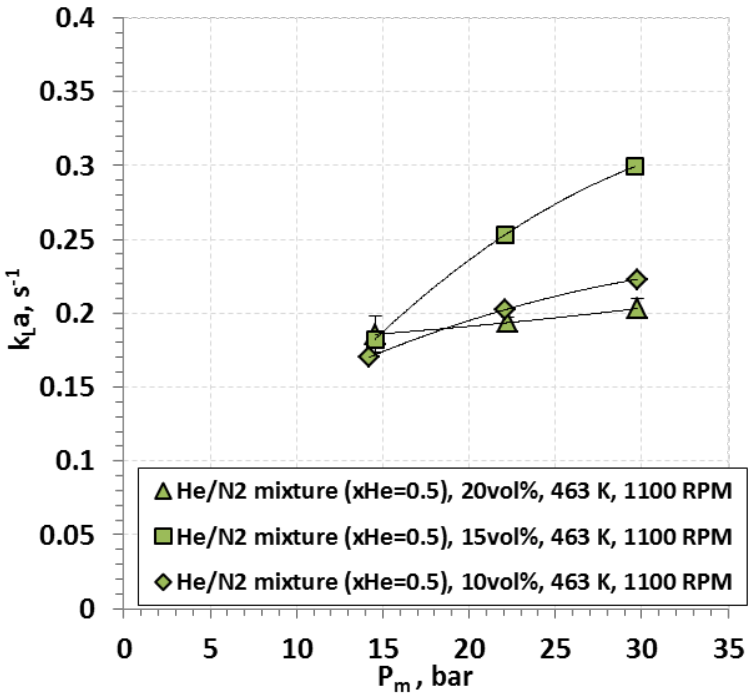

Figure 7.11: Effect of solid concentration on the overall k_La in the paraffins mixture (He/N_2=1)

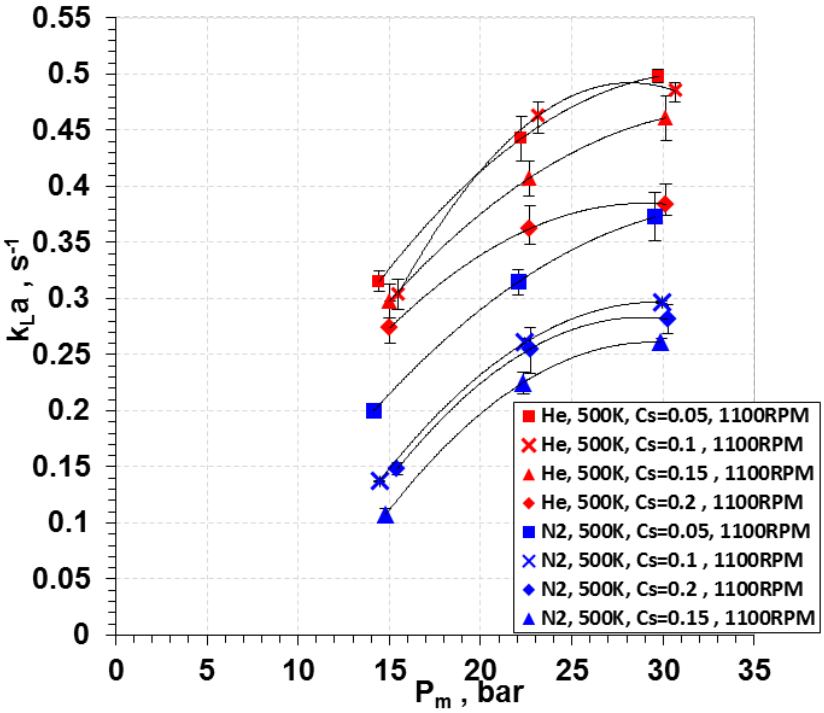

Figure 7.12: Effect of solid concentration on overall k_La in the reactor wax, (He and N_2)

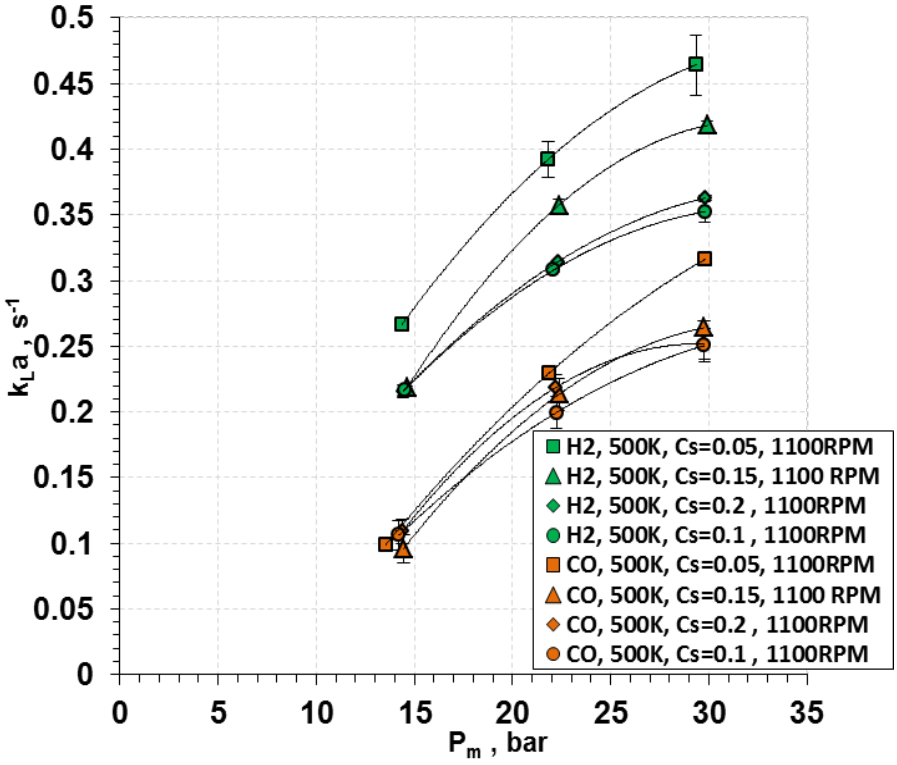

Figure 7.13: Effect of solid concentration on overall $k_L a$ in the reactor wax, (H_2 and CO)

7.2.2 Effect of pressure and gas density on $k_L a$

Figure 7.14 shows that increasing gas density by adding N_2 to He at 400 K in the absence of solid particles appeared to decrease the overall mass transfer coefficients for the mixtures. Indeed, N_2 which has higher density than He at the same conditions showed the lowest mass transfer coefficients as can be observed in this figure.

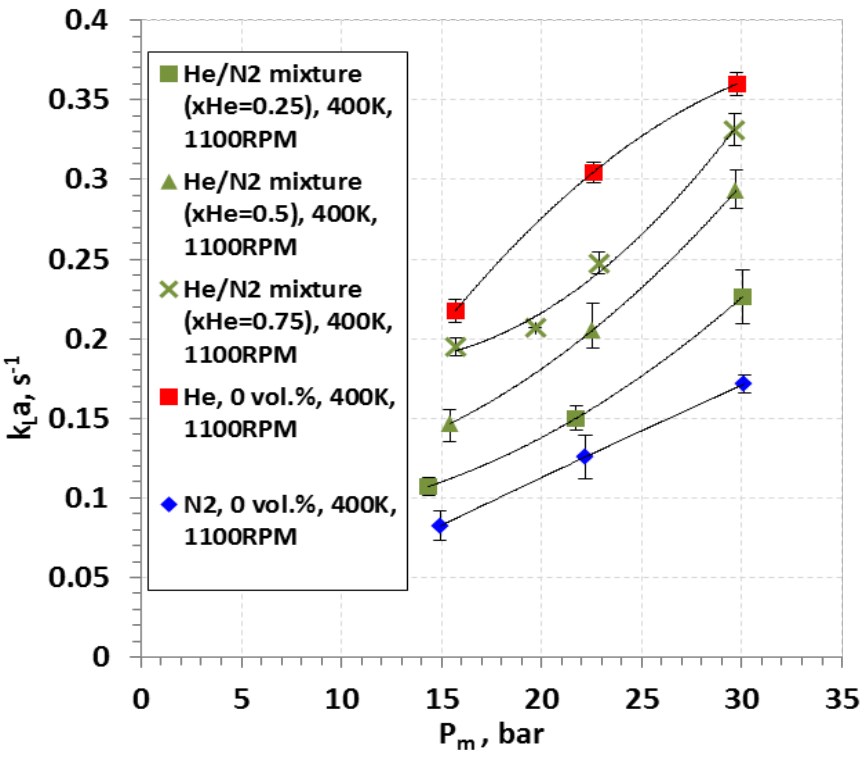

Figure 7.14: Effect of pressure (density) on the overall k_La in the paraffins mixture

The effect of pressure on k_La of He, N_2, H_2 and CO as single gases and in various mixtures of He/N_2 and H_2/CO in the molten reactor wax was investigated under the following conditions: T = 500 K, C_s = 5-20 vol%, P =15-30 bar; and the experimental results with C_s = 20 vol% are presented in Figures 7.15 and 7.16. As can be seen in both figures, the pressure has a strong effect on k_La of the four gases including the mixtures (y_{He}=0.25, 0.5, 0.75) and (y_{H_2} =0.25, 0.5, 0.75). The k_La values appeared to level off at about 27 bars. CO and N_2 appeared to behave similarly and seemed to have the smallest mass transfer coefficients, while He and H_2 appeared to be in a good agreement and had the greatest values within the pressure range investigated at 500 K. Also, as can be seen the gradual decrease of the gas density by diluting the CO or N_2 with H_2 or He, respectively, leads to a systematic increase of the overall mass transfer coefficients of the corresponding gaseous mixtures.

This effect can be attributed to the alteration of the physico-chemical properties of the gas-liquid system with increasing pressure. Increasing pressure increases the gas solubility, which decreases both liquid viscosity and liquid surface tension. Decreasing liquid viscosity

increases the gas diffusivity into the liquid-phase and subsequently k_L since the k_L is directly proportional to the gas diffusivity (D_{AB}) to the power 0.5 (penetration theory) or the power 1 (two-film theory). Also, the decrease of surface tension with increasing pressure decreases the gas bubble size [69, 73] which in turn increases the gas-liquid interfacial area, a. Thus, both k_L as well as a, and subsequently $k_L a$ are expected to increase with rising pressure.

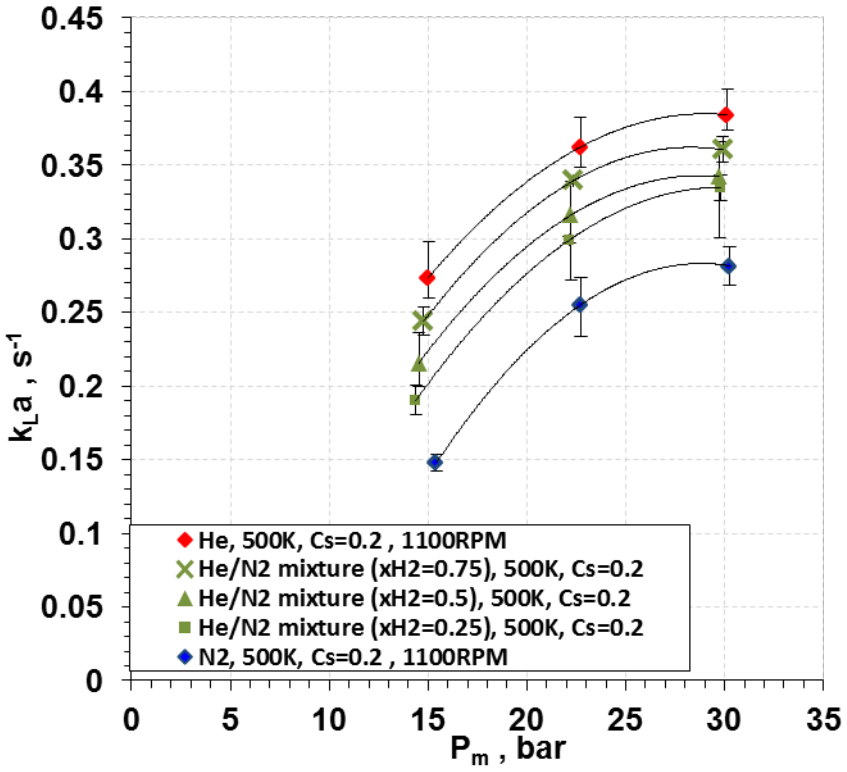

Figure 7.15: Effect of pressure on overall $k_L a$ of He and N_2 in the molten reactor wax

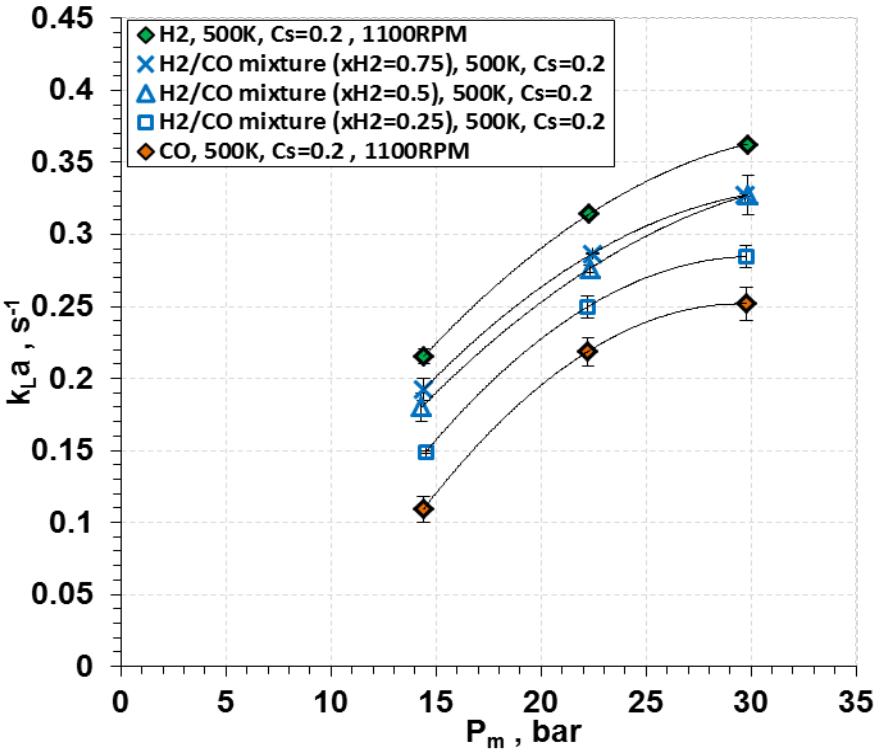

Figure 7.16: Effect of pressure on overall k_La of H_2 and CO in the molten reactor wax

7.2.3 Effect of composition and gas nature on k_La

In the paraffins mixture, the effect of gas nature and composition on the overall k_La values of He and N_2 can be seen in Figure 7.14. Also, in the reactor wax, the effects of gas nature and composition on the overall k_La are represented in Figure 7.15 for N_2 and He and in Figure 7.16 for and H_2, CO. The k_La values of He and H_2 as a single-gas were found to be greater than those of N_2 and CO respectively, under similar operating conditions in the (C_{12}-C_{13}) paraffins mixture and in the reactor wax. This is in agreement with previous findings where k_La values were found to follow the diffusivity/molecular weight. Also, it can be seen that k_La values of the gaseous mixture lie between the values obtained for N_2 and He or H_2 and CO as single gases. Moreover, changing the gas composition towards higher concentration of He or H_2 brings k_La values of the associated mixture closer to those of He or H_2 and vice-versa with N_2 and CO. Thus, the overall k_La values appear to follow the molecular weight of the gas mixture.

7.2.4 Effect of temperature on k_La and the mass transfer ratio

The effect of temperature on k_La of N_2 and He each as a single gas or gas mixture of He/N_2 =1 in the (C_{12}-C_{13}) paraffins liquid mixture is presented in Figures 7.17 and 7.18. As can be observed, increasing temperature resulted in an increase of the k_La values for both He and N_2 as single gases and as 50/50 mixture. Similarly, the k_La of H_2 and CO were found to be affected by the change in temperature as shown in Figure 7.17. An average of 37% increase in k_La of H_2 and an average of 428% rise in k_La of CO when increasing temperature from 300 K to 463 K can be noted. This behavior is in agreement with available literature data for comparable gas-liquid systems [19, 20, 45].

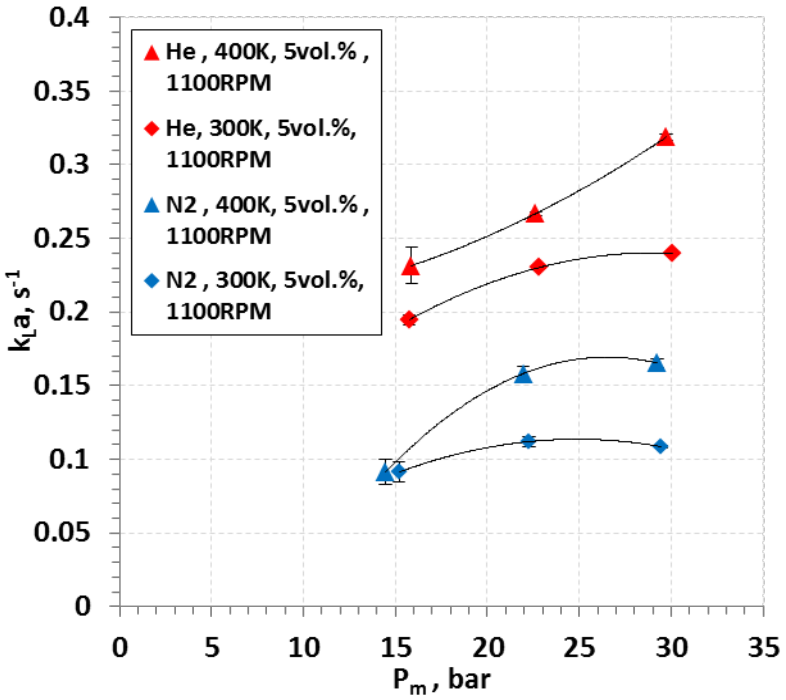

Figure 7.17: Effect of temperature on the volumetric mass transfer coefficient of He and N_2 in the paraffins mixture (C_S = 5 vol%)

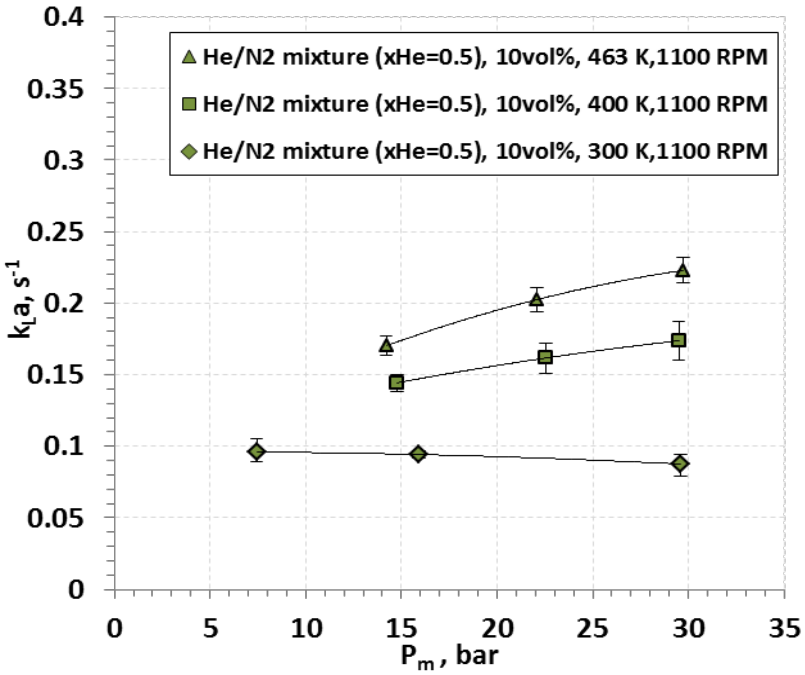

Figure 7.18: Effect of temperature on volumetric mass transfer coefficient of He/N_2=1 in the paraffins mixture (C_S = 10 vol%)

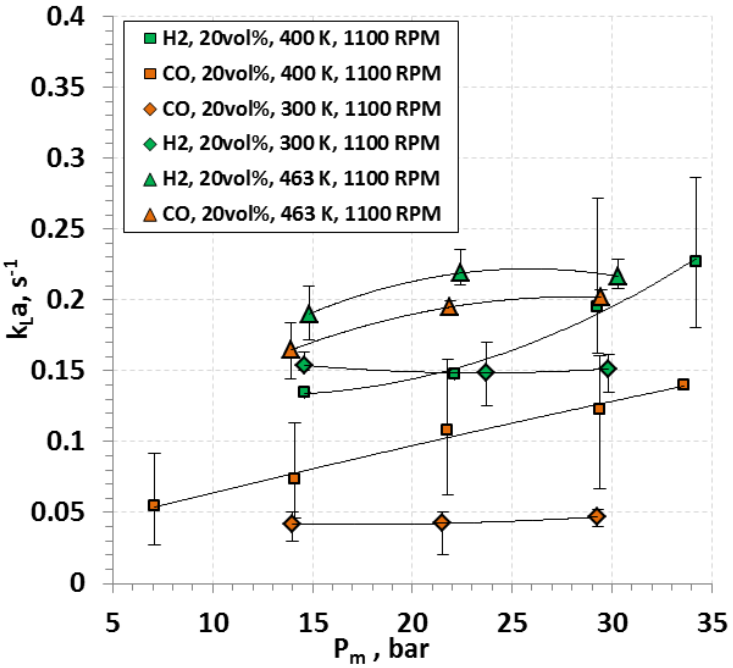

Figure 7.19: Effect of temperature, (gas nature) on volumetric mass transfer coefficient of H_2 and CO in the paraffins mixture (C_S = 20 vol%)

The effect of temperature on the overall and individual mass transfer coefficients of a gas mixture containing 50% He in the paraffins liquid mixture was studied at up to 463 K in the presence of 10 vol% solids. The overall k_La, as well as the individual k_La of He and N_2 at a constant gas density of 9.7 kg/m^3 are plotted as functions of temperature in Figure 7.20 and as can be seen, k_La values increase with increasing temperature from 300 to 400 K and the overall k_La values appear to level off after 400 K. This behavior can be attributed to the decrease of both viscosity and surface tension of the liquid-phase which led to higher diffusivity, and therefore k_L values, as well as large gas-liquid interfacial area. It should be noted that in the case of He in the gas mixture, its k_La values are only slightly affected by the temperature when compared with that of N_2 whose values increase about 50% from 300 to 400 K. This resulted in the decrease of the ratio of the mass transfer coefficient of He to that of N_2 with increasing temperature from 2.24 to about 1.51 as can be seen in Figure 7.21. The ratio of the square root of the diffusivities of He to that of N_2 as predicted by the correlation by Erkey et al [74] is also shown in the same figure and decrease from 1.66 to about 1.59. This decrease of the mass transfer coefficient ratio with increasing temperature from 300 to 400 K suggests that the data obtained at 300 K could have probably inherited some experimental errors due to possible plugging of the holes with solid particles on the agitated shaft during k_La measurements.

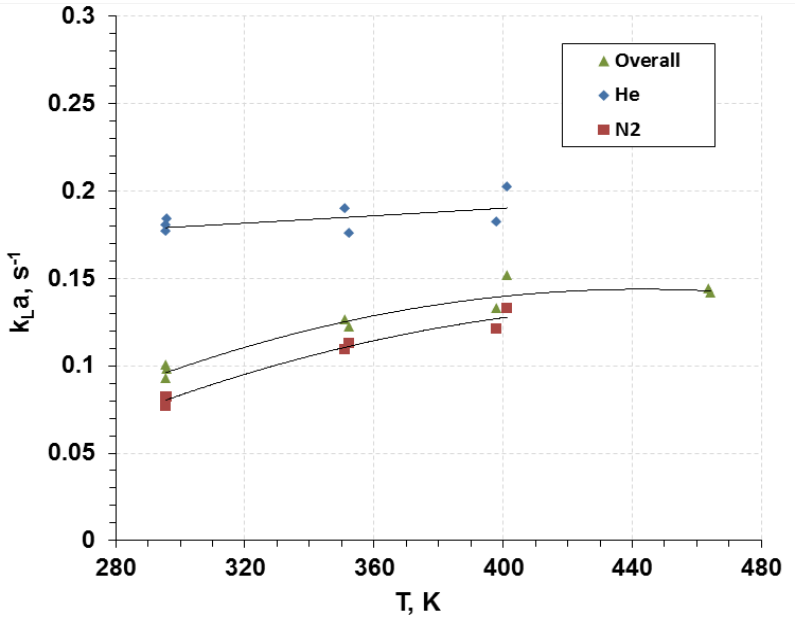

Figure 7.20: Effect of temperature on $k_L a$ in the paraffins mixture (He/N_2 gas mixture ($xHe = 0.5$); ρ_G=9.7 kg/m^3; C_S = 10 vol%; N = 1100 RPM)

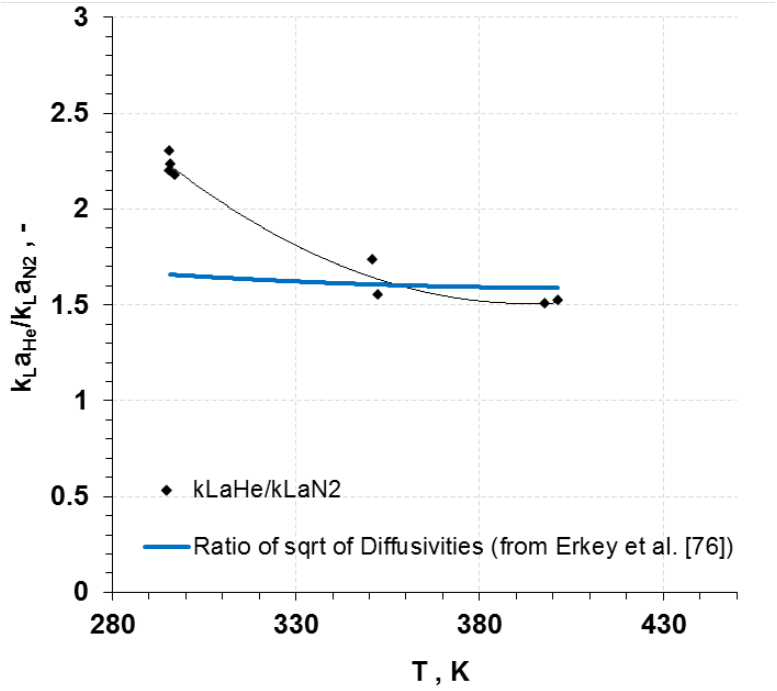

Figure 7.21: Effect of temperature on the ratio of the mass transfer coefficients in the paraffins mixture (He/N_2 gas mix ture ($x_{He} = 0.5$); ρ_G=9.7 kg/m^3; C_S = 10 vol%; N = 1100 RPM)

The effect of temperature on k_La of N_2 and He each as single gas in the reactor wax with no solid particles was investigated at up to 500 K and presented in Figures 7.22 and 7.23, respectively. As can be observed, increasing temperature considerably increases the k_La values for both gases.

The volumetric mass transfer coefficients of H_2 and CO in the reactor wax with solid concentration of 20 vol% are presented in Figure 7.24. Under these conditions, increasing temperature from 400 to 500 K resulted in about 21% increase of k_La for CO, whereas the increase is only about 10% for H_2.

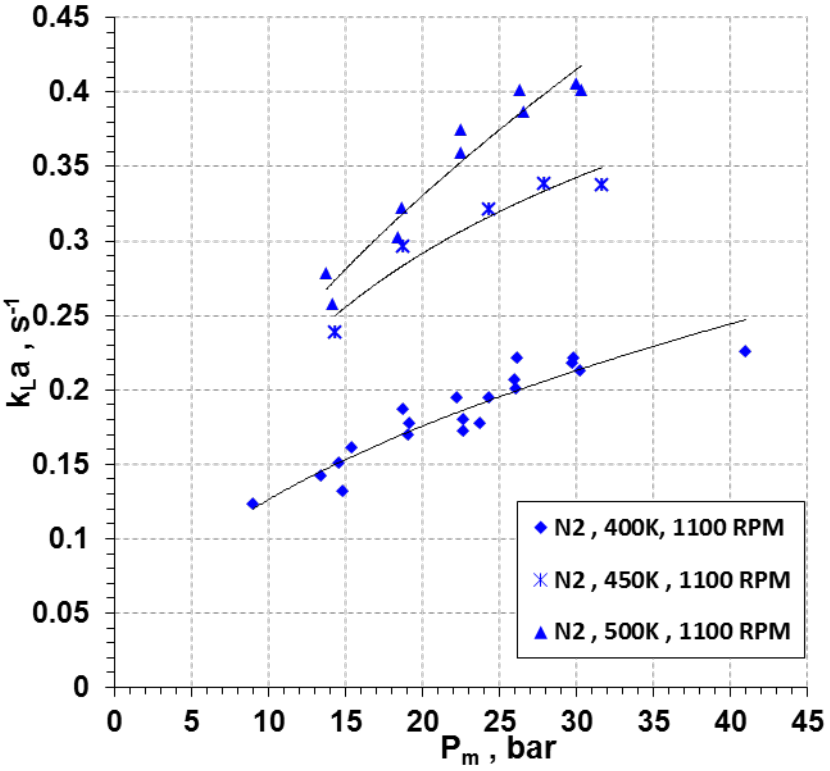

Figure 7.22: Effect of temperature on k_La of N_2 in the reactor wax

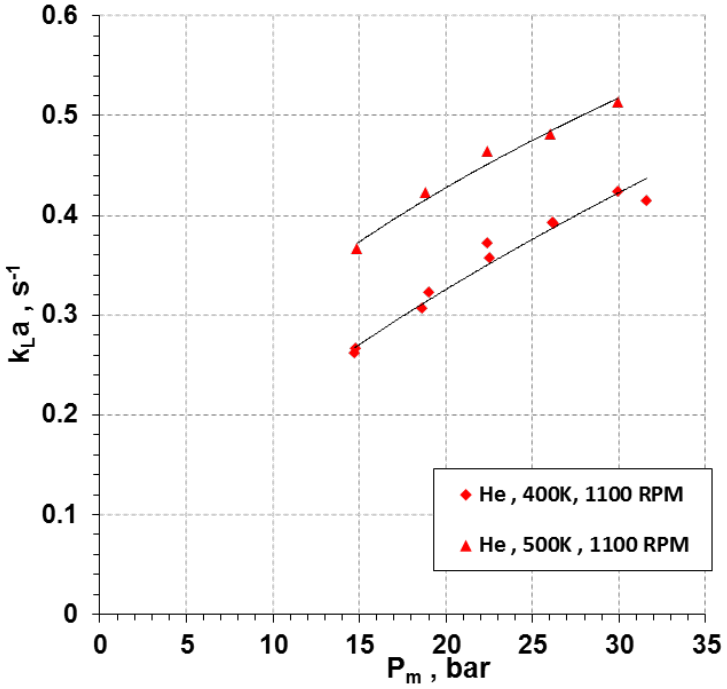

Figure 7.23: Effect of temperature on $k_L a$ of He in the reactor wax

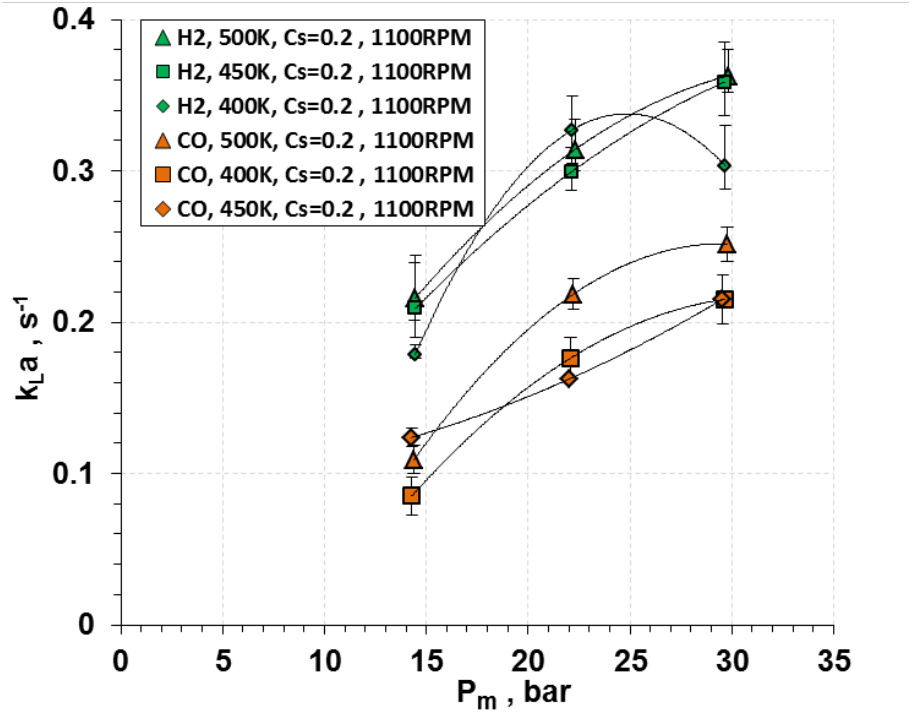

Figure 7.24: Effect of temperature on the volumetric mass transfer coefficient of H_2 and CO in the reactor wax; (C_S = 20 vol%)

7.2.5 Effect of mixing speed on k_La

Figure 7.25 shows the effect of mixing speed on the volumetric liquid-side mass transfer coefficient at 400 K, for N_2 as a single-gas in the reactor wax. As can be seen in this figure, increasing mixing speed strongly increases the volumetric liquid-side mass transfer coefficient, k_La, which is in agreement with numerous investigations [17, 19, 34, 35, 69]. The increase of the volumetric liquid-side mass transfer coefficient with mixing speed can be attributed to the increase of the liquid-side mass transfer coefficient k_L and/or the gas-liquid interfacial area, a. Increasing mixing speed increases the turbulence and shear rate in the reactor [39, 75], which reduces the gas-liquid film thickness Δ, leading to the increase of the mass transfer coefficient; hence, $k_L = D_{AB}/\Delta$. Also, increasing mixing speed increases the pumping capacity of the impeller, and, consequently, more gas bubbles are induced into the liquid through the hollow shaft, which increase the gas holdup. The increase of the number of gas bubbles in the reactor could lead to a slight increase of the Sauter-mean bubble diameter due to bubble coalescence. An increase of the gas holdup could lead to an increase of the gas-liquid interfacial area and, hence, to a small increase of the Sauter-mean bubble diameter. Since Calderbank and Moo-Young [76] reported that k_L is directly proportional to d_S, k_L increase with mixing speed. Thus, the combined effects of increasing mixing speed on the mass transfer coefficient and the gas-liquid interfacial area led to the increase of k_La values as shown in Figure 7.25.

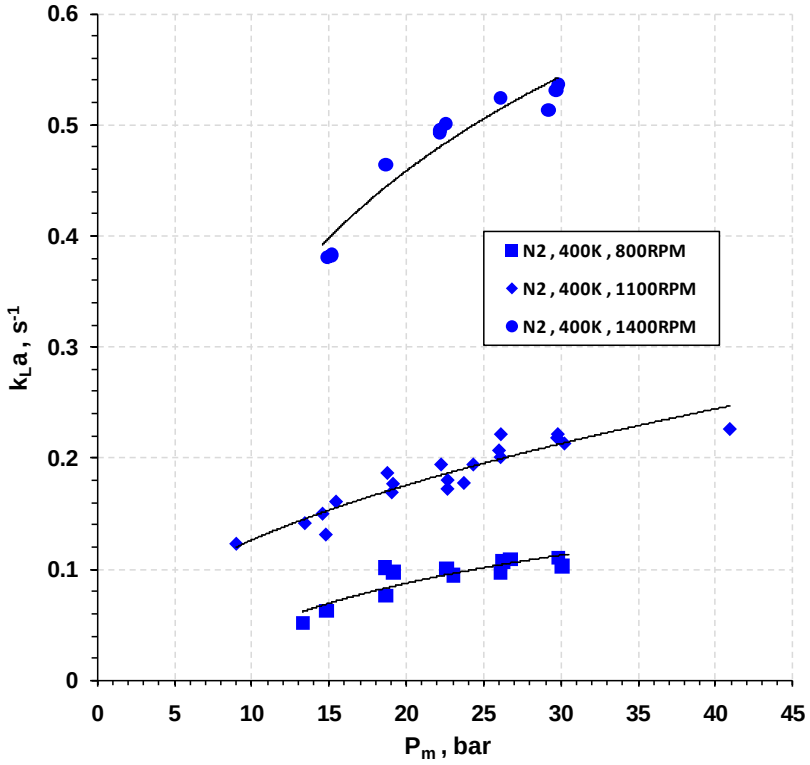

Figure 7.25: Effect of mixing speed on k_La of N_2 in the reactor wax

7.2.6 Effect of liquid nature on k_La

The effect of the liquid nature on the k_La values of N_2, He and H_2, CO is shown in Figures 7.26 and 7.27. Considering the lower viscosity and surface tension of the paraffins mixture as compared with those of the reactor wax, k_La values could be expected to be greater when using paraffins mixture as the liquid-phase. As can be seen in Figures 7.26 and 7.27, however, the mass transfer coefficients for the four gases (He, N_2, H_2 and CO) in the more viscous reactor wax are greater than those in the lower viscosity paraffins mixture. This behavior can be related to the presence of foam in the agitated reactor in the case of the reactor wax, while no froth whatsoever was observed when using the paraffin mixture. The froth appeared to increase the gas-liquid interfacial area (a) and subsequently k_La values for both gases in the reactor wax.

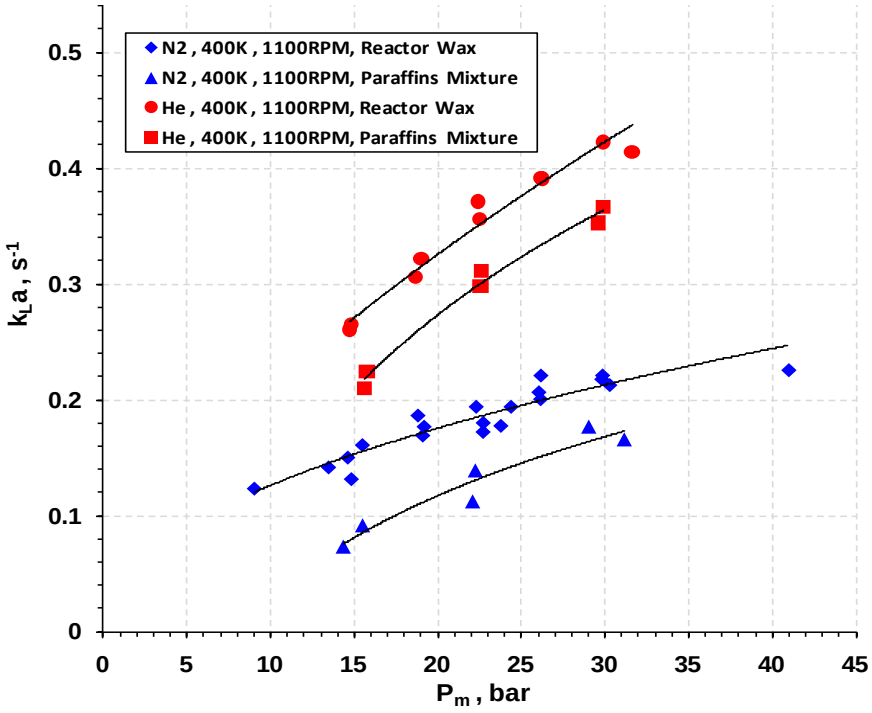

Figure 7.26: Effect of liquid nature on k_La of He and N_2 in the paraffins mixture

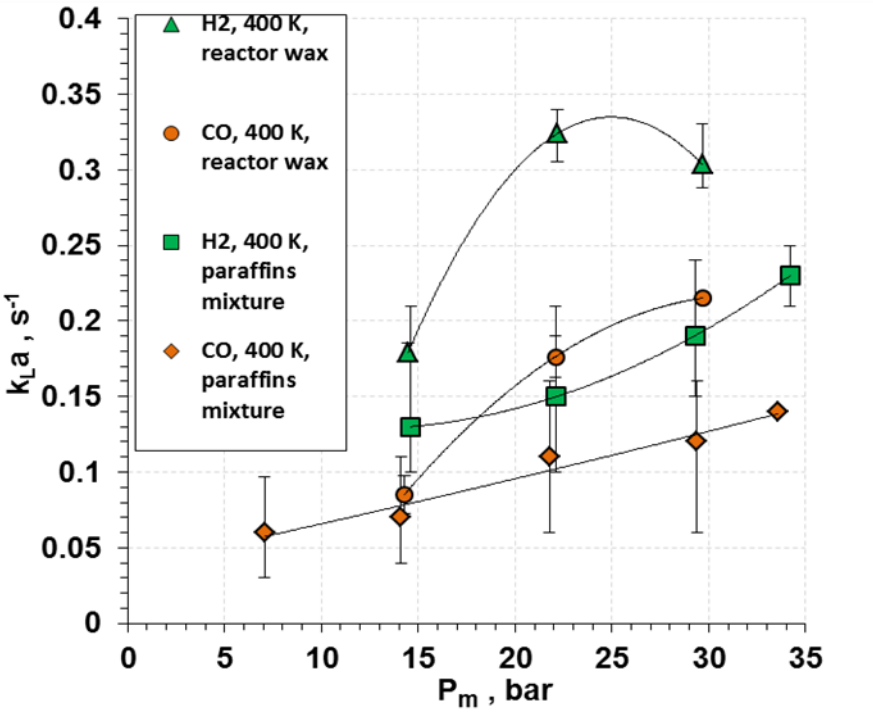

Figure 7.27: Effect of liquid nature on k_La of H_2 and CO in the reactor wax

7.2.7 Relationship between overall and individual mass transfer coefficients

For each experiment with a gas mixture, 3 volumetric mass transfer coefficients can be obtained from the 3 P-t curves: one for the overall gas (k_La), and one for each of the individual components in the gas mixture when using the Mass Spectrometer. He (k_La_{He}), N_2 (k_La_{N2}), are the components investigated in this study. Since the total amount of gas absorbed is the sum of those of each gas, the following relationship can be written:

$$-\frac{dn_G}{dt} = k_La(C^* - C_L)V_L = -\frac{dn_{G,He}}{dt} - \frac{dn_{G,N2}}{dt} = k_La_{He}(C^*_{He} - C_{L,He})V_L + k_La_{N2}(C^*_{N2} - C_{L,N2})V_L \quad (7\text{-}5)$$

Expressing the overall k_La as a function of the individual k_La:

$$k_La = \frac{k_La_{He}(C^*_{He} - C_{L,He}) + k_La_{N2}(C^*_{N2} - C_{L,N2})}{(C^* - C_L)} \quad (7\text{-}6)$$

Since at the beginning of the absorption $C_L = 0$ and $C^* = C^*_{He} + C^*_{N2}$, Equation (7-6) can be rearranged into:

$$k_La = \frac{k_La_{He}C^*_{He} + k_La_{N2}C^*_{N2}}{C^*_{He} + C^*_{N2}} \quad (7\text{-}7)$$

Using the solubility data obtained and the correlations presented in the sections 6.3.1 and 6.3.2. Equation (7-7) can be used as a mean to check the different experimental mass transfer coefficients obtained. Figure 7.28 shows the overall k_La values obtained from Equation (7-7) versus the measured overall k_La values, and as can be seen there is a good agreement between them.

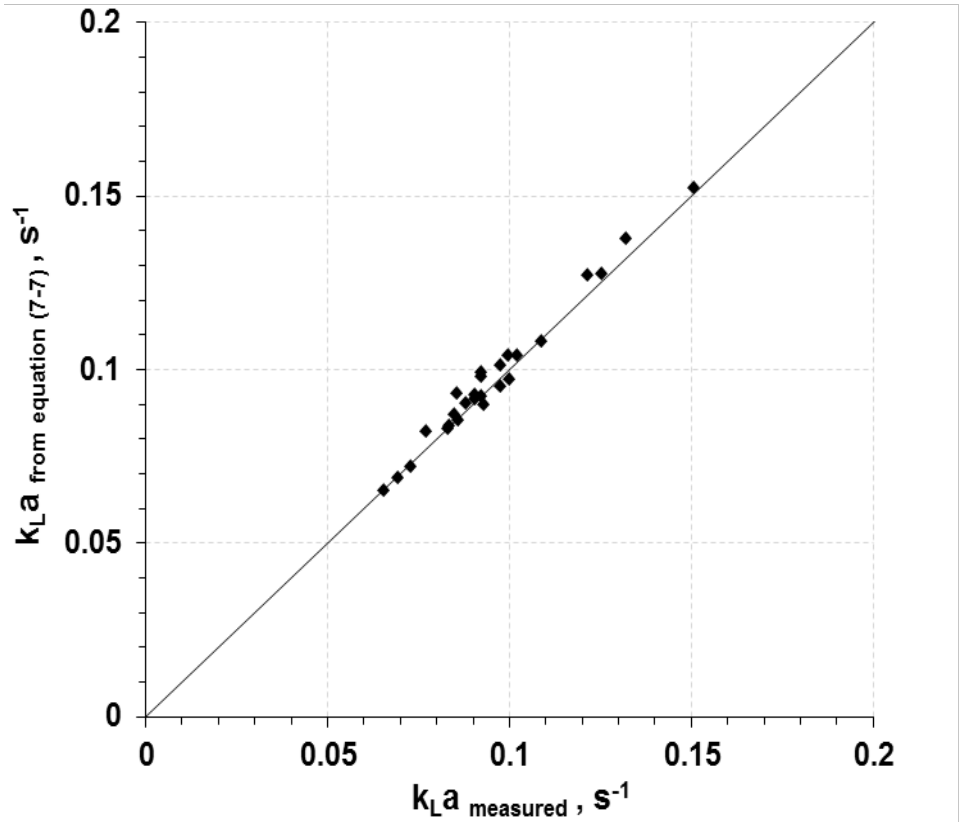

Figure 7.28: Overall k_La obtained from equation (7-7) versus overall k_La measured (He/N_2 gas mixture; C_S=10 vol%; N=1100 RPM)

The importance of Equation (7-7) resides in the fact that the mass transfer coefficient for each component in a gas mixture containing two-components can be calculated. As a matter of fact, this new relationship is a major finding of this research project.

8.0 CONCLUSIONS

The equilibrium solubility (C^*) and volumetric liquid-side mass transfer coefficient, (k_La) for four different gases (He, CO, N_2 and H_2) in two different liquids (C_{12}-C_{13} paraffins mixture and Sasol reactor wax) were measured in a 4-liter agitated reactor operating in a gas-inducing mode under typical conditions of Fischer-Tropsch synthesis. The effects of operating variables, including pressure (4-45 bars), temperature (300 – 500 K), mixing speed (800-1400 RPM), and Puralox alumina particles (mimicking F-T catalyst) concentration (0 - 20 vol%) on k_La and C^* values were investigated. At a given set of operating variables, the transient physical gas absorption technique was used to obtain k_La from the transient behavior and C^* at thermodynamic equilibrium. From the experimental data obtained the following conclusions can be derived:

- The C^* values for the four gases in the two liquids were found to linearly increase with the solute gas partial pressure at constant temperature and the data were modeled using Henry's Law. The effect of temperature on C^* was described using an Arrhenius-type equation, where the apparent activation energy of gas absorption was found to be dependent on temperature.
- The solubility values of the four gases in the two liquids followed the order: $C^*_{CO} > C^*_{N2} > C^*_{H2} > C^*_{He}$ which is in agreement with the behavior of the solubility parameters for the components used. Also, under similar pressure and temperature, C^* values of the four gases in the C_{12}-C_{13} paraffins liquid mixture were greater than those in the Sasol reactor wax. This behavior was attributed to the significant differences in hydrocarbon chain lengths of two liquids.

- The k_La values of the four gases in the two liquids were found to increase with increasing mixing speed, temperature and pressure. The increase of k_La values was greater from 15 to 23 bar than from 23 to 30 bar.
- The k_La values of the four gases in the paraffins mixture as well as in the Sasol reactor wax were observed to decrease with increasing solid concentration from 0 to 20 vol%.
- Under similar operating conditions, comparable k_La values were observed for N_2 and CO, whereas the values for H_2 were slightly different from those of He due to the difference between their molecular weights as well as diffusivities and solubilities in the two liquids.
- Under similar operating conditions, k_La values for the four gases were found to be higher in the reactor wax than those in the C_{12}-C_{13} paraffins mixture. This behavior was related to the greater interfacial area created by the observed steady froth with the reactor wax while no froth was observed with the paraffins mixture.
- A new empirical relationship for calculating the individual mass transfer coefficient of any component in a gaseous mixture knowing its overall mass transfer coefficients is proposed. This relationship is very important for the determination of the H_2 and CO mass transfer coefficients in the syngas using an adequate correlation for predicting the overall mass transfer coefficient under typical F-T operating conditions. This, of course, requires the knowledge of the diffusivity and the solubility of CO and H_2 at reactor conditions which can be measured or predicted using available software packages.

APPENDIX A

ERROR ANALYSIS AND SAMPLE CALCULATIONS

Following the procedure proposed by Lemoine [69] error analysis was made.

Let x_i be the i-th independent variable to be considered and Δx_i is the error in x_i.

Let F be a function of those independent variables: $F=f(x_1, x_2,\ldots, x_i,\ldots, x_n)$

The differential of this function can be calculated as follows:

$$dF = \sum_{i=1}^{n} \left.\frac{\partial F}{\partial x_i}\right|_{x_{j\neq i}} dx_i \qquad \text{(A-1)}$$

The error can then be estimated as:

$$\Delta F = \sum_{i=1}^{n} \left| \left.\frac{\partial F}{\partial x_i}\right|_{x_{j\neq i}} \right| \Delta x_i \qquad \text{(A-2)}$$

Therefore, expressions of the errors for the different measured parameters can be derived in the following manner:

Solubility, C^*:

The solubility is calculated using the following equation:

$$C_i^* = \frac{N_{i,I} - N_{i,F}}{V_L} \qquad \text{(A-3)}$$

$N_{i,I}$ and $N_{i,F}$ are calculated from:

$$N_{i,I} = \frac{P_{i,I} V_G}{R T_{r,I}} \qquad \text{(A-4)}$$

$$N_{i,F} = \frac{P_{i,F} V_G}{R T_{r,F}} \tag{A-5}$$

The initial average ($Tr,_I$) and final average ($Tr,_F$) temperatures are calculated as:

$$T_{r,I} = \frac{T_{I,gas} + T_{I,liq.}}{2} \tag{A-6}$$

$$T_{r,F} = \frac{T_{F,gas} + T_{F,liq.}}{2} \tag{A-7}$$

The gas-phase volume is estimated from:

$$V_G = V_r - \left(\frac{m_L}{\rho_L} + \frac{m_{cat.}}{\rho_{cat.}} \right) = V_r - V_L - V_{cat.} \tag{A-8}$$

Thus, the independent variables in the solubility, C^* are:

$$C^* = f(V_r, V_L, V_{cat.} P_{r,I}, T_{r,I}, P_{r,F}, T_{r,F}) \tag{A-9}$$

The error in the experimental solubility value can be estimated as:

$$\Delta C^* = \left|\frac{\partial C^*}{\partial P_{r,I}}\right| \Delta P_{r,I} + \left|\frac{\partial C^*}{\partial T_{r,I}}\right| \Delta T_{r,I} + \left|\frac{\partial C^*}{\partial P_{r,F}}\right| \Delta P_{r,F} + \left|\frac{\partial C^*}{\partial T_{r,F}}\right| \Delta T_{r,F} + \left|\frac{\partial C^*}{\partial V_r}\right| \Delta V_r + \left|\frac{\partial C^*}{\partial V_L}\right| \Delta V_L + \left|\frac{\partial C^*}{\partial V_{cat.}}\right| \Delta V_{cat.} \tag{A-10}$$

The needed partial derivatives are:

$$\frac{\partial C^*}{\partial P_{r,I}} = \frac{(V_r - V_L - V_{cat.})}{R V_L T_{r,I}} \tag{A-11}$$

$$\frac{\partial C^*}{\partial T_{r,I}} = -\frac{(V_r - V_L - V_{cat.}) P_{r,I}}{R V_L T_{r,I}^{\ 2}} \tag{A-12}$$

$$\frac{\partial C^*}{\partial P_{r,F}} = -\frac{(V_r - V_L - V_{cat.})}{R V_L T_{r,F}} \tag{A-13}$$

$$\frac{\partial C^*}{\partial T_{r,F}} = \frac{(V_r - V_L - V_{cat.}) P_{r,F}}{R V_L T_{r,F}^{\ 2}} \tag{A-14}$$

$$\frac{\partial C^*}{\partial V_r} = \frac{1}{R V_L} \cdot \left(\frac{P_{r,I}}{T_{r,I}} - \frac{P_{r,F}}{T_{r,F}} \right) \tag{A-15}$$

$$\frac{\partial C^*}{\partial V_L} = -\frac{V_r - V_{cat.}}{RV_L^{\,2}} \cdot \left(\frac{P_{r,I}}{T_{r,I}} - \frac{P_{r,F}}{T_{r,F}} \right) \tag{A-16}$$

$$\frac{\partial C^*}{\partial V_{cat.}} = -\frac{1}{RV_L} \cdot \left(\frac{P_{r,I}}{T_{r,I}} - \frac{P_{r,F}}{T_{r,F}} \right) \tag{A-17}$$

The volume of the liquid and catalyst phase in the reactor is given by:

$$V_L = \frac{m_L}{\rho_L} \tag{A-18}$$

$$V_{cat.} = \frac{m_{cat.}}{\rho_{cat.}} \tag{A-19}$$

The errors in the liquid and solid volumes are:

$$\Delta V_L = \left| \frac{\partial V_L}{\partial m_L} \right| \Delta m_L + \left| \frac{\partial V_L}{\partial \rho_L} \right| \Delta \rho_L \tag{A-20}$$

$$\Delta V_{cat.} = \left| \frac{\partial V_{cat.}}{\partial m_{cat.}} \right| \Delta m_{cat.} + \left| \frac{\partial V_{cat.}}{\partial \rho_{cat.}} \right| \Delta \rho_{cat.} \tag{A-21}$$

The required partial derivatives are:

$$\frac{\partial V_L}{\partial m_L} = \frac{1}{\rho_L} \Delta m_L \tag{A-22}$$

$$\frac{\partial V_L}{\partial \rho_L} = -\frac{m_L}{\rho_L^{\,2}} \Delta \rho_L \tag{A-23}$$

$$\frac{\partial V_{cat.}}{\partial m_{cat.}} = \frac{1}{\rho_{cat.}} \Delta m_{cat.} \tag{A-24}$$

$$\frac{\partial V_{cat.}}{\partial \rho_{cat.}} = -\frac{m_{cat.}}{\rho_{cat.}^{\,2}} \Delta \rho_{cat} \tag{A-25}$$

Volumetric Mass Transfer Coefficient, $k_L a$

$k_L a$ values are calculated using equation (6-26):

$$\frac{P_{i,F}}{P_{i,I}} \ln \left[\frac{P_{i,I} - P_{i,F}}{P_{i,t} - P_{i,F}} \right] = k_L a.t \tag{A-26}$$

The independent variables used in this expression are:

$$k_L a = f(P_{r,F}, P_{r,I}, P_{r,t}, t) \quad \text{(A-27)}$$

Therefore, the error for the volumetric mass transfer coefficient is calculated from equation (6-26) as follows:

$$\Delta k_L a = \left|\frac{\partial k_L a}{\partial t}\right|\Delta t + \left|\frac{\partial k_L a}{\partial P_{r,F}}\right|\Delta P_{r,F} + \left|\frac{\partial k_L a}{\partial P_{r,I}}\right|\Delta P_{r,I} + \left|\frac{\partial k_L a}{\partial P_{r,t}}\right|\Delta P_{r,t} \quad \text{(A-28)}$$

The needed partial derivatives are:

$$\frac{\partial k_L a}{\partial t} = \frac{-1}{t^2}\frac{P_{r,F}}{P_{r,I}}\ln\left(\frac{P_{r,I} - P_{r,F}}{P_{r,t} - P_{r,F}}\right) \quad \text{(A-29)}$$

$$\frac{\partial k_L a}{\partial P_{r,F}} = \frac{1}{tP_{r,I}}\left[\ln\left(\frac{P_{r,I} - P_{r,F}}{P_{r,t} - P_{r,F}}\right) + \frac{P_{r,F}\left(P_{r,I} - P_{r,t}\right)}{\left(P_{r,I} - P_{r,F}\right)\left(P_{r,t} - P_{r,F}\right)}\right] \quad \text{(A-30)}$$

$$\frac{\partial k_L a}{\partial P_{r,I}} = \frac{1}{t}\left[\frac{P_{r,F}}{P_{r,I}}\frac{1}{\left(P_{r,I} - P_{r,F}\right)} - \frac{P_{r,F}}{(P_{r,I})^2}\ln\left(\frac{P_{r,I} - P_{r,F}}{P_{r,t} - P_{r,F}}\right)\right] \quad \text{(A-31)}$$

$$\frac{\partial k_L a}{\partial P_{r,t}} = \frac{P_{r,F}}{tP_{r,I}}\frac{-1}{\left(P_{r,t} - P_{r,F}\right)} \quad \text{(A-32)}$$

An example of error calculation of C^* and $k_L a$ is provided in Table A.1.

Run #: 3W400H1_20_(15b/22.5b/30b) Date: 08-12-2011

System: Gas: H_2

Liquid: Sasol reactor wax

Solid: Puralox alumina particles

Operating Conditions:

C_S = 20 vol%	V_L = 0.00144 m^3	$\rho_{cat.}$ = 1170 kg/m^3
N = 1100 rpm	$V_{cat.}$ = 0.00036 m^3	m_L = 1.0564128 kg
V_r = 0.00383084 m^3	ρ_L = 733.62 kg/m^3	$m_{cat.}$ = 0.4212 kg

Errors:

ΔV_r = 0 m^3	$\Delta P_{r,F}$ = 3972 Pa	Δm_L = 0.0001 kg
ΔV_L = 1.37x10^{-7} m^3	$\Delta T_{r,I}$ = 0.1 K	$\Delta m_{cat.}$ = 0.0001 kg
$\Delta V_{cat.}$ = 3.27x10^{-8} m^3	$\Delta T_{r,F}$ = 0.1 K	Δt = 0 s
$\Delta P_{r,I}$ = 3972 Pa	$\Delta \rho_L$ = 0 kg/m^3	
$\Delta P_{r,m}$ = 3972 Pa	$\Delta \rho_{cat.}$ = 0 kg/m^3	

Table A.1: Sample error calculation

$P_{r,I}$	$T_{r,I}$	$P_{r,F}$	$T_{r,F}$	$P_{r,m}$	t	C^*	$\Delta C^*/C^*$	k_La	$\Delta k_La/k_La$
bar	*K*	*bar*	*K*	*bar*	*s*	mol/m^3	*%*	s^{-1}	*%*
15.027	403.1	14.03	402.9	14.2	11.1	38.47	11.8%	0.176	23.55%
22.495	401.7	21.95	402.9	22.01	8.3	59.50	6.9%	0.305	18.42%
30.012	400.5	29.47	401.4	29.5	9.0	79.93	4.8%	0.292	14.58%

APPENDIX B

EXAMPLE $k_L a$ CALCULATIONS

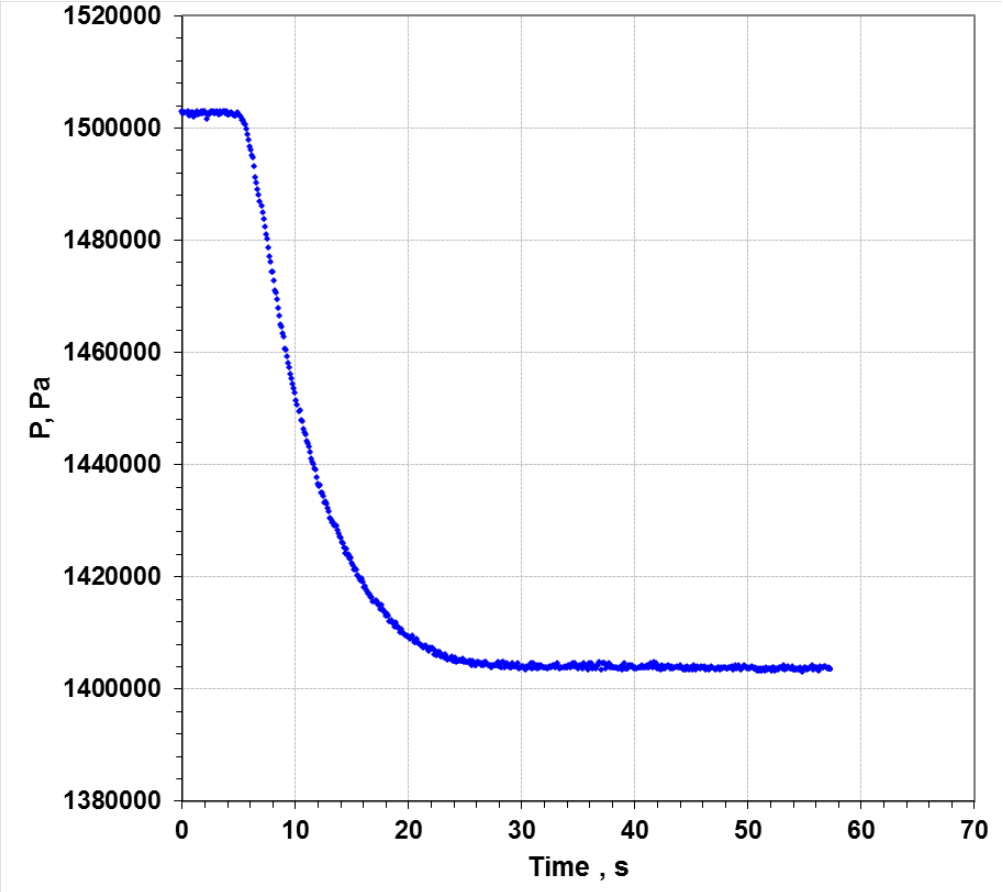

Figure B.1: Typical experimental Pressure vs. time curve showing the transient gas-absorption behavior for the run #: 3W400H1_20_(15b/22.5b/30b)

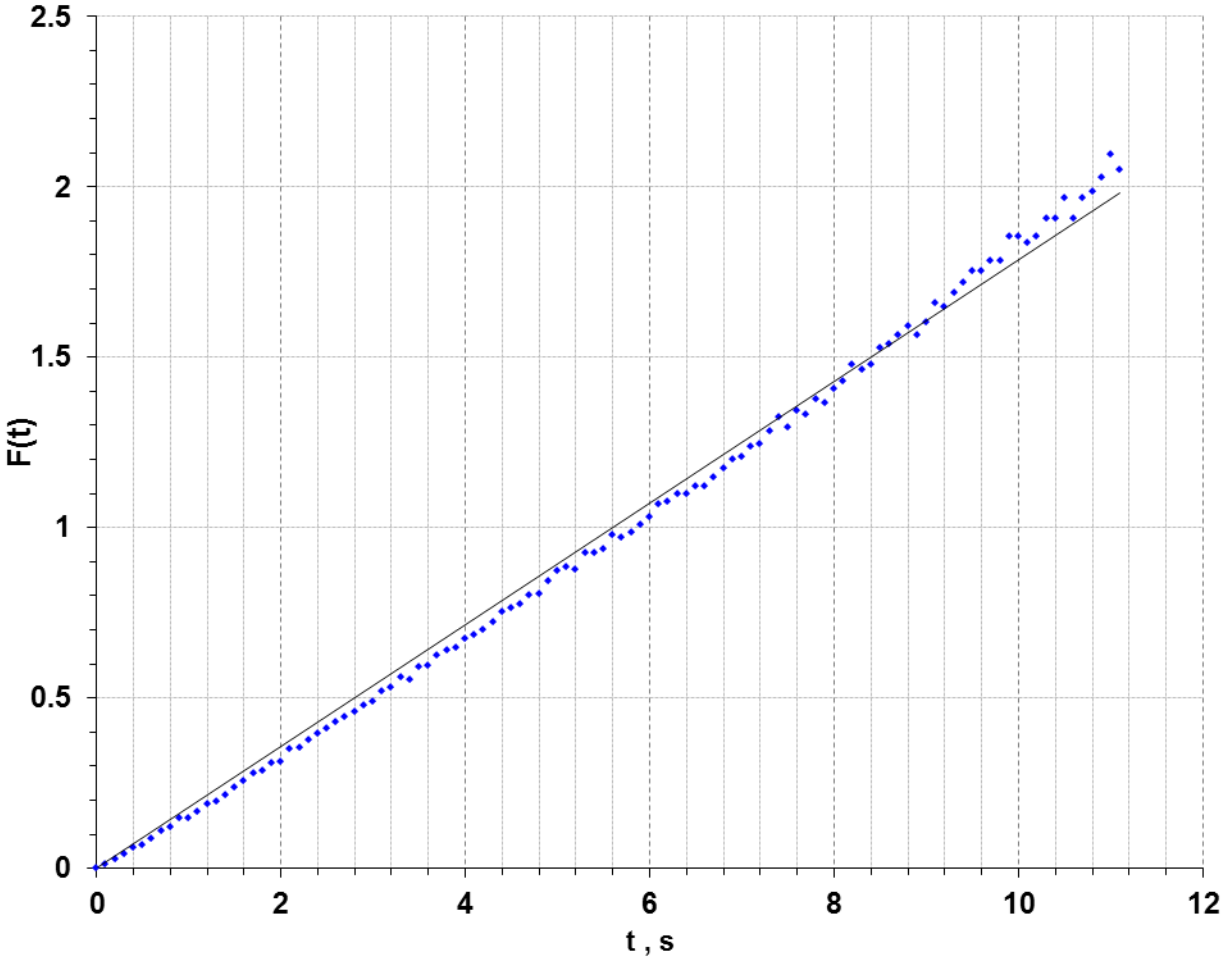

Figure B.2: A plot of F(t) from equation (6-26); run # : 3W400H1_20_(15b/22.5b/30b)

BIBLIOGRAPHY

1. CIA, *World economy overview*. THE WORLD FACTBOOK, 2011.

2. Global, B., *Global oil reserves*. 2011.

3. Review, A.E., *Annual Energy Review*. 2008, 2009.

4. Administration, U.S.E.I., *Annual Energy Outlook 2011*. 2011.

5. Agency, I.E., *World Energy Outlook 2011*. 2011.

6. Vosloo, A.C., *Fischer-Tropsch: a futuristic view*. Fuel Processing Technology, 2001. **71**(1-3): p. 149-155.

7. Dry, M.E., *Present and future applications of the Fischer-Tropsch process*. Applied Catalysis A: General, 2004. **276**(1-2): p. 1-3.

8. Wilhelm, D.J., et al., *Syngas production for gas-to-liquids applications: technologies, issues and outlook*. Fuel Processing Technology, 2001. **71**(1-3): p. 139-148.

9. Liu, G., et al., *Making Fischer−Tropsch Fuels and Electricity from Coal and Biomass: Performance and Cost Analysis*. Energy & Fuels, 2010. **25**(1): p. 415-437.

10. Lemoine, R., A. Behkish, and B.I. Morsi, *Hydrodynamic and Mass Transfer Characteristics in Organic Liquid Mixtures in a Large-Scale Bubble Column Reactor for the Toluene Oxidation Process*. Industrial & Engineering Chemistry Process Design and Development, 2004. **43**(19): p. 6195-6212.

11. Zwietering, T.N., *Suspending of solid particles in liquid by agitators*. Chemical Engineering Science, 1958. **8**(3-4): p. 244-253.

12. Narayanan, S., et al., *Suspension of solids by mechanical agitation*. Chemical Engineering Science, 1969. **24**(2): p. 223-230.

13. N. Sharma, R. and A. A. Shaikh, *Solids suspension in stirred tanks with pitched blade turbines*. Chemical Engineering Science, 2003. **58**(10): p. 2123-2140.

14. Armenante, P.M., E.U. Nagamine, and J. Susanto, *Determination of correlations to predict the minimum agitation speed for complete solid suspension in agitated vessels.* The Canadian Journal of Chemical Engineering, 1998. **76**(3): p. 413-419.

15. Murugesan, T., *Critical Impeller Speed for Solid Suspension in Mechanically Agitated Contactors.* Journal of Chemical Engineering of Japan, 2001. **34**(3): p. 423-429.

16. Lewis, W.K. and W.G. Whitman, *Principles of Gas Absorption*. Industrial & Engineering Chemistry, 1924. **16**(12): p. 1215-1220.

17. Chang, M.Y. and B.I. Morsi, *Solubilities and mass transfer coefficients of carbon monoxide in a gas-inducing reactor operating with organic liquids under high pressures and temperatures.* Chemical Engineering Science, 1992. **47**(13-14): p. 3541-3548.

18. Huang, S.H., et al., *Solubility of synthesis gases in heavy n-paraffins and Fischer-Tropsch wax*. Industrial & Engineering Chemistry Research, 1988. **27**(1): p. 162-169.

19. Deimling, A., et al., *Solubility and mass transfer of CO and H2 in Fischer—Tropsch liquids and slurries.* The Chemical Engineering Journal, 1984. **29**(3): p. 127-140.

20. Albal, R.S., et al., *Mass transfer coefficients and solubilities for hydrogen and carbon monoxide under Fischer-Tropsch conditions.* Chemical Engineering Science, 1984. **39**(5): p. 905-907.

21. Chou, J.S. and K.C. Chao, *Solubility of synthesis and product gases in a Fischer-Tropsch SASOL wax*. Industrial & Engineering Chemistry Research, 1992. **31**(2): p. 621-623.

22. Ronze, D., et al., *Hydrogen solubility in straight run gasoil.* Chemical Engineering Science, 2002. **57**(4): p. 547-553.

23. Tong, J., et al., *Solubilities of Nitrogen in Heavy Normal Paraffins from 323 to 423 K at Pressures to 18.0 MPa*. Journal of Chemical & Engineering Data, 1999. **44**(4): p. 784-787.

24. van Vuuren, D.S., J.R. Hunter, and M.D. Heydenrych, *The solubility of various gases in Fischer-Tropsch reactor wax.* Chemical Engineering Science, 1988. **43**(6): p. 1291-1296.

25. Tsai, F.-N., et al., *Solubility of methane, ethane, and carbon dioxide in a Mobil Fischer—Tropsch wax and in n-paraffins.* The Chemical Engineering Journal, 1988. **38**(1): p. 41-46.

26. Ghosh, A., W.G. Chapman, and R.N. French, *Gas solubility in hydrocarbons—a SAFT-based approach*. Fluid Phase Equilibria, 2003. **209**(2): p. 229-243.

27. Chou, J.S. and K.C. Chao, *Correlation of synthesis gas solubility in n-paraffin solvents and Fischer—Tropsch waxes.* Fluid Phase Equilibria, 1989. **46**(2-3): p. 179-195.

28. Wang, Y.N., et al., *Correlation for gas–liquid equilibrium prediction in Fischer–Tropsch synthesis*. Fuel, 1999. **78**(8): p. 911-917.

29. Campanella, E.A., *Correlation and prediction of synthesis gas solubility in n-paraffin systems*. Chemical Engineering & Technology, 1997. **20**(6): p. 371-377.

30. Tsai, F.N., et al., *Solubility of methane, ethane, and carbon dioxide in a Mobil Fischer-Tropsch wax and in n-paraffins*. Chemical Engineering Journal (Amsterdam, Netherlands), 1988. **38**(1): p. 41-6.

31. Huang, S.H., et al., *Solubility of synthesis gases in heavy n-paraffins and Fischer-Tropsch wax*. Industrial & Engineering Chemistry Research, 1988. **27**(1): p. 162-9.

32. Chou, J.S. and K.C. Chao, *Correlation of synthesis gas solubility in n-paraffin solvents and Fischer-Tropsch waxes*. Fluid Phase Equilibria, 1989. **46**(2-3): p. 179-95.

33. Gao, W., R.L. Robinson, Jr., and K.A.M. Gasem, *High-Pressure Solubilities of Hydrogen, Nitrogen, and Carbon Monoxide in Dodecane from 344 to 410 K at Pressures to 13.2 MPa*. Journal of Chemical and Engineering Data, 1999. **44**(1): p. 130-132.

34. Karandikar, B.M., et al., *Effect of water on the solubilities and mass transfer coefficients of gases in a heavy fraction of Fischer-Tropsch products*. Canadian Journal of Chemical Engineering, 1987. **65**(6): p. 973-981.

35. Karandikar, B.M., et al., *Effect of water on the solubility and mass transfer coefficients of CO and H2 in a Fischer-Tropsch liquid*. The Chemical Engineering Journal, 1986. **33**(3): p. 157-168.

36. Huang, S.H., H.M. Lin, and K.C. Chao, *Experimental investigation of synthesis gas solubility in Fischer-Tropsch reactor slurry*. Fluid Phase Equilibria, 1987. **36**: p. 141-148.

37. Campanella, E.A., *Correlation of solubilities of carbon monoxide, carbon dioxide, and hydrogen in paraffins*. Journal of Chemical Engineering of Japan, 1993. **26**(1): p. 48-51.

38. Inga, J.R., *Scaleup and Scaledown of Slurry Reactors: A New Methodology*, in *Chemical and Petroleum Engineering Department*1997, University of Pittsburgh: Pittsburgh, PA. p. 339.

39. Tekie, Z., J. Li, and B.I. Morsi, *Mass Transfer Parameters of O2 and N2 in Cyclohexane under Elevated Pressures and Temperatures: A Statistical Approach*. Industrial & Engineering Chemistry Research, 1997. **36**: p. 3879-3888.

40. Ronze, D., et al., *Hydrogen solubility in straight run gas oil*. Chemical Engineering Science, 2002. **57**(4): p. 547-553.

41. Breman, B.B., et al., *Gas-Liquid Solubilities of Carbon Monoxide, Carbon Dioxide,Hydrogen, Water, 1-Alcohols (1 < n < 6), and n-Paraffins (2 < n < 6) in Hexadecane, Octacosane, 1-Hexadecanol, Phenanthrene, and Tetraethylene Glycol at Pressures up to 5.5 MPa and Temperatures from 293 to 553 K*. Journal of Chemical and Engineering Data, 1994. **39**(4): p. 647-666.

42. Hichri, H., et al., *Gas-liquid mass-transfer coefficients in a slurry batch reactor equipped with a self-gas-inducing agitator*. Industrial & Engineering Chemistry Research, 1992. **31**(8): p. 1864-1867.

43. Behkish, A., et al., *Mass transfer characteristics in a large-scale slurry bubble column reactor with organic liquid mixtures*. Chemical Engineering Science, 2002. **57**(16): p. 3307-3324.

44. Miller, S.A., A. Ekstrom, and N.R. Foster, *Solubility and mass-transfer coefficients for hydrogen and carbon monoxide in n-octacosane*. Journal of Chemical and Engineering Data, 1990. **35**(2): p. 125-127.

45. Inga, J.R. and B.I. Morsi, *Effect of catalyst loading on gas/liquid mass transfer in a slurry reactor: a statistical experimental approach*. Canadian Journal of Chemical Engineering, 1997. **75**(5): p. 872-881.

46. Albal, R.S., et al., *Mass transfer in multiphase agitated contactors*. The Chemical Engineering Journal, 1983. **27**(2): p. 61-80.

47. Zaidi, A.L., M.; Ralek and Deckwer, *Mass Transfer in the Liquid Phase Fischer-Tropsch Synthesis*. German Chemical Engineering, 1979. **2**: p. 94-102.

48. Ledakowicz, S., H. Nettelhoff, and W.D. Deckwer, *Gas-liquid mass transfer data in a stirred autoclave reactor*. Industrial & Engineering Chemistry Fundamentals, 1984. **23**(4): p. 510-512.

49. Hsu, Y.-C., et al., *Ozone Transfer into Water in a Gas-Inducing Reactor*. Industrial & Engineering Chemistry Research, 2002. **41**(1): p. 120-127.

50. Hsu, Y.-C., R.Y. Peng, and C.-J. Huang, *Onset of gas induction, power consumption, gas holdup and mass transfer in a new gas-induced reactor*. Chemical Engineering Science, 1997. **52**(21-22): p. 3883-3891.

51. Sridhar, T. and O.E. Potter, *Interfacial areas in gas--liquid stirred vessels*. Chemical Engineering Science, 1980. **35**(3): p. 683-695.

52. Oguz, H., A. Brehm, and W.D. Deckwer, *Gas/liquid mass transfer in sparged agitated slurries*. Chemical Engineering Science, 1987. **42**(7): p. 1815-1822.

53. Joosten, G.E.H., J.G.M. Schilder, and J.J. Janssen, *The influence of suspended solid material on the gas-liquid mass transfer in stirred gas-liquid contactors*. Chemical Engineering Science, 1977. **32**(5): p. 563-566.

54. Ruthiya, K.C., et al., *Mechanisms of physical and reaction enhancement of mass transfer in a gas inducing stirred slurry reactor*. Chemical Engineering Journal, 2003. **96**(1-3): p. 55-69.

55. Teramoto, M., et al., *Effects of pressure on liquid-phase mass transfer coefficients*. Chemical Engineering Journal (Amsterdam, Netherlands), 1974. **8**(3): p. 223-6.

56. Deimling, A., et al., *Solubility and mass transfer of carbon monoxide and hydrogen in Fischer-Tropsch liquids and slurries*. Chemical Engineering Journal (Amsterdam, Netherlands), 1984. **29**(3): p. 127-40.

57. Maalej, S., B. Benadda, and M. Otterbein, *Influence of pressure on the hydrodynamics and mass transfer parameters of an agitated bubble reactor*. Chemical Engineering & Technology, 2001. **24**(1): p. 77-84.

58. Dietrich, E., et al., *Raney-nickel catalyzed hydrogenations: Gas-liquid mass transfer in gas-induced stirred slurry reactors*. Chemical Engineering Science, 1992. **47**(13-14): p. 3597-3604.

59. Chen, J.-H., et al., *Application of gas-inducing reactor to obtain high oxygen dissolution in aeration process*. Water Research, 2003. **37**(12): p. 2919-2928.

60. Lekhal, A., et al., *Gas-liquid mass transfer in gas-liquid-liquid dispersions*. Chemical Engineering Science, 1997. **52**(21-22): p. 4069-4077.

61. Kluytmans, J.H.J., et al., *Mass transfer in sparged and stirred reactors: influence of carbon particles and electrolyte*. Chemical Engineering Science, 2003. **58**(20): p. 4719-4728.

62. Yaws, C.L., *Chemical Properties Handbook*1999: McGraw-Hill.

63. Satterfield, C.N. and G.A. Huff, *Product Distribution from Iron Catalyst in Fischer-Tropsch Slurry Reactors*. Industrial & Engineering Chemistry Process Design and Development, 1982. **21**(3): p. 465-470.

64. Patzlaff, J., et al., *Studies on product distributions of iron and cobalt catalyzed Fischer-Tropsch synthesis*. Applied Catalysis A: General, 1999. **186**(1-2): p. 109-119.

65. Gao, W., R.L. Robinson, Jr., and K.A.M. Gasem, *Improved Correlations for heavy n-paraffin physical properties*. Fluid Phase Equilibria, 2001. **179**(1-2): p. 207-216.

66. Marano, J.J. and G.D. Holder, *General Equation for Correlating the Thermophysical Properties of n-Paraffins, n-Olefins, and Other Homologous Series. 2. Asymptotic*

Behavior Correlations for PVT Properties. Industrial & Engineering Chemistry Research, 1997. **36**(5): p. 1895-1907.

67. Marano, J.J. and G.D. Holder, *A General Equation for Correlating the Thermophysical Properties of n-Paraffins, n-Olefins, and Other Homologous Series. 3. Asymptotic Behavior Correlations for Thermal and Transport Properties*. Industrial & Engineering Chemistry Research, 1997. **36**(6): p. 2399-2408.

68. Wilke, C.R. and P. Chang, *Correlation of diffusion coefficients in dilute solutions*. American Institute of Chemical Engineering Journal, 1955. **1**: p. 264-270.

69. Lemoine, R., *Hydrodynamics, Mass Transfer and Modeling of the Liquid-Phase Toluene Oxidation Process*, in *Chemical and Petroleum Engineering Department*2005, University of Pittsburgh: Pittsburgh, PA.

70. Tekie, Z., et al., *Gas-liquid mass transfer in cyclohexane oxidation process using gas-inducing and surface-aeration agitated reactors*. Chemical Engineering Science, 1997. **52**(9): p. 1541-1551.

71. Soriano, J.P., *Mass Transfer Characteristics in an Agitated Slurry Reactor Operating Under Fischer-Tropsch Conditions*, in *Chemical and Petroleum Engineering Department*2005, University of Pittsburgh: Pittsburgh. p. 137.

72. Hildebrand, J.H.S., Robert Lane, *The solubility of nonelectrolytes*. Vol. 3rd ed. 1955 New York, United States Reinhold : s.n. .

73. Behkish, A., et al., *Gas holdup and bubble size behavior in a large-scale slurry bubble column reactor operating with an organic liquid under elevated pressures and temperatures*. Chemical Engineering Journal, 2007. **128**(2-3): p. 69-84.

74. Erkey, C., J.B. Rodden, and A. Akgerman, *A Correlation for Predicting Diffusion Coefficients in Alkanes*. The Canadian Journal of Chemical Engineering, 1990. **68**: p. 661-665.

75. Tekie, Z., et al., *Gas-Liquid Mass Transfer in Cyclohexane Oxidation Process Using Gas-Inducing and Surface-Aeration Agitated Reactors*. Chemical Engineering Science, 1997. **52**(9): p. 1541-1551.

76. Calderbank, P.H. and M.B. Moo-Young, *The continuous phase heat and mass-transfer properties of dispersions*. Chemical Engineering Science, 1961. **16**(1-2): p. 39-54.